Alkali metals in combustion

of biomass with coal

Alkali metals in combustion
of biomass with coal

PROEFSCHRIFT

ter verkrijging van de graad van doctor
aan de Technische Universiteit Delft,
op gezag van de Rector Magnificus Prof. dr. ir. J.T. Fokkema,
voorzitter van het College voor Promoties,
in het openbaar te verdedigen op dinsdag, 23 januari 2007 om
10.00 uur

door

Michał Piotr GLAZER

Master of Science
Poznan University of Technology, Poland
geboren te Poznań, Polen.

Dit proefschrift is goedgekeurd door de promotor:

Prof. dr.-Ing. H. Spliethoff

Samenstelling promotiecommissie:

Rector Magnificus	voorzitter
Prof. Dr. -Ing. H. Spliethoff	Technische Universiteit Delft, Promotor
Prof. dr. J.A. Moulijn	Technische Universiteit Delft
Prof. Dr. -Ing. I. Obernberger	Technische Universiteit Eindhoven
Prof. dr. Th. H. van der Meer	Universiteit Twente
Prof. dr. M. Hupa	Åbo Akademi
Dr. ir. W de Jong	Technische Universiteit Delft
Dr. ir. J. Kiel	ECN

Copyright © 2006 by M.P. Glazer

All rights reserved. No part of the material protected by this copyright notice may be reproduced or utilized in any form or by any means, electronic or mechanical, including photocopying, recording or by any information storage and retrieval system, without the prior permission of the author.

Typeset by the author with the LaTeX Documentation System.

Author email: michal_glazer@hotmail.com

Contents

List of abbreviations **1**

1 Introduction **3**
1.1 Straw . . . 3
1.2 Straw as a fuel . . . 3
1.3 Technologies for co-firing . . . 4
1.3.1 Grate co-firing with biomass . . . 4
1.3.2 Pulverized fuel co-firing with biomass . . . 5
1.3.3 Fluidized bed co-firing with biomass . . . 5
1.4 Problems related with straw, co-combustion issues . . . 6
1.5 Distributed CHP plants . . . 7
1.6 EU demonstration 25MW high efficiency straw fired power plant 7
1.7 Motivation and scope of the dissertation . . . 9
1.8 Methodology . . . 10
1.9 Outline of this thesis . . . 11

2 Alkali metals behavior under combustion conditions **13**
2.1 Alkali metals, S and Cl in straw and coal . . . 13
2.2 The fate of alkali metals and interactions with S, Cl and Si . . . 15
2.3 Possible alkali getters . . . 20
2.3.1 Kaolin . . . 25
2.3.2 Co-combustion with coal and sequestering of alkalis . . . 26
2.4 Conclusions and research requirements . . . 28

3 Experimental investigation of alkali metal release within CFBC systems **29**
3.1 Introduction - investigation of alkali metals in combustion systems 29
3.2 Combustion facility - CFB reactor . . . 31
3.3 Non-intrusive gaseous alkali metals measurements - ELIF technique . . . 34
3.3.1 ELIF limitations and consideration of errors . . . 34
3.3.2 Optical access . . . 35
3.3.3 Laser excitation and fluorescence detection . . . 35
3.4 Experimental techniques . . . 36
3.4.1 Fuels and CFBC tests . . . 36
3.4.2 Fly ash and bed material investigation with SEM/EDS . . . 38

3.5 Results . . . 40
3.6 Discussion . . . 44
3.6.1 ELIF campaigns . . . 44
3.6.2 SEM/EDS analysis of the particles . . . 52
3.7 Conclusions . . . 53

4 Chemical equilibrium modelling of combustion system 55
4.1 Introduction to chemical equilibrium . . . 55
4.1.1 Enthalpy . . . 55
4.1.2 Standard Enthalpy of Reaction . . . 55
4.1.3 Standard Enthalpy of Formation . . . 56
4.1.4 Activation Energy . . . 56
4.1.5 Spontaneous Reaction . . . 56
4.1.6 Energy and Spontaneity . . . 56
4.1.7 Entropy . . . 57
4.1.8 The Gibbs free energy . . . 57
4.1.9 Entropy and Chemical Reactions . . . 57
4.1.10 Temperature dependence of the Gibbs free energy . . . 58
4.1.11 Standard-State Free Energy of Formation . . . 58
4.2 Chemical Equilibrium Definitions . . . 59
4.2.1 The Equilibrium Constant . . . 59
4.2.2 Free Energy Changes and Equilibrium Constants . . . 59
4.2.3 A General Approach to Gibbs free energy . . . 60
4.2.4 Gibbs Energy Minimization . . . 62
4.3 Thermodynamic equilibrium calculations - approach . . . 63
4.4 Results . . . 66
4.5 Discussion . . . 66
4.6 Conclusions . . . 75

5 Fundamental investigation of KCl - kaolin interactions 77
5.1 Introduction . . . 77
5.2 Experimental . . . 78
5.2.1 Thermogravimetric reactor . . . 78
5.2.2 Sample holder . . . 79
5.2.3 Samples and experimental conditions . . . 79
5.3 Results and discussion . . . 80
5.3.1 Evaporation of KCl . . . 80
5.3.2 Morphology investigation with SEM . . . 81
5.3.3 Elemental composition of samples . . . 84
5.3.4 Cross section investigation with SEM/EDS and X-ray mapping . . . 89
5.4 Conclusions . . . 91

6 Final conclusions and recommendations **95**
6.1 Conclusions 95
6.1.1 Experimental work 95
6.1.2 Modelling work 96
6.2 Recommendations 97
6.2.1 Experimental work 97
6.2.2 Modelling work 98

References **99**

A Structural changes during rapid devolatilization of high alkali bio-fuels **109**
A.1 Introduction 109
A.2 Experimental apparatus 109
A.3 Results and discussion 111
A.4 Conclusions 114

B Alkali sampling on pilot scale CFB **117**
B.1 Introduction 117
B.2 Problem outline 118
B.3 Problem solving 118
B.4 Conclusions 123

C Wet gas trapping measurement protocol **125**

D Alkali measurements with batch techniques **127**
D.1 Wet trapping method - principles and experimental setup 127
D.2 Results 129
D.3 Discussion 129

E SEM/EDS analysis of the CFBC samples **133**

F SEM/EDS analysis of kaolin samples **139**

Summary **151**

Samenvatting **153**

Selected Publications **155**

Curriculum Vitae **157**

Acknowledgments **159**

List of abbreviations

CFBC - Circulating Fluidized Bed Combustion

CHP - Combined Heat and Power

DE - Diatomaceous Earth

DTA/TGA - Differential Thermal Analysis/Thermogravimetric Analysis

EHN - Energia Hidroelectrica De Navarra

ELIF - Excimer Laser Induced Fragmentation (ELIF) fluorescence spectroscopy

FTIR - Fourier Transform Infra Red

HIAL - HIgh ALkali

MBMS - Molecular Beam Mass Spectrometry

MBM - Meat and Bone Meal

NDIR - Non Dispersive Infra Red

PEARLS - Plasma Excited Atomic Spectroscopy

PMT - Photomultiplier

SEM/EDS - Scanning Electron Microscopy/Energy Dispersion Spectroscopy

SFG - Simulated Flue Gas

SI - Surface Ionization

TG - Thermogravimetric

XRD - X-ray Diffraction

Chapter 1
Introduction

1.1 Straw

Straw is a product of growing commercial crops especially cereal grain (Fig. 1.1). It can be considered as by product. Every year more than 300 Mton of straw is produced just within Europe [European Renewable Energy Council, 2000]. Wheat and barley constitute for about 80% of produced straw. The annual production of straw within the EU is influenced by EU internal agricultural policies and depends on cereal prices, weather during growth and harvest, etc. At present straw is being used for [Nikolaisen, 1998]:

- agriculture's own production (for livestock housing systems)
- as heat source for grain drying and heating in agriculture
- for energy production
- soil fertilization (the amount of straw left after accounting for above application).

1.2 Straw as a fuel

The need for renewable energy sources as a substitute for fossil fuels is still growing. The utilization of different forms of biomass seems to be an opportunity to reduce the CO_2 emissions and fulfill the demands of the Kyoto protocol [United Nations, 1997]. Almost zero net CO_2 emissions for biomass are becoming attractive also from an economical point of view, in many countries tax for excessive CO_2 emissions has been introduced. According to the EU directive the combustion of straw alone and co-combustion with coal should be promoted to reach the aim of 8% of the current primary energy supplied from bio-sources in 2010 [Spliethoff et al., 2001] and help to reduce the CO_2 emissions by up to 366 Mt per year [European Commission, 1998b] in the existing power plants and the newly built ones. Most of the European countries



Figure 1.1: Straw harvesting

use mainly fossil fuels such as coal, oil or natural gas for energy production but there is still more and more attention paid to the utilization of agricultural residues. Among the biofuels the herbaceous ones, like straw seem to be promising for utilization. As already mentioned 300 Mton of biofuels such as straw called also high alkali [HIAL] biofuels, is available every year on the EU common market and can be used for example small decentralized CHP plants [European Renewable Energy Council, 2000].

Straw usually contains 14-20% water which is vaporised during the combustion process. The dry matter left is mainly composed of less than 50% carbon, 6% hydrogen. The oxygen content is quite high and can be at a level of 42%. Moreover there is small amount of nitrogen, sulfur, silicon and other elements like alkali metals (sodium and potassium) and chloride.

1.3 Technologies for co-firing

1.3.1 Grate co-firing with biomass

There are a number of power plants operating based on the grate firing technique. Many different forms of grate firing exist, among others there are: fixed beds, vibrating beds, moving and travelling beds together with rotating kilns [van Loo and Koppejan, 2002]. The advantage of grate firing and co-firing is that it can handle untreated fuel very often with high moisture content. As

a drawback the efficiency of electricity production is quite low and oscillates between 10-30% [Veijonen, 2005; Obernberger, 1998; Hein and Bemtgen, 1998]. Because of the robust construction, grate firing is well suited for dealing with problematic fuels like straw and there are coal power plants which have been retrofited to partial use of biomass [Hein and Bemtgen, 1998; Brem, 2003].

1.3.2 Pulverized fuel co-firing with biomass

Pulverized fuel combustion is based on a finely ground fuel as a feed. The fuel is then transported to the combustor where it is burnt and as a result energy is produced as (combined) heat and power. For pulverized fuel combustion fuel requirements are much higher than for fluidized bed or grate firing [Mann and Spath, 2001]. In case of fossil fuels like coal, the particle size should not be larger than about 100μm within whole range. The reason is twofold. Residence time in pulverized coal reactors is relatively short so the fuel size has to be small in order to achieve full conversion. Also because of the oxygen diffusion to the particle the size is limiting factor. In case of biomass fuels and their higher reactivity the size can be increased but it should not be more than 1mm [Heikinnen, 2005]. High temperatures in pulverized fuel boilers prevent wide use of biomass, especially straw in such boilers due to slagging and fouling problems.

1.3.3 Fluidized bed co-firing with biomass

CFB technology implementation is growing fast. There are currently over 1200 CFBC plants worldwide [McMullan, 2004; Cleve, 1999] with a total installed capacity of some 65GWth. Looking how the installed capacity is divided between continents the dominant application region to date is Asia where approximately 52% of total capacity is installed. In Europe there is 22%, the North America accounts for some 26% of the worldwide capacity. It has to be stressed that most of the Asian capacity is located in China where the number of CFBC plants is close to 900 with an average capacity of 30MWth. So far succesful scale up has been achieved upto 300MWe and CFB boilers are competitive to PF technology because of the ability to use low grade fuels at low cost and low environmental impact. Nowadays there are new, more than 400MWe supercritical power plants being built, for example in Lagisza, Poland [PowerTechnology, 2006].

Eventhough CFB technology offers great fuel flexibility, most of the mentioned capacity operates on coal. There is a chance for further development lowering environmental impact. This can be done by implementing biomass for energy production [de Jong, 2005; Oniszk-Poplawska et al., 2003]. Great fuel flexibility offered by CFB boilers is an advantage and can be used to substitute coal by

biomass if down-stream problems with corrosion for example are solved. Combustion of straw is one of the options because of its availability. This would further increase competitiveness of CFB technology considering environmental issues. However still many issues concerning high temperature chemistry of combustion remain unknown. Corrosion, slagging and fouling are at this moment an unavoidable part of straw combustion. To implement biofuels broadly these issues have to be investigated, understood and solved. This thesis tries to answer some of the questions and presents the influence of operational conditions on alkali metals compounds release from high alkaline fuels. Moreover it does answer some fundamental questions concerning interactions between the main gaseous alkali compound KCl and kaolin, the most promising alkali getter.

1.4 Problems related with straw, co-combustion issues

Co-firing with fossil fuels, particularly coal, has received considerable attention, especially in Denmark, Finland, Sweden, the Netherlands and the USA. Biomass can be blended in differing proportions. Extensive tests show that biomass energy can provide about 15% of the total energy input, with modifications only to the feeding systems and burners. Co-firing has been evaluated for a variety of boiler technologies e.g. pulverised coal combustion, cyclones combustion, fluidised bed combustion, etc [Tillman, 2000]. The technical feasibility of biomass co-firing is largely proven, although serious problems on the long time scale basis still remain, e.g. effects on boiler efficiency, slagging, fuel feed control, combustion stability, fuel delivery, unsolved combustion chemistry in case of herbaceous high-alkali biofuels like straw, corrosion etc. [European Commission, 1998a; Schultz, 1998]. One reason why biomass co-firing has not been put into commercial practice is because the economics are unfavourable, due to the low cost of coal- and gas-based power plants. The costs of energy produced from straw varies in The Netherlands between 2.5-5 Euro/GJ comparing to 1.8-2.9 Euro/GJ for energy from coal [Scherpenzeel, 1999]. The most critical factors are fuel costs and the capital cost of the modifications to the power plant to permit co-firing. Yet despite all these problems, biomass co-firing with coal in existing power boilers seems to be one of the most economical ways to use biomass for energy on a large scale in the near future. Co-firing in existing coal-fired power plants makes it possible to achieve greater efficiency in converting biomass into electricity compared to for example 100% wood-fired boilers. For instance, biomass combustion efficiency to generate electricity would be close to 33%-37% when fired with coal. There are also important environmental benefits, e.g. lower sulphur oxide emissions and about a 30% re-

duction in oxides of nitrogen [World Energy Council, 2004].

It has to be pointed out that contrary to coal ash, ash originating from straw combustion because of high alkali metals content cannot be used for land filling and building materials. It can only be disposed to specially controlled disposal sites. This regulations determine somehow life-cycle of straw as fuel and causes utilization costs to be higher.

1.5 Distributed CHP plants

The most promising options for straw combustion and co-combustion seem to be small distributed power plants or Combined Heat and Power (CHP) plants. These plants can be located within areas where stable supply of straw can be guaranteed. Yearly supply contracts with farmers would create new jobs in local agricultural and provide an undisrupted flow of fuel for continuous operation. To avoid high transportation costs the size of such power plants should be designed in such a way that supply of the necessary amount of straw can be provided within relatively small radius. If a power plant can be combined with heat production the efficiency will be of course higher. For power plants with 100% straw combustion the material for heat exchangers and operational parameters should be carefully set and controled within acceptable limits. Biofuels, especially high alkali straw is a difficult fuel and special materials and power plant handling is required.

1.6 EU demonstration 25MW high efficiency straw fired power plant

With financial support from the European Community a 25MWe power plant completely fired with straw was built by EHN, the Spanish utility. The plant is located in the Navarra region of Spain, in the industrial estate of Sanüesa nearby Pamplona (Fig. 1.2). The aim of the project has been to demonstrate the implementation of highly advanced technology for biofuels utilization, especially difficult ones like straw [EHN, 2004]. The Sangüesa boiler is a grate firing boiler operating exclusively with straw. The power plant is not a CHP, it produces only electricity. Sanüesa power plant operates with high steam efficiency and steam temperature, an especially designed superheater minimizes slagging and fouling problems. The electrical efficiency is 32% while the boiler thermal efficiency is 92%. The power plant is an electricity generation facility based on renewable energy, which supplies a net amount of 25 MW of electricity to the grid. An additional power production of about 2.5 MW of electricity is



Figure 1.2: Straw fired power plant, EHN, Sangüesa, Spain

generated for consumption in the own operation systems of the plant, and heat production is nowadays released at the condensing system, which is cooled by a water intake from an irrigation channel of the Irati river. The plant operation availability is expected to be 8.000 hours/year, which leads to an annual electricity production of 200 GWh with 160 000 tons/year of straw. The technology is based on an innovative biomass boiler, together with a conventional steam circuit and steam turbine process (Fig. 1.3). The core technology is located in the boiler, which includes novel hanging platen superheaters for the steam, especially designed with special materials and shapes for minimizing corrosion on their surface. It also includes a vibrating hydrograte made of two different sections, and an innovative feeding system design, including safety devices for fire prevention.

As the utility reports, the plant was initially designed for using only straw but also mixtures of wood chips and straw up to 50% (thermal). At the moment, only for straw the investments in facilities and logistics have been carried out, but enough space is available for the construction of an additional barn and feeding systems for wood chips. The fuel consumption of the plant is 160 000 tons/year of straw, mainly of wheat, barley and corn, all of which is collected all around the region. Supply of straw is guaranteed by means of long-term contracts with local farmers and service companies. The plant's first connection to the grid was achieved on 25th June 2002. After several operation tests the plant has reached succesfully full load operation.

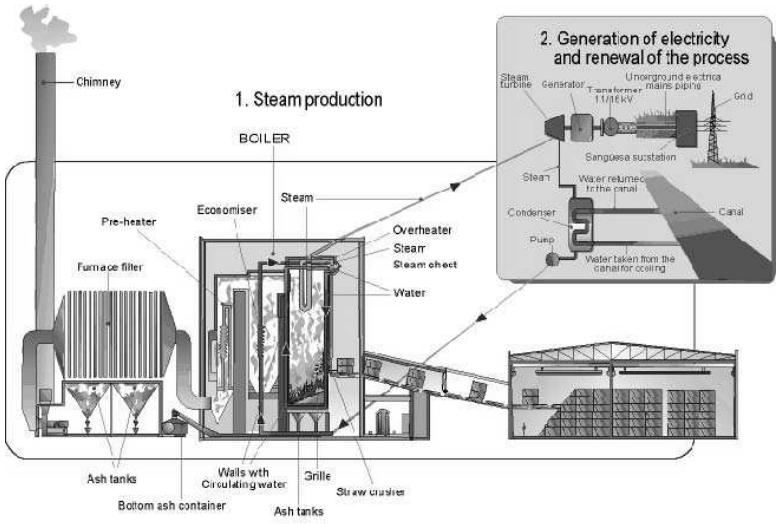


Figure 1.3: Straw fired power plant, power production cycle, EHN, Sangüesa, Spain (adapted from [EHN, 2004])

1.7 Motivation and scope of the dissertation

The existing unknowns and uncertainties in the chemistry of the release of alkali metals K and Na, S, Cl during the combustion process hinder successful, widespread introduction of high alkali biofuels like straw on the energy production market. Extensive research on alkali sequestering and alkali capture by additives is needed to reduce the operational costs and improve the reliability of the existing and newly built power plants.

Chlorine and alkali metals compounds present in straw are very problematic. The combination of alkali metals like potassium and sodium under combustion conditions leads to the production of gaseous and condensing potassium and sodium chloride that are troublesome for boiler operators. The alkali metals compounds being extremely corrosive and deposit forming at combustion conditions create a great risk of failure, unexpected shut downs and costly repairs. Moreover the ash originating from straw has a much lower melting temperature than of other fuels resulting in serious slagging and fouling of the installations.

In order to learn the mechanism responsible for the alkali sequestering in combustion systems, especially circulating fluidized beds, good sampling of the alkali metals is needed first. The implementation of the most up to date excimer

laser alkali sampling technique will be demonstrated within this thesis.

The high alkali (HIAL) straws selected for the experiments were characterized by a broad range of potassium contents, from average values to extremely high potassium content. This in combination with certain ratios of Cl and Si would lead to corrosion and deposit formation problems mentioned above. The reason for the selection was to discover the mechanisms responsible for alkali sequestering. This thesis aims to describe the mechanism based on the experimental data and chemical equilibrium modelling.

Finding a way to capture alkali metals by additives in combustion systems, circulating fluidized bed in particular, is the next issue this thesis is aiming at. The screening of possible alkali metals sorbing additives will be presented. Further more fundamental investigation of the most promising additive, alumina-silicate clay - kaolin, a natural constituent of coal ash, are shown and novel results are presented.

1.8 Methodology

This thesis intends to clarify the aspects of high temperature chemistry of straw combustion focusing on the chemistry of alkali metals compounds and their sequestering. For this purpose advanced experimental and modeling techniques are used.

Under this scope 8 different herbaceous biofuels have been chosen. From them 4 high alkali straw types from Denmark and Spain varying substantially with their ash composition have been selected for further investigation to realize the defined goals.

In order to measure the gaseous alkali compounds two techniques were screened and tested. Some tests have been performed using wet trapping batch technique. In the end the gaseous alkali metals compounds in CFB combustion have been measured using Excimer Laser Induced Fluorescence (ELIF). ELIF is an on-line and in-situ modern measurement technique suitable for industrial application. Together with the ELIF measurements Scanning Electron Microscopy and Energy Dispersive Spectrometry (SEM/EDS) analysis of the biomass fuels are presented.

In order to get more insight into the mechanisms responsible for alkali sequestering an advanced chemical equilibrium modelling package - FactSage has been used to model the combustion system and predict the possible system composition. The package offers most comprehensive database tailored for

high temperature combustion systems.

In order to further investigate interactions between alkali metals and alumina-silicates a Thermogravimetric (TG) reactor has been used to study fundamental interactions between KCl and kaolin. The Scanning Electron Microscopy and Energy Dispersive Spectrometry (SEM/EDS) fulfilled the work with the composition and morphology study over the kaolin particles.

1.9 Outline of this thesis

This thesis presents experimental and modeling work concerning combustion of high alkaline straw in a CFB combustor. The influence of operating conditions and fuel composition on alkali release is analyzed and conclusions are drawn. Moreover fundamental interactions between gaseous potassium chloride and clay mineral kaolin under combustion conditions have been investigated. Together with experimental work on different facilities chemical equilibrium modelling on the system has been performed.

In **Chapter 2** a theoretical discussion and literature review concerning biomass combustion, especially straw is presented. An overview of available research, knowledge is discussed and unknowns are pointed out. Together with the literature overview on straw combustion and alkali related issues, possible alkali metal getters are presented and their applicability discussed.

In **Chapter 3** the main experimental findings concerning CFB combustion and co-combustion tests are presented. Results are based on the ELIF measurements campaigns. To present a complete overview of the system SEM/EDS analysis of ash and bed material is presented and discussed.

In **Chapter 4** the modelling work on the multicomponent combustion system is presented. Chemical equilibrium modelling work was aimed to reveal information on possible reactions and paths of alkali sequestering within the system. Results are discussed, taking into account changing parameters and fuel composition within the system.

In **Chapter 5** the fundamental studies concerning interactions between gaseous potassium chloride and kaolin performed at Åbo Akademi (Finland) are presented and discussed. This study has been carried out in the framework of Marie-Curie exchange programme. The research reveals interesting interactions and dependencies for this most promising alkali sorbing additive.

In **Chapter 6** the final conclusions summarizing experimental and modelling

work are presented. Moreover, recommendations for further scientific work are pointed out.

In **Appendix A** a preliminary investigation of straw combustion using a heated grid apparatus is presented. Morphology changes during rapid heating up are discussed.

In **Appendix B** the sampling of gaseous alkali compounds at combustion conditions is presented. Difficulties and solutions to certain problems experienced during measurements campaigns on CFB combustor are described.

In **Appendix C** the wet trapping measuring protocol is listed.

In **Appendix D** the results of alkali measurements using batch techniques are presented.

In **Appendix E** additional SEM/EDS scans presenting the composition of CFBC sampled material are presented. The material include various samples of the bed material, fly ash and filter ash from the reactor.

In **Appendix F** additional EDS scans of the composition of the kaolin samples having been in contact with gaseous KCl at reactor conditions are presented.

Chapter 2

Alkali metals behavior under combustion conditions

2.1 Alkali metals, S and Cl in straw and coal

Alkali metals together with Si, S and Cl play an important role in combustion systems because they are responsible for slagging and fouling, corrosion attack and deposits formations and in case of fluidized beds for bed agglomeration. Whenever analyzing the behavior of biofuels and coal during combustion process one has to focus first on the elemental composition of the fuels itself. The way how the particular elements are bound in the structure of the fuel and how they can be released during combustion conditions should be investigated. Coal and biomass, especially herbaceous high alkali biofuels differ substantially.

In coal, alkali metals are believed to be bound with organic compounds as cations associated with carboxylic acids or as inorganic compounds. In the form of the inorganics they may exist as simple soluble salts or to be associated with silicates (crystalline). In the form of silicates they are non-water soluble [Raask, 1985; Hald, 1994]. According to Raask most of sodium in low rank coals is organically bound. In high rank coal sodium is rather found in the form of soluble salts. Moreover it is associated with alumino-silicates such as $Na_2O{\cdot}Al_2O_3{\cdot}[SiO_2]_6$. Potassium occurs mostly in the form of alumino silicates [Huffaman et al., 1990] [Raask, 1985] namely $K_2O{\cdot}[Al_2O_3]_3{\cdot}[SiO_2]_6{\cdot}[H_2O]$ and $K_2O{\cdot}Al_2O_3{\cdot}[SiO_2]_6$ and hence it is not easily released to the gas phase during thermal conversion processes.

It was suggested that part of the alkalis in the coal is present in the form of

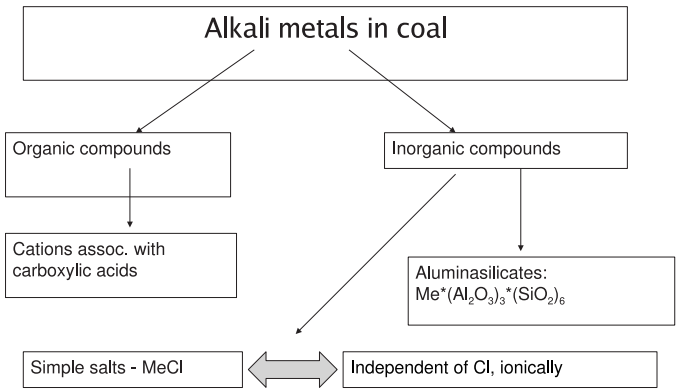


Figure 2.1: Alkali metals in coal

chloride mainly NaCl in the pores of coal [Gottwald et al., 2001]. For a part of sodium not bound with alumino-silicates there is a discussion whether it is present together with Cl and in a form of water soluble, easily released NaCl [Raask, 1985] or it is independent of Cl and linked ionically to the coal surface [Manzoori and Agarwal, 1992]. The independent Na, Cl binding was suggested by some researchers because the measurements reveal that chlorine as HCl(g) is released independently at much lower temperatures than sodium [Raask, 1985; Thompson and Argent, 1999]. On the other hand a mechanism was proposed by Hald [Hald, 1994], Manzoori [Manzoori and Agarwal, 1992] and Raask [Raask, 1985] in which alkali species during release as chlorides may react with i.e. kaolin present in coal or sulfur with liberation of HCl(g). A scheme of the distribution of alkali metals in coal is presented in figure 2.1. It has to be pointed out that in straw the sodium content in general is comparable with coal but it may contain about ten times more potassium. Alkalis, especially potassium, play an essential role in plant metabolism and is present in organic structures as simple, easy accessible inorganic compounds. Potassium is known to be an essential plant nutrient and plays an important role in osmotic processes inside plant cells. A schematic distribution of alkali metals in biomass is presented in figure 2.2.

Chemical fractionation experiments show that over 90% of the potassium in high alkali biofuels like straw is available as either water soluble or ion exchangeable material [Miles, 1996; Jenkins et al., 1996] and also in very interesting work by Zevenhoven et al. [Zevenhoven-Onderwater et al., 2001]. On the contrary the sodium content in biomass is much lower than potassium. It has been suggested [Wornat et al., 1995] that because of the high level of oxygen in biomass, K and Na are bound with the oxygen containing functionalities within

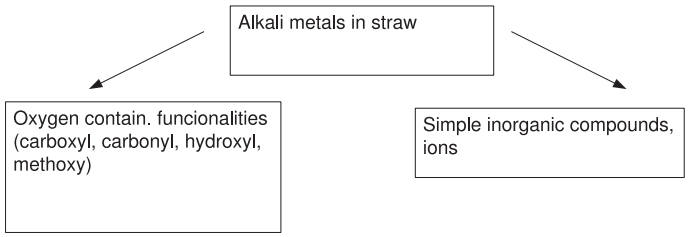


Figure 2.2: Alkali metals in straw

the organic matrix so the vaporization behavior of the alkali metals under combustion conditions will resemble that of low-rank coals. Potassium appearance as discrete KCl particles was also suggested. There is a general agreement that the organically bound potassium in biomass has a high mobility and can be easily released [Gottwald et al., 2002a].

Considering the mode of occurrence of chlorine and sulfur these elements occurs in biomass in anionic forms as plant nutrients. In coal most of the sulfur is present in the form of pyrite, and chlorine is present in the form of NaCl as discrete coal mineral particles or in ionic form in the coal structure [Raask, 1985; Mukherjee and Borthakur, 2003]. The content of silica in straw as well as in coal is relatively high. Silica compounds in high alkali biomass strengthen the original plant structure. In coal silica is bound in form of alumino-silicates.

2.2 The fate of alkali metals and interactions with S, Cl and Si

During the first stages of decomposition fuel particles dry and devolatilize. In this process the hydrocarbons, CO, CO_2 and H_2O are released from the fuel particle. In case of combustion in CFBC, the high heating rates promote rapid devolatilization. It was suggested that the alkali release in case of biomass may already start during the devolatilization of the biomass fuel at relatively low temperatures [Davidsson et al., 2002b]. The elemental pyrolysis studies done by them concerning birchwood material and wheat straw [Davidsson et al., 2002c] in a single particle pyrolysis reactor with a surface ionization (SI) detector reveal that alkali species are released around 400°C. Further increase in the temperature caused an increased amount of alkalis detected. The authors suggest that there are two different types of alkalis, namely the pyrolysis alkalis, organically bound in the structure of the fuel and the ash alkalis emitted in the higher temperature range. It was also observed that for the small fuel

samples these two stages of the detected release overlap because of the high heating rate in the reactor. Moreover Davidsson [Davidsson et al., 2002c] observed that small particles release more alkali per unit initial particles mass than large one during rapid pyrolysis of birchwood particles . According to literature [Jensen et al., 2000b] during pyrolysis experiments with relatively low heating rates of 50°C/s HCl was the main Cl containing component. Further on during char combustion KCl and KOH were released. Wornat and co-workers [Wornat et al., 1995] suggest that after the devolatilization process if the temperature is high enough several inorganic transformations take place. Especially the alkali metals will experience surface migration, vaporization to the gas phase or coalescence with incorporation into the fuel silicate structures or for coal into alumino-silicate structures [Jensen et al., 2000b]. Not all alkalis from high alkali biomass are released to the gas phase. It was observed by many researchers [Miles et al., 1996; Baxter et al., 1998;
Olsson et al., 1997; Olsson et al., 1998; Gottwald et al., 2002a] that Cl acts as a shuttle in transporting potassium from the fuel structure outside. It is believed that Cl is more responsible for the amount of alkali vaporized than the alkali concentration in fuel itself [Baxter et al., 1998; Kaufmann, 1997]. Depending on the conditions in a reactor (reducing, oxidizing environment) the alkalis can be released in the form of chlorides, hydroxides, sulphates [Gabra et al., 2001]. Potassium chloride is among the most stable, high-temperature, gas-phase alkali containing species.

According to Hald [1994] the gaseous alkali metal content increases with:

- increasing temperature
- decreasing pressure
- increasing chlorine content in the fuel
- decreasing sulfur content in the fuel if the conditions are oxidizing

A complete mechanism in a batch pyrolysis reactor was suggested for Cl and K release from straw [Jensen et al., 2000b]. They observed that in the temperature range of 200-400°C the organic matrix of the fuel was decomposed and suggested that in this temperature range most of Cl and K was transferred from the fuel structure to a liquid tar phase. Also, substantial HCl(g) release in this temperature range was measured. Potassium is expected to be present in the form of condensed KCl and K_2CO_3 and to be built in the char matrix structure. It was observed that release of HCl from coal similarly to biomass starts at about 200°C with visible increase between 300°C and 400°C and is finished at about 600°C [Schoen, 1956; Edgecombe, 1956]. At 400-700° Jensen and co-workers [Jensen et al., 2000b] did not find significant amounts

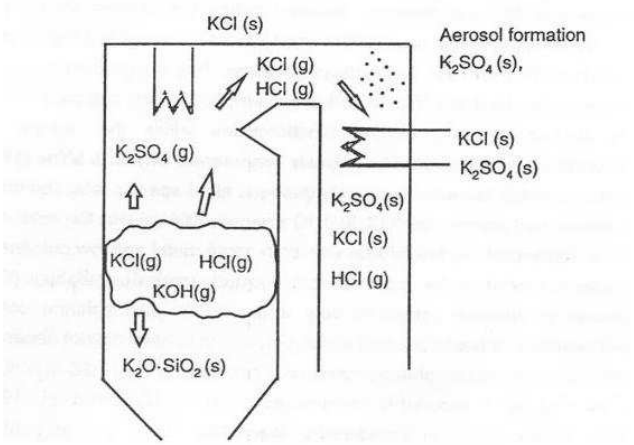


Figure 2.3: Path of potassium within combustion systems [adapted from Nielsen, 1998]

of K or Cl released to the gas phase. Opposite to Davidsson and co-workers [Davidsson et al., 2002b; Davidsson et al., 2002a; Davidsson et al., 2002c] others [Jensen et al., 2000b] did not observe significant release of potassium below 700°C. In the temperature range of 700-830°C all potassium evaporates in the form of KCl, whereas the rest of potassium was suggested to react with silicon to form potassium silicates, in the higher temperature range between 830-1000°C decomposition of K_2CO_3 took place and potassium was released as KOH or free K atoms. Above that range it was suggested that potassium is supposed to be released from the char matrix and the potassium silicates. A schematic distribution of potassium within combustion systems is presented in figure 2.3
The alkali metal release during the combustion of several biomass/coal blends was investigated by Dayton [Dayton et al., 1999a; Dayton et al., 1999b] in a high-temperature alumina-tube flow reactor. The sampling was done using a direct sampling, molecular beam mass spectrometer (MBMS), it revealed the higher emissions of gaseous HCl as compared to the combustion of pure fuels itself, on the contrary the emissions of KCl(g) and NaCl(g) decreased during co-combustion. Also Spliethoff and co-workers [Spliethoff et al., 2001] reported higher HCl emissions during co-firing of straw and coal in a FB boiler with a straw thermal input of 60%. The experimental findings [Dayton et al., 1999a] were compared with chemical equilibrium calculations with good agreement. The authors suggest a mechanism responsible for the decrease in the alkalis emissions namely by transformation of alkalis into condensed forms to Sanidine ($KAlSi_3O_8$) and Albite ($NaAlSi_3O_8$) minerals. The main part of sulfur both in coal and biomass is released to the gas phase in the form of SO_2, but it is

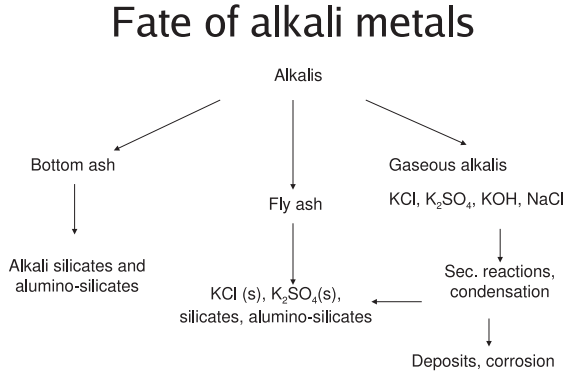


Figure 2.4: Fate of alkali metals in combustion systems

favorable that SO_2 will react with KCl to form K_2SO_4. The mechanism from one point of view may help to bind SO_2 and lower SO_2 emissions but from another alkali sulphates are responsible together with alkali chlorides for heavy deposits formation on the heat exchanger surfaces. For coal there was no significant loss of alkalis below 800°C [Raask, 1985]. Potassium is present in coal mainly as alumino-silicates. The potassium connected to alumino-silicates is usually stable.

At normal CFB combustor temperatures in the range 800°C-900°C the alkali compounds are distributed between the bottom ash, alkali metals in the fly ash particles and the gaseous alkali metal compounds. Due to interactions with SiO_2 and Al_2O_3 part of the alkalis in the fuel convert into silicates and alumino-silicates. In this form they are not available for vaporization [Wornat et al., 1995] and stay bound into bottom and fly ash particles [Chirone et al., 2000].

A schematic distribution of alkali metals within combustion systems is presented in figure 2.4. During coal and straw co-combustion it is likely that more alkalis are recombined in the alumino-silicates structures. If there is silica present in the system, which is the case during biomass combustion, the alkali metals in the form of oxides, hydroxides or metalo-organic compounds will form low melting eutectics with silicates [Miles et al., 1996]. Silica has a relatively high melting temperature of 1700°C but the melting point of mixtures with the main component of biomass ashes, potassium oxide, in the ratio 32% K_2O and 68% SiO_2 lower this temperature to 769°C. According to Wei and coworkers [Wei et al., 2002] potassium is combined with alumino-silicates from the coal to form $KAlSi_2O_6$[s] solid mineral, which at combustion temperatures

does not take part in the deposition process on the furnace inner surfaces. On the contrary when the share of straw increases the alkalis are supposed to react with the simple silica compounds present in the biomass fuel particle itself which result in formation of $K_2Si_4O_9$[liq], which with other alkali-silica compounds have the tendency to produce a mixture of low meting eutectics and are responsible for sticky deposits and bed agglomeration. According to Lin [Lin et al., 2003] potassium was found to be the most responsible for causing agglomeration and in the end defluidization. The molten ash coat the surfaces of the bed material, promoting agglomeration and defluidization in FBC. Thermodynamic equilibrium calculations have been performed to identify the stable silica, potassium, chlorine and sulfur species, the potassium silicates were found to be the main form present in the bed. This was confirmed with the experiments [Jensen et al., 1997]. During combustion of straw, potassium is the main alkali compound in the operation temperatures for CFBC that will be released to the gas phase in the form of KCl and KOH and subsequently will react with SO_2 present in the gas phase to K_2SO_4.

In coal power plants alkali salts in flue gases can be very harmful for turbomachinery. In most of the conditions however, a significant amount of alkali vapors will be converted into sulfates. Depending on the conditions, the sulfate can condense on fly ash particles or nucleate in the form of an aerosol [Scandrett and Clift, 1984]. According to Hald [Hald, 1994] the gaseous alkalis in contact with the colder heat exchanger surfaces will condense. The condensation phenomena may already appear on the fly ash particles occurring together with the reactions with silica compounds. Moreover condensation of the pure alkali metals particles in the gas phase and subsequent deposition is also possible. Because K_2SO_4 has a higher melting point than KCl it is prone to condensation and deposition at already high temperatures. There is a ongoing discussion [Nielsen et al., 2000b; Nielsen et al., 2000a; Nielsen, 1998] whether the sulfation reaction with KCl and SO_2 occur already in the gas phase or after condensation in the molten solid phase. Investigation performed by Nielsen and co-workers [Nielsen et al., 2000b; Nielsen et al., 2000a; Nielsen, 1998] and others [Baxter et al., 1998; Baxter, 1993], Andersen [Andersen, 1998] based on observations at different combustion units indicate that the deposits formation process for KCl and K_2SO_4compounds is mainly characterized by condensation and thermophoresis phenomena which form the first sticky, inner layer of the deposits. The outer deposit layer is dominated by potassium, silicon and calcium and builds up mainly by inertial impaction phenomena and consists mainly of the individual ash particles. Volatile sodium was observed to be released in some part as NaCl(g) and NaOH(g); the non-volatile part is combined with ash components [Wei et al., 2002]. Ash deposition and alkali vapor condensation were studied during CFB combustion of forest residue in a 35 MW

co-generation plant [Valmari et al., 1999b]. It was observed that the deposition mechanisms differ depending on the size of ash particles. For coarse ash particles deposition rate was observed to be largely due to large inertial and turbulent impaction and extensive deposition was observed. On the other hand for submicron particles thermophoresis and diffusion were the main mechanisms responsible for deposition. Thermophoresis and diffusion are not so effective as direct impaction so the deposition rate for submicron particles was smaller even though their efficiency to stick to boiler inner surfaces is high [Hansen et al., 1999]. It was pointed out that submicron particles creating a sticky layer of deposits may attract coarse ash particles retention on the deposit layer. A theoretical analysis indicates that gas to particle conversion occurs during the cooling of the flue gas by the homogeneous nucleation of K_2SO_4 particles, which act as condensation nuclei for the subsequent condensation of KCl [Christensen et al., 1998].

A model for conversion of gaseous AOH and ACl (where A stands for alkali like K or/and Na) to alkali sulfates was developed [Glarborg and Marshall, 2005]. The model relies on a detailed chemical kinetic model for the high-temperature gas-phase interactions between alkali metals, the O/H radical pool, and chlorine/sulfur species. Particular attention is paid to alkali hydrogen sulfates and alkali oxysulfur chlorides as potential gas-phase precursors of A_2SO_4. Sulfation is initiated by oxidation of SO_2 to SO_3. According to the model, SO_3 subsequently recombines with alkali hydroxide or alkali chloride to form an alkali hydrogen sulfate or an alkali oxysulfur chloride. The calculations reveal these compounds to be stable enough in the gas phase to work as precursors for formation of alkali sulfates. Sulfation is completed by a number of shuffle reactions, which are all expected to be fast, although they involve stable molecules. Sulfation of KCl was studied in the gas and molten phase in a laminar entrained flow reactor [Iisa et al., 1999]. The experiments were performed at 900-1100°C. Small particles of KCl were partially evaporated and allowed to react with SO_2. The results suggest that the most of KCl sulfation will take place in gas phase. The conversion in the condensed phase will be very limited.

2.3 Possible alkali getters

Many possible alkali getters are reported in literature. The choice for a proper sorbing material is not always straightforward and should be done together with analysis of the combustion system and fuel itself. But in general desired characteristics can be pointed out. A potential sorbent should be characterized by [Punjak et al., 1989]:

- high temperature stability
- rapid rate of adsorption
- high loading capacity
- transformation of alkali compounds into a less corrosive form
- irreversible adsorption to prevent the release of adsorbed alkali during process fluctuations
- being cheap

Mclaughin [McLaughin, 1990] carried out a screening study for candidate materials and used simultaneous thermal analysis (STA) technique to divide the investigated materials as non-getters and getters. The ones that did not display an interaction between the minerals and the NaCl salt were classified as non-getters, these were as follows:

- α-Alumina (αAl_2O_3)
- γ-Alumina (γAl_2O_3)
- Andalusite (Al_2SiO_5)
- Celestite ($SrSO_4$)
- Kyanite (Al_2SiO_5)
- Silicon Carbide (SiC)
- Silimanite (Al_2SiO_5)

Materials which exhibited significant interaction with NaCl upon heating were classified as possible getters, these were:

- Attapulgite (magnesium-alumina-silicate)
- Kaolinite ($Al_2Si_2O_5(OH)_4$)
- Bauxite (Al_2O_3)
- Barytes ($BaSO_4$)
- Calcium Montmorillonite (Fullers Earth, complex formula of multiple elements, smectide group)
- diatomaceous earth (shells of phytoplankton)
- Emathlite (70% SiO_2, 10% Al_2O_3; 5% MgO, Fe_2O_3, TiO_2, CaO, K_2O, Na_2O)

- Pumice (extrusive volcanic rock)

- Pyrophillite ($Al_2Si_2O_5(OH)$)

Most of the possible additives are based on Al-Si system because aluminosilicates are able to bind alkalis in their structure [Steenari, 1998]. Al-Si based getters were reported [Ohmann and Nordin, 2000], where kaolin was found to be an effective one [Gottwald et al., 2001] in removing alkalis from biomass combustion systems. Apart from the Al-Si based getters there are a number of experimental data reported with dolomite and limestone as additives [Coda et al., 2001]. Ohman and co-workers [Ohmann and Nordin, 2000] tried to investigate bed agglomeration phenomena during fluidized bed combustion of biomass fuels and to find a possible prevention method. By adding kaolin up to an amount of 10% w/w of the total amount of the bed they managed to increase the initial bed agglomeration temperature about 150°C. Steenari [Steenari, 1998] reported kaolin to be effective in absorbing and reacting with potassium compounds from straw. The reaction paths were influenced by particle size, temperature and gas composition. Moreover, kaolin was found to be more effective than dolomite. Punjak and co-workers [Punjak et al., 1989] in their earlier study with adsorption of NaCl proved that kaolinite is a very effective sorbent, however the kinetics of adsorption were found to depend on the gaseous atmosphere. They described the process in a typical atmosphere as a combination of adsorption and chemical reaction influenced by the intraphase transport of alkali inside the porous kaolinite. Besides kaolinite, emathlite and bauxite were tested. Bauxite was observed to have the highest initial capture rate but kaolinite had the highest capacity.

An important difference in the sorption characteristics of the kaolinite, emathlite and bauxite is the reversibility of the adsorption process [Punjak et al., 1989; Scandrett and Clift, 1984]. It was found that after saturation, no desorption was observed for kaolinite and emathlite, but bauxite lost approximately 10% of its total weight gain. It was suggested that not the same mechanism is responsible for the adsorption for the three sorbents. Literature finding concerning Emathlite, Diatomaceous Earth and Kaolinite indicating the maximum sorbing capacity are shown in table 2.1. Investigation of the saturated kaolinite by means of XRD reveals that it contains primarily nephelite and carnegieite which are sodium aluminosilicates polymorphs with the chemical formula $Na_2O \cdot Al_2O_3 \cdot 2SiO_2$. Nephelite has a high melting point at 1526^oC.

Besides clay based additives bauxite is very often mentioned in literature as possible alkali getter [Turn et al., 2001, Dou et al., 2003]. However in case of bauxite the physical adsorption phenomenon is partly responsible for alkali uptake [Turn et al., 1998a]. The XRD spectrum for as-received bauxite shows the

Table 2.1: Amount of alkali metals absorbed per g of sorbent [Turn et al., 1998a]

	Absorbed amount in mg/g of the getter
Emathlite	150-190
Diatomaceous	18
Kaolinite	max. 266

presence of α-quartz, corundum and hematite. The XRD results on fully saturated bauxite indicate the formation of nephelite and carnegieite produced by a reaction similar to that in kaolinite but the amount of silica in bauxite is not sufficient to account for all the adsorbed alkali [Turn et al., 1998a]. Apparently, the rest of the alkali is present as glassy products or physisorbed chloride not detectable by XRD. The authors tested straw of various types with respect to the formation of crystalline compounds and high temperature reactions in ash, as well as sintering and melting behavior in a fluidized bed gasification. The major part of potassium was observed to contribute together with silica to low ash melting point (potassium silicates). The authors found a high content of potassium but also high levels of silicon were found in straw samples. Ash from rape straw was shown to be mainly crystalline, whereas ash produced from wheat and barley contained significant amounts of amorphous material. The high amount of amorphous material was related to a low melting temperature,as the specific combination of Si and K resulted in formation silicate-rich amorphous ash even at 550°C. They observed that reducing conditions intensified reactions between kaolin and potassium species.

Most material characterized as non-getters are a modification of $Al_2O_3{\cdot}SiO_2$. But the difference is that the charge on the lattice is balanced and does not contain any interlayer cations, nor any water or hydroxyl groups. The tight crystal structure means that the silica lattice is far less accessible to attack by water than more open layered structures found in the getters [McLaughin, 1990]. Six commercially available materials have been tested as granular sorbents to be used in granular-bed filters for the removal of gaseous alkali metal compounds from the hot (1073 to 1153 K) flue gas of pressurized fluidized-bed combustors [Lee and Johnson, 1980]. Moreover, by the same authors tests were performed in a laboratory fixed bed combustor/alkali sorbing facility using PFBC gases [Lee et al., 1992]. The authors observed that sodium was the major alkali-vapor species present in the flue gas of coal combustion. The main finding from this investigation was that Diatomaceous Earth (DE) and activated bauxite were the two most promising sorbents. Clays are known to be effective in alkali binding into their aluminum silicates structure. DE is a sedimentary rock of

marine or lacustrine deposition. Chemically, it consists primarily of silicon dioxide and various amounts of impurities such as clay, carbonaceous matter, iron oxide, sand, etc. Alkalis react mainly with silica but may react also with the impurities there are clay minerals. The retention of gaseous alkali by DE was found to be attributed to chemical reaction with alkali metal compounds to form water-insoluble alkali metal silicates. In contrast, activated bauxite primarily captures the gaseous alkali metal chlorides by an adsorption mechanism. The sorbing capabilities for these two sorbents were found to be related to their internal surfaces areas and to increase with temperature for DE and decrease with temperature for bauxite [Lee and Johnson, 1980].

The kinetics and mechanism of adsorption of NaCl vapor on kaolinite were studied at 800°C under both nitrogen and simulated flue gas (SFG) atmospheres [Punjak and Shadman, 1988]. The authors observed that under nitrogen atmosphere both chlorine and sodium were retained by the sorbent. However, under the simulated flue gas conditions, only sodium was retained. In both cases the adsorption was irreversible. Comparison of data for adsorption experiments under SFG and nitrogen atmosphere shows a significant effect of gas composition on the adsorption. It was suggested that the effect of water and not oxygen is of prime importance. For example, the alkali-loading capacity of kaolinite under SFG was higher than that under N_2. From the research it appears that the adsorbed NaCl reacts with kaolinite when water is present to form nephelite and volatile HCl. The kinetics of adsorption was mainly influenced by two types of diffusion:

- diffusion through the adsorbent pores where adsorption is simultaneously taking place
- diffusion through a saturated layer of sorbent formed on the outside of the sorbent particles

If there would be only physical adsorption a model compounds like KCl would be found only on the surface of getter particle. Physical adsorption is characterized by van der Waals or dispersion forces which are weak intermolecular interactions. Physical adsorption is generally reversible if the vapor pressure of the adsorbate is reduced. Moreover it is known that the system reaches equilibrium very fast. Due to the long range nature of the attractive forces, physical adsorption may form several layers of adsorbed gas molecules on the solid surfaces. As the number of layers increases, the adsorption process approaches one of condensation [Fisher, 1977]. On the other hand chemisorptive interactions between the solid surface and the adsorbed molecule are much stronger. Chemisorption is mainly responsible for gas-solid reactions and catalysis with chemical reaction involved and chemisorption can only occur as monolayer. As a result, chemisorption may be slow and display rate behavior characteristic of

processes possessing an activation energy. Gases which have been chemisorbed may be difficult to remove and may leave the surface altered [Turn et al., 1998b]. In Chapter 5 the fundamental studies concerning interactions between gaseous potassium chloride and kaolin are presented and discussed. The research reveals interesting interactions and dependencies for this most promising alkali sorbing additive. Because of that the following paragraph presents theoretical information about kaolin.

2.3.1 Kaolin

The major constituent of kaolin is the clay mineral kaolinite, $Al_2Si_2O_5(OH)_4$. This mineral has a layered structure that undergoes several transformations during heating (figure 2.5). Steenari and co-workers [Steenari, 1998] presents a whole mechanism of kaolin transformation. At 100-200°C adsorbed water is being released and between 400°C and 600°C hydroxyl groups located between silicates layer leave the structure. Without water an amorphous mixture of SiO_2 and Al_2O_3 called meta-kaolinite remains. Metakaolinite can be called the dehydration product of kaolinite. New crystalline products start to form when the temperature exceeds 900°C. Although all the interlayer hydroxy particles leave the structure of kaolin about 450°C. Clay may retain hydroxyl groups up to 900°C, above that temperature the lattice collapses. In the absence of water vapor in the gas stream, the residual hydroxyl groups in the structure of the clay minerals may be sufficient for the formation of alkali alumino-silicates. Drury [Drury et al., 1962; McLaughin, 1990] noted that in the presence of water vapor at high temperature, hydroxyl groups are readilly regenerated into the silica lattice through the reaction:

$$\equiv\mathbf{Si\text{-}O\text{-}Si}\equiv\mathbf{(s)} + \mathbf{H_2O(g)} \Longleftrightarrow \mathbf{2}\equiv\mathbf{Si\text{-}OH(s)}$$

The addition of water to the carrier gas may re-hydroxylate the silica lattice, making it more accessible to alkali and thus increasing the uptake of straw originating alkalis [Mulik et al., 1983; McLaughin, 1990]. The potential sorbing reaction between kaolin and for instance gaseous KCl can be summarized within two steps as below.

$$2KCl_{(g)} + A \rightleftharpoons A^*2KCl \text{ slow (rate limiting) (1)}$$

$$A^*2KCl + H_2O_{(g)} \rightleftharpoons K_2O^*A + 2HCl_{(g)} \text{ rapid (2)}$$

Where A stands for a vacant active site on meta-kaolin surface and can be expanded to:

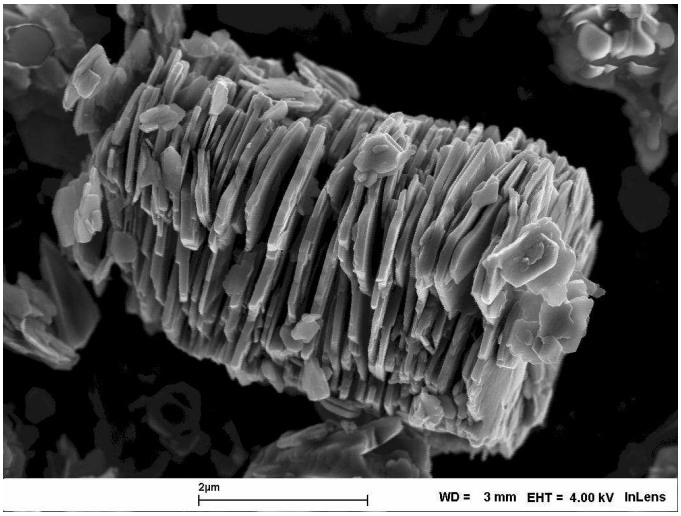


Figure 2.5: Kaolin particle, magnification 15k

$K_2O*A = K_2O*Al_2O_3*2SiO_2 = 2KAlSiO_4$

The changes in ash melting point after kaolin addition can be explained by the adsorption of potassium-containing species on the the surfaces of kaolinite and meta-kaolinite particles. This is followed by diffusion into and reaction with the aluminum silicate structure. Two crystalline reaction products were found, hexagonal $KAlSiO_4$ (kalsilite) and $KAlSi_2O_6$ (leucite) associated with melting temperatures of 1165-1250°C for the ash-mixtures. The melting temperature increases as the alumina content is increased [Turn et al., 1998b]. The molar ratio of Si to Al is 1 for kalsilite and 2 for leucite which indicates that kalsilite is a more direct product from meta-kaolinite than leucite which demands the incorporation of one more silica unit.

2.3.2 Co-combustion with coal and sequestering of alkalis

Alkali capture by natural compounds from coal like sulfur and alumino-silicates was reported [Aho and Ferrer, 2004, Furimsky and Zheng, 2003] and moreover [Haÿrinen et al., 2004; Coda et al., 2001]. Experiments with a pilot scale CFB reactor with MBM blends and coal were performed. Chlorine concentrations in deposits could be reduced through increase of SO_2 concentrations in the surrounding gas. Alkali sequestering was reported to be promoted through sulfation with release of HCl. Alkalis were also trapped by aluminum sili-

cates. The authors report that binding of alkali species by aluminosilicates should be possible under fluidized bed conditions where the flue gas phase residence time is 2-3s. Such reactions can occur simultaneously with sulfation. The presence of aluminum rich phases in the fly ash leads to less sticky ash on heat transfer surfaces. Similar findings are presented by other researchers [Dayton et al., 1999a]. As a drawback, they confirmed that co-firing promotes release of gaseous HCl. Experiments were performed with a high-temperature alumina-tube reactor. During combustion of Imperial wheat straw blends, more HCl (g) was detected than expected. Blending coal with the high-chlorine containing wheat straws seems to yield more HCl vapor than expected based on the linear combination of the amount of HCl released during combustion of the pure fuel separately. On the other hand the amount of KCl(g) was less than expected. It was reported that co-combustion of different biomass types may result in useful interactions to decrease or totally inhibit Cl deposition and bed agglomeration[Aho and Ferrer, 2004]. Co-combustion tests of pulp sludge with ash composition similar to kaolin were done together with biomass. The main finding confirmed that aluminum and silicon concentrations in the inorganic part should be maximal and other elements minimal to get the desired effect. Experiments were carried out in a CFB reactor with MBM blended with three types of coal. MBM is characterized by a high Cl content and coal contains protective elements like Al, Si and S. Alkali aluminosilicate formation was the main alkali sequestration path, dominating over sulfation. Presence of sulfur did not prevent alkali chloride deposition, underlining the weakness of the sulfation effect [Aho and Ferrer, 2005]. There is ongoing discussion whether the sulfur content is the most important for sequestering of Cl during biomass combustion [Robinson et al., 2002]. The authors of this paper claim that the primary interaction between the biomass and coal during co-firing is the reaction of the sulfur from the coal with the alkali species from the biomass. The interaction between alkali chlorides from straw with sulfur from coal was said to reduce the stickiness of fly ash and deposit material and hence reduce the deposition characteristics relative to the unblended straw. Moreover apart from the fly ash interaction sulfation of alkali chlorides within deposits is said to be the major type of interactions within deposits. Coda and co-workers [Coda et al., 2001] for bubbling fluidized bed experiments observed that when kaolin was added to the system gaseous alkali chlorides converted to alkali aluminum silicates in the form of the coarse ash and HCl was released. Release of gaseous HCl on the other hand is considered to be problematic as well because of strongly corroding properties of this gas. Al-containing additives increased HCl formation and decreased Cl concentration in the fly ash. In the case of Al-Si based additives, evidence was found for the formation of alkali alumina silicates from alkali chlorides. The aluminum silicates were transferred mainly to the coarse fly ash fraction.

2.4 Conclusions and research requirements

There is a need for more detailed investigation of the behavior of straw in CFB combustors. There is a scarcity of data available on coal-straw co-combustion in CFB systems. Blending may play an important role from operational and environmental point of view in future straw utilization. The knowledge how to handle difficult, renewable fuels would be then very important.

There is a need to have a deeper look alumina-silicates minerals present naturally in coal and represented by kaolin and their abilities to capture the gaseous alkali metals originating from straw. The information which mechanisms are responsible for the capture would provide more knowledge about the combustion processes resulting in the lower operational costs for power utilities on a longer time scale.

Chapter 3

Experimental investigation of alkali metal release within CFBC systems

3.1 Introduction - investigation of alkali metals in combustion systems

Alkalis, especially potassium, play an essential role in plant metabolism and are present in organic structures as simple, easily accessible and mobile inorganic compounds. Potassium plays an important role in osmotic processes inside plant cells. Wornat and co-workers [Wornat et al., 1995] suggest that because of the high level of oxygen in biomass, K and Na are associated with the oxygen-containing functionalities within the organic matrix, so the vaporization behavior of the alkali metals under combustion conditions will resemble that of low-rank coals. Potassium appearance as discrete KCl particles was also suggested. There is a general agreement that the metabolically active potassium in biomass has high mobility and can readily be released.

Biofuels such as straw are characterized with extremely high alkali metals content, which in combination with certain ratios of Cl and Si leads to corrosion and deposits formation and in case of fluidized bed technology defluidization problems. High-temperature corrosion associated with biomass combustion is often being reported at power plants using biofuels, especially high chlorine and alkaline straw [Baxter et al., 1998; Sander and Henriksen, 2000]. Deposit formation on relatively cold heat exchanging surfaces is another widely recognized problem. The sticky ash particles deposit on the heat transfer surfaces and continue to build-up preventing optimal heat transfer, hindering the flue gas flow and in extreme cases with high growing rate can lead to unscheduled shutdowns [Miles et al., 1996]. Locally high concentrations of chlorine from chloride

deposits were observed to substantially increase the corrosion rates of the heat exchanging surfaces [John, 1984]. Therefore extensive research is needed to reduce the operational costs and improve the reliability of the existing and newly built power plants. To prevent above-mentioned operational problems, a clear understanding of the complex behavior of alkali metals during combustion is needed. Many factors remain still unknown.

The classical, batch method for alkali sampling is so called wet chemical method [Hald, 1994]. In this method gaseous alkali metals are substracted from the system. The concentration in flue gases is then calculate by means of relating together amount of the gas and alkali sampled. The wet chemical method is very prone to errors and difficult to apply. Substantial differences may arise between the measurements in the same experimental conditions. The wet trapping method has been applied but because of the difficulties with assessing the amount of alkali compounds measured the method was rejected. Some experimental data are presented in **Appendix D** together with accompanying discussion.

Currently several modern techniques exist whereby alkali compounds can be sampled directly from the flue gases on-line and even in-situ. In recent years, three have been employed increasingly, namely ELIF, SI, and PEARLS. The ELIF technique is based on excimer laser induced fragmentation fluorescence and this laser technique is sensitive essentially only to gas-phase species of sodium and potassium [Gottwald et al., 2001; Gottwald et al., 2002b]. Plasma excited alkali resonance line spectroscopy (PEARLS) is based on dissociation of alkali compounds by mixing a sample gas with a nitrogen plasma jet generated with a non-transferred dc plasma torch. Surface Ionization (SI) alkali detector is based on phenomena of ionization of alkali metals upon desorption from a hot Pt surface. SI detects alkali both in the gas phase and on aerosol particles. PEARLS, apart from measuring gaseous alkalis can also detect also particles below 10μm. Surface ionization (SI) and PEARLS techniques were described in detail elsewhere [Haÿrinen et al., 2004; Tran et al., 2005].

The objective of this work was to investigate the influence of fuel composition and combustion conditions on the release of the alkali compounds to the gas phase during combustion and co-combustion of high alkali straw with coal at different ratios based on energy basis in a Circulating Fluidized Bed Combustor (CFBC).

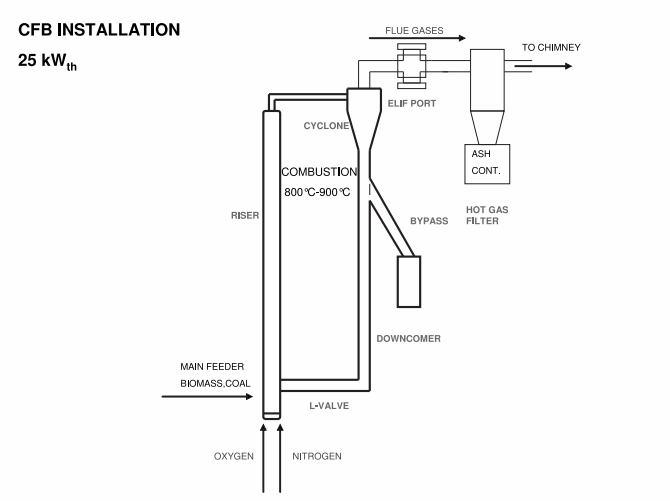


Figure 3.1: Circulating Fluidized Bed Combustor at Section Energy Technology, TU Delft

3.2 Combustion facility - CFB reactor

The CFB test rig (Fig. 3.1, Fig. 3.2) available within TU Delft is 5 m high with an inner riser diameter of 80 mm. The thermal output for the combustion experiments was about 25 kW and is operated atmospherically. The installation is started with an electrical preheating; the temperature within the system can be controlled. The average operational temperature is between 750°C to 850°C with a maximum level of 900°C. The reactor operates with standard silica sand as a bed material, with particle diameters between 0.3 – 0.6 mm. The installation is equipped with a screw-based feeding system that consists of three independently controlled screw feeders with variable feeding rates for different fuel/additives mixtures (upper part) and a main feeder that transports the mixture to the reactor (lower part). The installation is equipped with sampling ports at different heights of the riser and downcomer. Combustion experiments can be performed with variable fuel composition, feeding rates and feeding position. Further downstream, after the cyclone but before a hot gas filtering unit the installation has been equipped with an optical access point/optical port for ELIF measurements. The experiments were performed at 850°C as a mean temperature in the reactor and approximately 750°C at the ELIF port. Downstream of the optical port, the reactor is equipped with the hot gas filter installation based on four ceramic textile BWF candles and operating at 450°C on average.

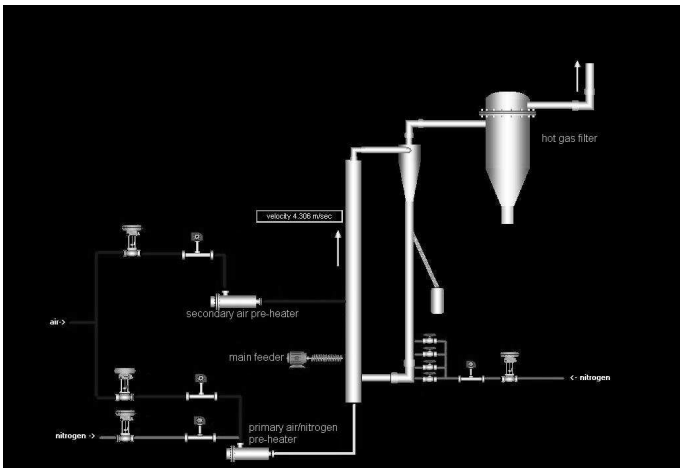


Figure 3.2: CFBC - P&ID

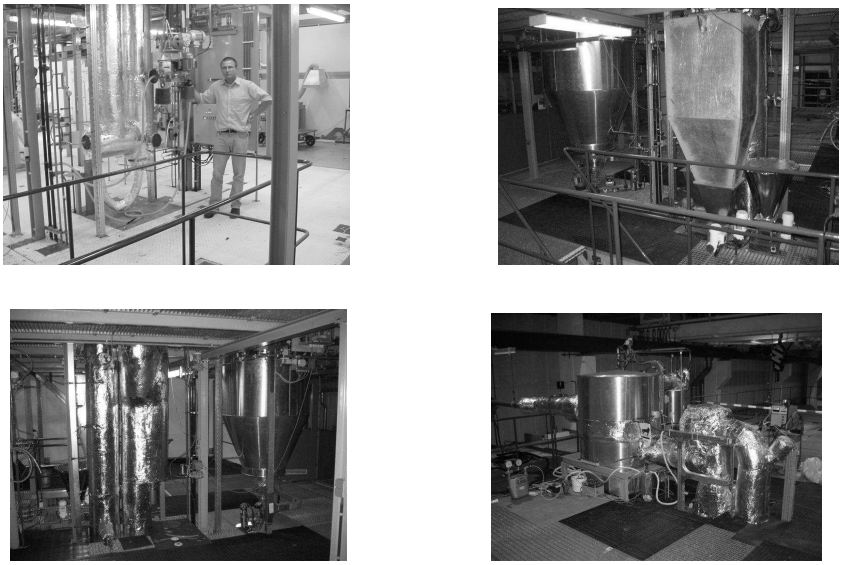


Figure 3.3: CFBC - different views, top right - feeding system, top left - fuel bunkers, bottom right - rear view, bottom left - top level with the laser ports

The main features of the installation are [Siedlecki, 2003]:

- insulated riser, cyclone, downcomer and L-valve;

- primary (fluidization) air and nitrogen preheater ($\Phi_{h,\,max}$ = 5.7 kW, $\Phi_{m,\,max}$ = 40 kg/h , T_{max} = 400°C);
- secondary air inlet and preheater ($\Phi_{h,\,max}$ = 3.7 kW, $\Phi_{m,\,max}$ = 18 kg/h, T_{max} = 400°C);
- automated control valves for air and nitrogen, operated from the control room;
- circulation nitrogen valve, with 4 admission points;
- separate sand, coal and biomass screw feeding systems, with common main screw feeder. A rotary valve device between the main screw feeder and the separate feeders should prevent the flue gases from escaping into the sand and fuel bunkers;
- two feeder connection points at different heights (one feeding point operated at a time);
- two access points for manual sand feed (one on the riser and one on the downcomer);
- hot gas filter of the BWF candle-type, with 4 candles. The filter is electrically heated and insulated to keep its temperature at a minimum of 350°C in order to prevent the condensation of water. At the bottom of the filter a solids removal system is present;
- electrical trace heating reactor preheat system ($\Phi_{h,\,max}$ = 14.8 kW);
- downcomer bypass pipe with bucket and valve;
- 7 thermocouples distributed over the riser, and single thermocouples installed in the downcomer, filter inlet and filter outlet. These thermocouples are monitored on-line during operation;
- 9 dp-cells installed to measure the pressure drop over the different parts of the installation, monitored on-line;
- advanced software for process operation, control and data acquisition;
- gas analysis equipment for on-line measurement of CO_2 (NDIR, range 0 – 20 vol%) , O_2 (paramagnetic, ranges 0 – 21 vol% and 0 – 25 vol%) and CO levels (NDIR, ranges 0 – 800 ppmv, 0 – 10000 ppmv, 0 – 10 vol%).
- Fourier Transfer Infra Red (FTIR) gas analyzers for measuring HCl - measurements not successful
- Infra Red SO_2 analyzer - measurements not fully successful

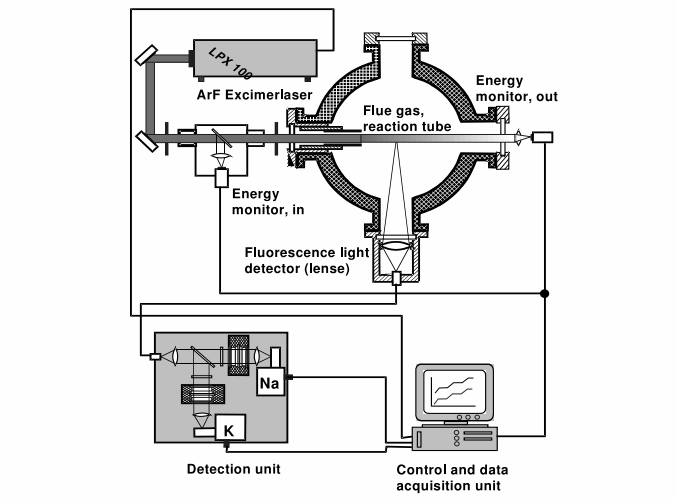


Figure 3.4: ELIF - measuring principles

3.3 Non-intrusive gaseous alkali metals measurements - ELIF technique

The ELIF method uses pulsed, ArF-excimer laser light at 193 nm to photodissociate alkali compounds and simultaneously excite electronically the alkali atoms formed. Fluorescence from the excited Na(3^2P) or K(4^2P) states can easily be detected in the visible region. For *in-situ* ELIF measurements, optical access windows in the flue gas pipe are required where the excitation light can enter the flue gas region and from which the fluorescence emission is collected and lead to a detector (photomultiplier, PMT) for continuous monitoring.

3.3.1 ELIF limitations and consideration of errors

Since the laser energy densities used are only a few mJ/cm^2, only gas-phase alkali is monitored. Also, because of the fixed excitation wavelength of 193 nm and the low energy used, only chloride and hydroxide can be detected with the present system. It has to be stressed that chlorides are definitely the main species under the conditions the measurements were done. Had there beenno chlorine in the system and/or the temperaturewere very high, above about 1400°C, hydroxides would play the role as well [Monkhouse and Glazer, 2006]. In order to detect sulfates, either a shorter wavelength (<190 nm) or a much higher (ca. x 100) energy density would be required [Gottwald et al., 2001;

Schurmann et al., 2001]. On the other hand, a higher energy density also leads to the vaporization of aerosol particles in the flue gas, so that the advantage of discrimination towards gas-phase alkali is lost.

The uncertainty in the measured alkali concentrations is composed of statistical variations and systematic errors. Statistical fluctuations (laser energy measurement, fluorescence detection) about a "true" value measured under constant conditions can be reduced by averaging over sufficient laser shots. In the case of very low signals, a compromise may have to be made between measurement precision and temporal resolution. In this work, averaging over 50 shots was judged to be sufficient, since the systematic errors in the total error are the dominant factors. Systematic errors are introduced through using supplementary data (calibration constant, quenching constants for individual collision partners (N2, O2 etc.), laser energy in the measurement volume) that are used for the calculation of the absolute alkali concentrations.

From the statistical and systematic errors, total error limits of around 25-30% of the absolute concentrations can be estimated. However, for alkali molecule concentrations above 20-25 ppm, a further error is introduced, since then enough alkali atoms are generated by photolysis to cause self-absorption effects. In this case, the fluorescence curve of growth for alkali atoms starts to deviate significantly from linearity (see paper of Chadwick et al. 1997).

3.3.2 Optical access

The set up for ELIF used for the measurements at the CFB combustor, is shown in Fig. 3.4. The optical access to the flue gas pipe consisted of four ports holding Suprasil quartz windows. The Suprasil quartz windows are essential for the laser access because of the short (UV) laser wavelength, but are also preferred for thermal stability. Therefore the detection windows were also made of this material. The windows were mounted in flanges of thermally/mechanically stable materials. The optical access port can withstand the actual operating conditions and the system is designed to minimize heat loss by the flanges. The Suprasil windows were flushed continuously with nitrogen, to keep them free of fly ash.

3.3.3 Laser excitation and fluorescence detection

Alkali compounds in the flue gas are photolyzed using laser energy densities of several mJ/cm^2 and with frequency of 6.4 Hz. Then ELIF signals are averaged over 50 shots and time resolution of 12 s is obtained. The laser energy entering and leaving the optical access ports is monitored constantly and

provides a measure of the effective beam transmission. The fluorescence from excited potassium and sodium atoms is detected by two separate photomultipliers. To reduce undesired radiation due e.g. to incandescence, atomic line filters 0.2 nm width/central wavelength 589 nm for sodium and 1nm/768 nm for potassium, respectively, are placed in front of the detectors. Unwanted emission is also suppressed by a time gate on the photomultipliers. The exchangeable neutral density filters prevent detector saturation at high alkali concentration levels and further suppress background radiation. In the set-up used in these experiments, an optical fiber cable was used to transmit the fluorescence light from the optical access to the detection system. The calibration of the system has been described in detail elsewhere [Gottwald et al., 2001; Schurmann et al., 2001]. The laser set-up build on the CFBC is shown on Fig. 3.5 and Fig. 3.6.

3.4 Experimental techniques

3.4.1 Fuels and CFBC tests

Special bio-fuels characterized by their very high alkali metal content were selected among others for this research. Four kinds of straw originating from Spain were used: HIAL 3 - Wheat Marius, HIAL 4 – Rape, HIAL 7 – Brasica Carinata, HIAL 9 – Maize. Together with these bio-fuels, Columbian hard coal was used in co-combustion experiments in order to investigate the synergetic effect of co-combustion on gas phase alkali content. The chemical composition of the fuels is given in table 3.1 and the ash composition in table 3.2. In order to better characterize the straw, the ratios of certain elements are given in table 3.3. For the selected fuels, K/Cl, 2K/S, K/Si and S/Cl ratios were of special interest. The ratios may determine the behavior of the fuels for combustion processes. The certain elements like potassium, silica, sulfur and chlorine and their ratios may give a clue to understanding the final composition of the bed material, fly ash and etc. The ratio will determine how alkali metals are sequestered in the system and what kind of final products can be expected. The synergy effect of some elements (for example potassium, alumina and silica) is expected to have huge impact on the final products and will be discussed further chapter 3 and 4. The fuel was cut and pelletized to prepare it for the screw feeding system. The average pellet size was 15 mm by 8 mm (Fig. 3.7). The coal was dried, crushed and sieved and the average size fraction used was 1-3 mm. The measurements were done at a reactor temperature of approximately 850°C, the temperature at the ELIF optical access point was no less than 750°C. Single tests were done for 750°C in the reactor. The combustion tests were done for 100% of every fuel and in the case of co-combustion for 80 % coal -20 % biomass and 50 % coal – 50 % biomass on an energy basis.

Table 3.1: Fuel composition (oxygen by difference) together with LHV

Fuel	HIAL3	HIAL4	HIAL7	HIAL9	COAL
LHV(exper.)	16,3MJ/kg	16,3MJ/kg	16,7 MJ/kg	16,4 MJ/kg	26.02 MJ/kg
Composition:	Wt %	Wt %	Wt %	Wt %	Wt %
Moisture	3.7	6.83	6.57	6.8	4.24
	Wt % dry	Wt % dry	Wt % dry	Wt % dry	Wt % dry
Ash	5.7	5	5.1	7.1	12.06
C	46	46	45	45	69.9
H	6.1	6.1	6	5.9	4.41
N	0.28	0.46	1.1	0.6	1.29
S	0.06	0.1	0.28	0.07	0.52
Cl	0.27	0.03	0.06	0.64	0.03

Table 3.2: Calculated ash composition of some elements in HIAL fuels and coal

	HIAL 3	HIAL 4	HIAL 7	HIAL 9	COAL
	% of Ash	% of Ash	% of Ash	% of Ash	% of Ash
SiO_2	64	9	2.5	33	60.6
Al_2O_3	0.3	2.3	0.3	3.7	20.6
Fe_2O_3	0.2	0.9	0.2	1.6	8.2
CaO	5.4	50	20	17	1.2
MgO	1.8	1.7	2.3	4.4	0.9
Na_2O	0.1	0.2	0.3	0.4	0.9
K_2O	17	12	40	22	4.1

Table 3.3: Molar ratios between problematic elements in HIAL fuels

	HIAL3	HIAL4	HIAL7	HIAL9
K/Cl	2.69	15.41	25.69	1.84
K/Si	0.34	1.74	20.36	0.86
S/Cl	0.25	3.69	5.16	0.12



Figure 3.5: ELIF laser installation build-on the CFBC (1)

3.4.2 Fly ash and bed material investigation with SEM/EDS

In order to get more information about the fate of alkali metals compounds in Circulating Fluidized Beds multiple samples of bed material and flying ash were collected (Table 3.4). The samples were then investigated with SEM/EDS technique. SEM/EDS technique is a modern technique for determining mor-

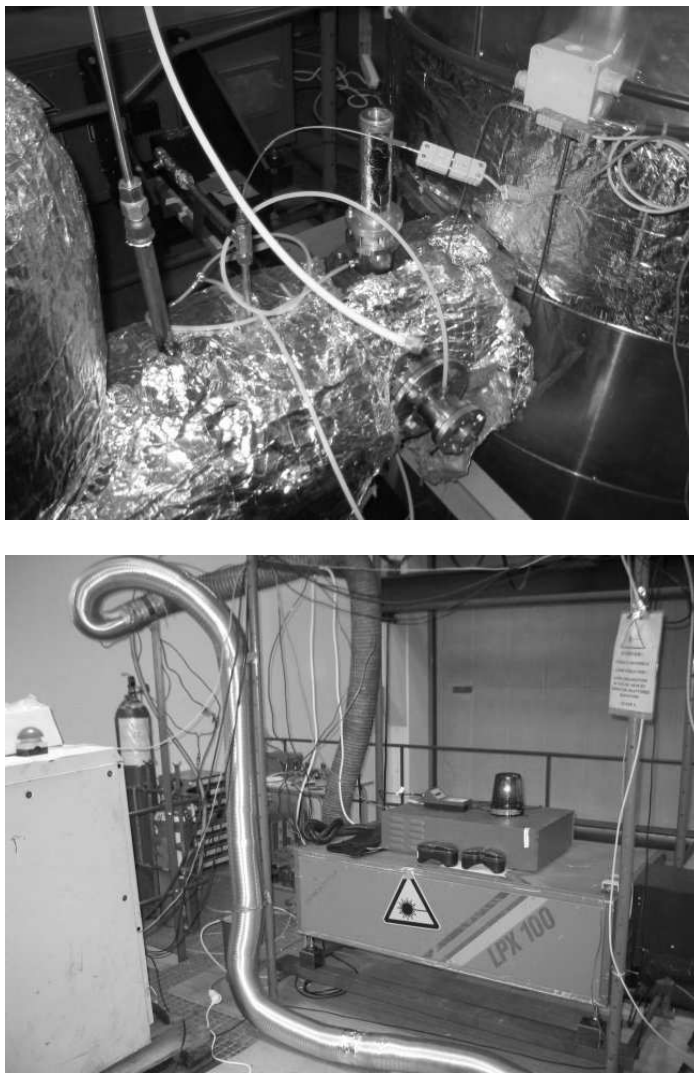


Figure 3.6: ELIF laser installation build-on the CFBC (2)

phology and composition of the investigated samples. It combines together Scanning Electron Microscopy (SEM) and Energy Dispersive Spectroscopy (EDS). In SEM systems electron beam is directed on the surface of the samples. Interaction with the sample creates emissions of electrons, using special detectors and electronic data acquisition systems an image of the surface is created as a result. Additionally SEM if coupled with a EDS detector information about



Figure 3.7: Four biomass fuels pelletized

elemental composition in form of spectra can be obtained.

The experimental data for combustion experiments applying the Delft CFB pilot scale test rig are presented in table 3.5.

3.5 Results

The results of the ELIF measurements are presented in table 3.6. The results for coal itself are all below ppm level. Results for the straw are two orders of

Table 3.4: Overview of the analyzed samples

Sample number	Type	Date	Fuel	Analysis	Remarks
1	bed mat.	05/05/04	coal	SEM/EDS	
2	bed mat.	05/05/04	coal	SEM/EDS	
3	fly ash	08/10/04	HIAL 9 – 100%	SEM/EDS	
4	filter ash	10/04/04	-	SEM/EDS	
5	clean sand	-	-	SEM/EDS	
6	filter ash	26/01/04	-	SEM/EDS	
7	filter ash	01/03/04	-	SEM/EDS	
8	fly ash	13/10/04	HIAL 9 – 50%	SEM/EDS	
9	FTIR port ash	03/02/04	HIAL 4 – 100%	SEM/EDS	
10	fly ash	03/02/05	HIAL 4 – 100%	SEM/EDS	

Table 3.5: Experimental data for the combustion experiments applying ELIF technique on the Delft CFB pilot scale test rig. The fuels ratio are based on the energy basis for the co-combustion tests biomass-coal. The flue gas composition before the ceramic filter. The velocity was calculated for conditions within the riser

Fuel	Fuel ratio	Exp. num.	air-main-supply	velocity	t.inlet-air	t_reactor	P.reactor	t.filter	O2	NO	CO	CO2	SO2
	% (en.basis)		kg/h	m/sec	deg.C	deg.C	bar	deg.C	vol%	vppm	vppm	vol%	vppm
coal	100	04_01	31.49	4.48	351	850	1.08	358	8.01	336	368	11.31	-
coal	100	04_02	31.52	4.49	352	750	1.08	358	6.03	140	777	13.33	-
HIAL 3	100	04_03	29.26	4.47	360	850	1.08	362	7.68	327	195	12.58	not det
HIAL 3	50	04_04	29.44	4.50	363	850	1.09	354	5.42	334	286	14.68	-
HIAL 9	100	04_05	28.75	4.37	364	850	1.08	374	6.16	238	1179	13.19	not det
HIAL 9	50	04_06	29.21	4.52	328	855	1.08	370	5.14	265	737	14.41	-
HIAL 4	100	04_07	30.05	4.47	360	850	1.11	350	6.64	281	310	14.63	not det
HIAL 4	50	04_08	29.66	4.38	368	850	1.15	350	6.38	373	190	13.72	-
HIAL 7	50	04_09	29.76	4.36	364	850	1.18	356	5.58	376	127	14.26	-
HIAL 7	100	04_10	31.46	4.53	369	900	1.18	354	4.31	304	435	15.90	not det
HIAL 3	20	04_11	29.51	4.47	360	890	1.13	351	4.70	296	305	13.63	171
HIAL 4	20	04_12	29.24	4.38	360	870	1.12	350	4.16	266	886	14.26	145
HIAL 7	20	04_13	29.13	4.37	360	875	1.13	359	3.20	284	417	14.87	-
HIAL 9	20	04_14	29.34	4.21	360	870	1.13	367	7.68	212	283	10.40	191

magnitude higher and show that combustion of the high alkali straw is characterized by comparatively very high gaseous alkali emissions, which are due largely to extremely high alkali content in the fuel itself.

The value obtained for 100% HIAL7 has to be considered qualitative, since the signal is strongly affected by self-absorption of the potassium fluorescence (see. DISCUSSION). For HIAL 9, 20%-80% combustion case, the highest values were measured among the fuels for this biomass-coal ratio. Based on the results for 20%-80% combustion case very significant values would be expected for HIAL 9 100% and 50%-50% combustion cases. Unfortunately the very high particulate content in the flue gas originating from this fuel blocked the optical access windows before stable conditions could be reached and prevented much of the signal reaching the detection system. The values for pure HIAL 3 and HIAL 4 combustion were in the tenths of ppm range. In order to better understand alkali metals sequestering measurement of gaseous HCl and SO_2 were performed. Unfortunately because of unresolved issues with the sampling line the measurements were not successful and cannot be included within results and further discussed. The HCl was measured by means of FT-IR and SO_2 by means of infra red analyzer. Few successful data on SO_2 are presented in the table 3.5.

Co-combustion with 50% of coal on energy basis lowered the flue gas alkali concentrations significantly (figure 3.8). The most effective reduction was observed for HIAL 3 and HIAL 7, while that for HIAL 4 was moderate. For 20%-80% straw/coal co-combustion, the decrease is an order of magnitude. Both K and Na concentrations were lower in co-combustion tests than in pure straw combustion, Conversely, only small additions of straw to coal lead to dramatic increases in gaseous alkali content in the flue gas.

The results of the SEM/EDS investigation of the bed material, fly ash and filter ash samples are shown in figure 3.9 till figure 3.18. The clean sand used as a bed material and the sand substracted from the reactor has been compared at the first instance (figure 3.9). Apart of the SEM image of the particles the composition of the particles obtained with EDS was included. The SEM/EDS analysis continues with investigation of different particles of fly ash. The results correspond to HIAL 9 and are characterized with great variety in composition and morphology as can be seen from SEM images and EDS scans. The fly ash is followed with filter ash (figure 3.16 to figure 3.18)

Name of Experiment	Exp. Number	$T_{reactor}$ [°C]	$T_{meas.\ point}$ [°C]	K [vppm] at 6% O_2	Na [vppm] at 6%O_2	Comments
100 % Hard Coal	04_01	850	760	0.18	0.01	
100 % Hard Coal	04_02	750	710	0.02	0	
100 % HIAL3	04_03	850	760	43.49	0.75	
100 % HIAL4	04_07	850	764	61.22	0.08	
100 % HIAL7	04_10	900	786	<200	0.29	See in the text
100 % HIAL9	04_05	850	792	no signal	no signal	See in the text
50 % HIAL3 – 50 % Coal	04_04	850	760	12.82	0.14	
50 % HIAL4 – 50 % Coal	04_08	850	731	50.49	0.08	
50 % HIAL7 – 50 % Coal	04_09	850	777	12.63	0.02	
50 % HIAL9 – 50 % Coal	04_06	855	770	no signal	no signal	See in the text
20 % HIAL3 - 80 % Coal	04_11	890	774	1.46	0.01	
20 % HIAL4 - 80 % Coal	04_12	870	769	10.02	0.03	
20 % HIAL7 - 80 % Coal	04_13	875	791	4.08	0.01	
20 % HIAL9 - 80 % Coal	04_14	870	772	36.08	0.12	

Table 3.6: ELIF measurements campaigns - results

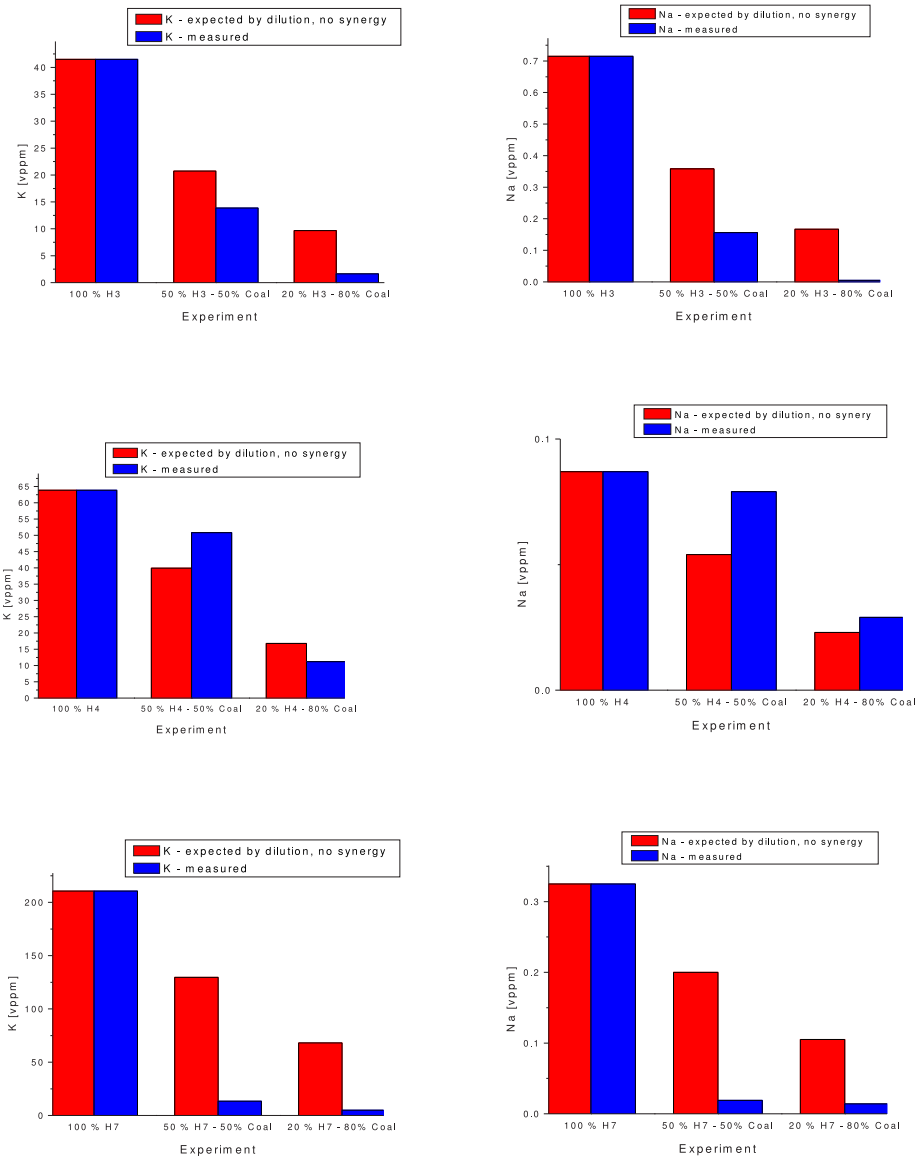


Figure 3.8: Co-combustion of HIAL fuels with coal - synergy effect (experiments, conditions at the measuring point T=750°C, p=atmospheric)

3.6 Discussion

3.6.1 ELIF campaigns

The results of the ELIF measurements show that very high amounts of gaseous alkali species are released to the gas phase from all types of straw investigated.

Although both potassium and sodium are readily released from the biomass, the sodium content in straw is comparable with that in coal, whereas the potassium content is ten times higher. This largely explains the different levels of K and Na found in the flue gas in case of CFBC experiments. During the experimental campaign with ELIF the highest release for both potassium and sodium was observed for HIAL 7. For Na, up to several hundred ppb were measured, but for K the corresponding values were 2-3 orders of magnitude higher. Now although only about 1% of the alkali molecules are actually photolyzed here, if the molecular concentration is above about 20 ppm, self-absorption of the alkali atom fluorescence (radiation trapping) will be significant. This has been discussed in the literature [Chadwick et al., 1996; Chadwick et al., 1997; Monkhouse, 2002] and means that the fluorescence versus concentration curve deviates from linearity. Thus in the several hundred ppm range (HIAL 7 100%) the actual values should be much higher. The quantification of this phenomenon for this type of application is under investigation. HIAL 7 is characterized by the high K content and the low chlorine content. Moreover, the observed reduction in gas-phase alkali on co-combustion is the most pronounced of all cases investigated. In addition, the relatively high sulfur content in HIAL 7 may play a role by forming condensable alkali sulfates [Wolf et al., 2005]. However, at the relatively moderate temperatures of FB combustion, most of the sulfates will be in condensable form and for the reasons given in the experimental part, are not detected by ELIF. Under the present conditions, it should be assumed that compounds detected by ELIF are mostly potassium and sodium chlorides.

For HIAL 9, very high potassium release would have been expected in the combustion process because of the high K level and the highest Cl content of all fuels. Several authors have shown [Baxter et al., 1998; Gottwald et al., 2001; Gottwald et al., 2002b] that Cl is more responsible for the degree of alkali vaporization than the alkali concentration in fuel itself. It was reported by several researchers [Gottwald et al., 2002b; Haÿrinen et al., 2004] that the gaseous alkali content in the flue gas may increase with the increasing chlorine content. Therefore the measured concentrations with ELIF could have been higher than for HIAL 7. However, this high level could not be fully detected in the case of 100% and 50-50% combustion, due to deterioration of the window transparency, as mentioned earlier.

It is believed that chlorine behaves as a shuttle for potassium transportation to the particle surface [Hansen et al., 1999] before release as KCl to the gas phase. The highest concentrations of alkalis in the case of 80-20% co-combustion experiments for HIAL 9 may indicate that for 100% and 50-50% combustion the value would also be very high. Time constraints meant that the repeat of this measurement had to be deferred to a later date. In the case of HIAL 3 with the

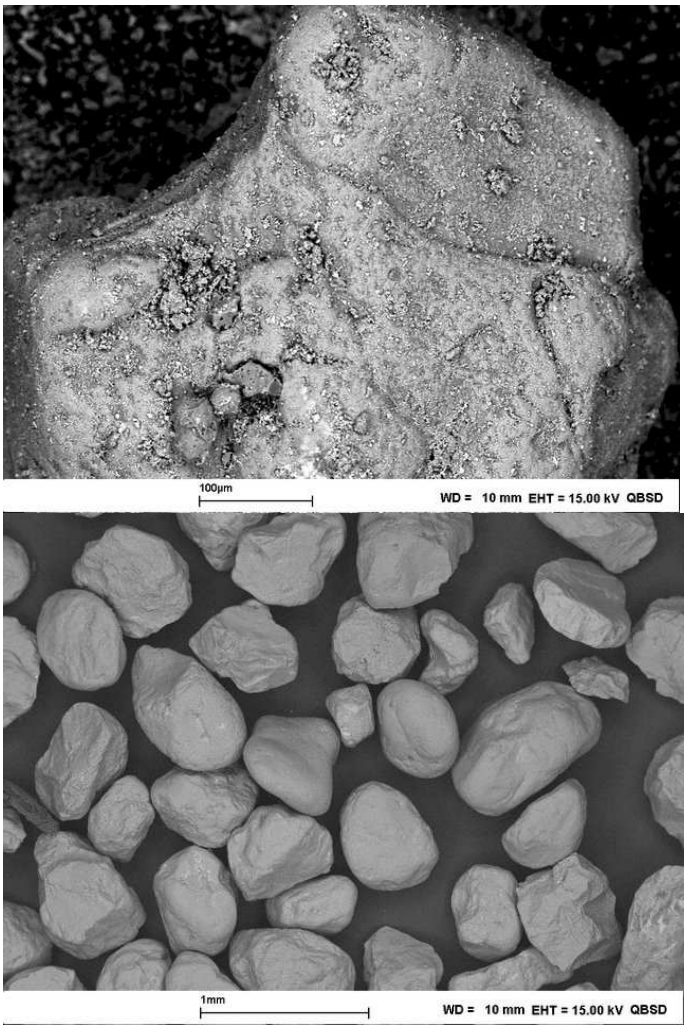


Figure 3.9: Bed material, upper - from the reactor (experiment 04_01, reference table 3.5), lower - clean sand

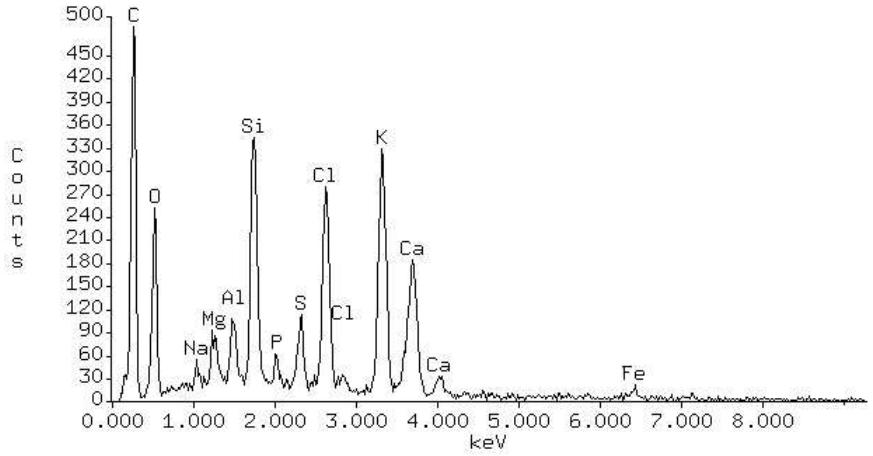
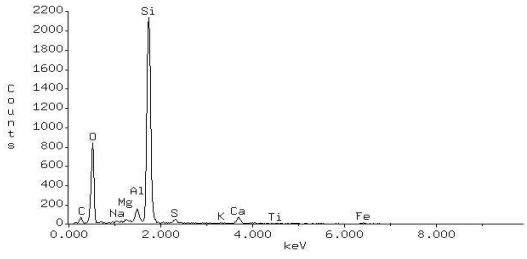


Figure 3.10: EDS analysis of bed material after experiments (figure 3.9 upper, experiment 04_01, reference table 3.5)



Element	k-ratio	Element	Atom %	Compound	Compound
	(calc.)	Wt %		Formula	Wt %
Na-K	0	0.3	0.27	Na2O	0.41
Mg-K	0	0.29	0.24	MgO	0.48
Al-K	0.02	2.12	1.61	Al2O3	4
Si-K	0.33	40.15	29.26	SiO2	85.88
K -K	0	0.02	0.01	K2O	0.03
Ca-K	0.02	2.55	1.3	CaO	3.57
S -K	0.01	1.12	0.71	SO3	2.79
Ti-K	0	0.09	0.04	TiO2	0.16
Fe-K	0.02	1.88	0.69	Fe2O3	2.68
O -K	—	51.48 S	65.87	—	—
Total		100	100		100

Figure 3.11: EDS analysis of bed material, clean sand (figure 3.9 lower)

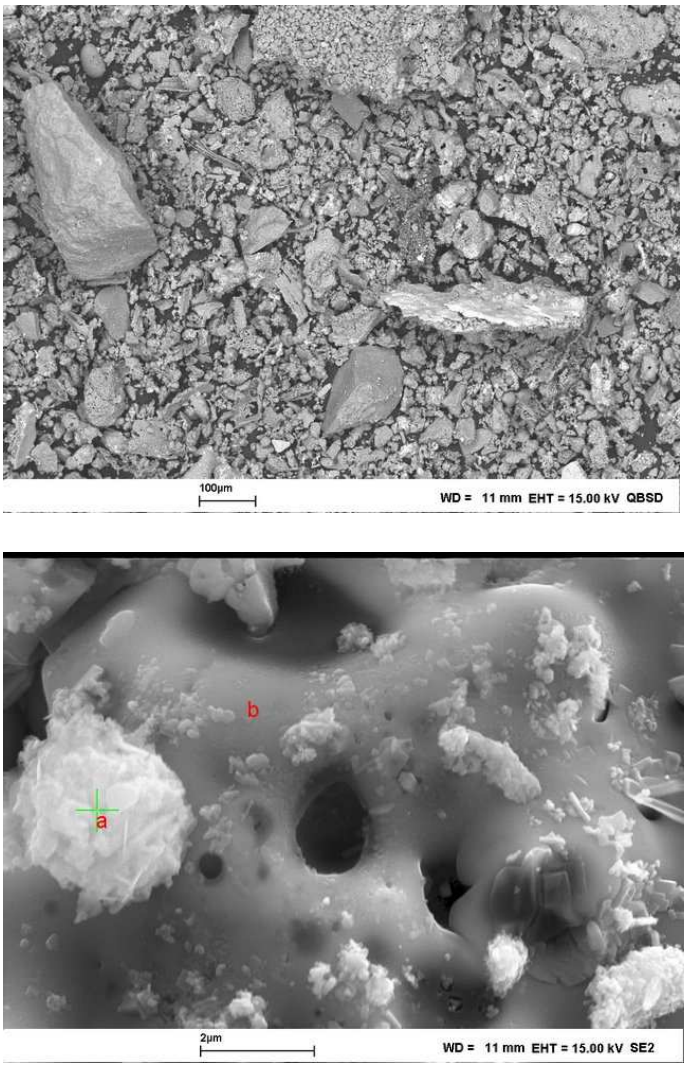


Figure 3.12: HIAL 9 100% (experiment 04_04, reference table 3.5)- fly ash (spot a and spot b marked on the lower figure)

highest Si content, the equilibrium may shift towards formation of non-gaseous compounds when the coal was added. Correspondingly, a strong decrease in flue gas alkali concentration was measured with ELIF. The formation of silicates, as can be seen in chapter 4, is especially favored if the amount of Cl in the system is low. For HIAL 9, in contrast, the equilibrium is shifted more

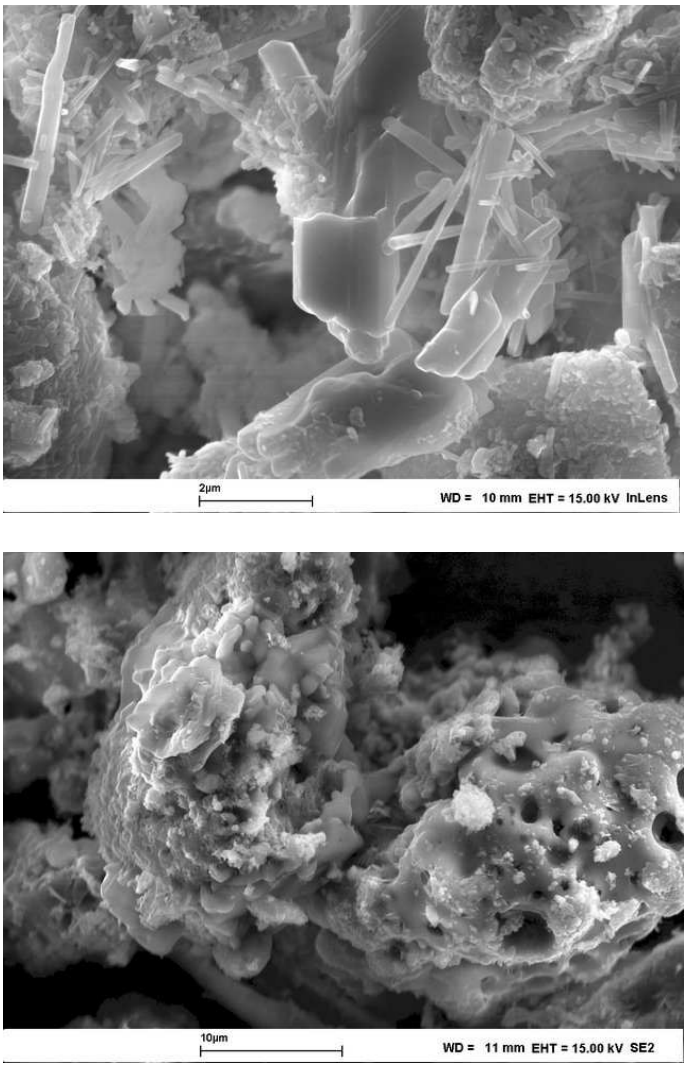
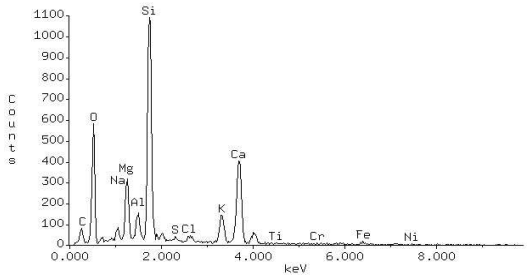


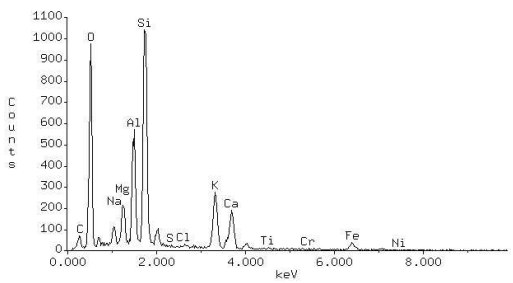
Figure 3.13: HIAL 9 (experiment 04_04, reference table 3.5)- fly ash

towards the chloride, because of the higher chlorine content. High release of alkali chlorides resulting from a large Cl fuel content has been observed experimentally [Gottwald et al., 2002b; Aho and Ferrer, 2004]. The concentrations of K and Na detected during the co-combustion experiments with ELIF were lower than expected just on the basis of mixing of pure fuels and the dilution effect (figure 3.8). The graphs present the expected concentrations of K, Na which



Element	ZAF	Element	Atom %	Compound	Compound
		Wt %		Formula	Wt %
Na-K	2.14	1.68	1.65	Na2O	2.26
Mg-K	1.62	5.91	5.5	MgO	9.8
Al-K	1.49	2.17	1.82	Al2O3	4.1
Si-K	1.3	20.88	16.82	SiO2	44.67
K -K	1.14	4.99	2.89	K2O	6.01
Ca-K	1.14	19.18	10.83	CaO	26.84
S -K	1.27	0.34	0.24	SO3	0.86
Ti-K	1.26	0.05	0.02	TiO2	0.08
Fe-K	1.23	1.67	0.68	Fe2O3	2.39
P -K	1.44	0.8	0.58	P2O5	1.82
Cl-K	1.24	1.16	0.74	Cl	1.16
O -K	4.17	41.17 S	58.22	—	—
Total		100	100		100

Figure 3.14: EDS analysis of fly ash HIAL 9 100%, spot a (figure 3.12)



Element	ZAF	Element	Atom %	Compound	Compound
		Wt %		Formula	Wt %
Na-K	2.13	2.27	2.19	Na2O	3.05
Mg-K	1.63	3.52	3.22	MgO	5.84
Al-K	1.46	8.68	7.16	Al2O3	16.39
Si-K	1.35	19.63	15.56	SiO2	42
K -K	1.16	9.09	5.17	K2O	10.95
Ca-K	1.15	7.34	4.08	CaO	10.27
S -K	1.29	0	0	SO3	0.01
Ti-K	1.24	0.25	0.12	TiO2	0.42
Fe-K	1.22	4.54	1.81	Fe2O3	6.49
P -K	1.47	1.89	1.36	P2O5	4.33
Cl-K	1.26	0.26	0.16	Cl	0.26
O -K	3.4	42.54 S	59.18	—	—
Total		100	100		100

Figure 3.15: EDS analysis of fly ash HIAL 9 100%, spot b (figure 3.12)

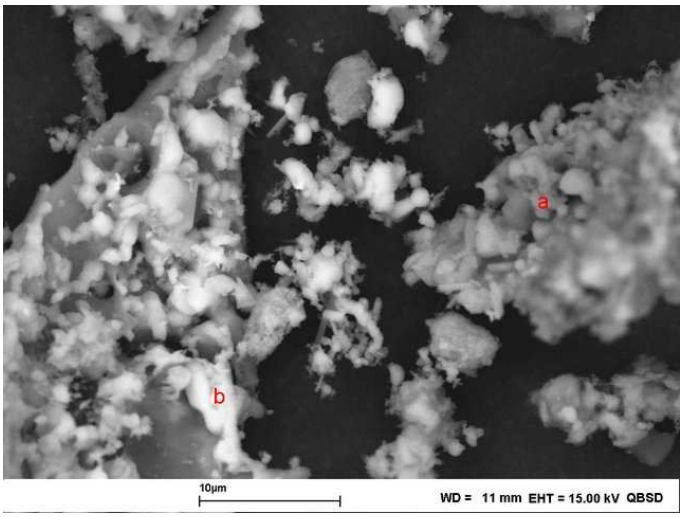
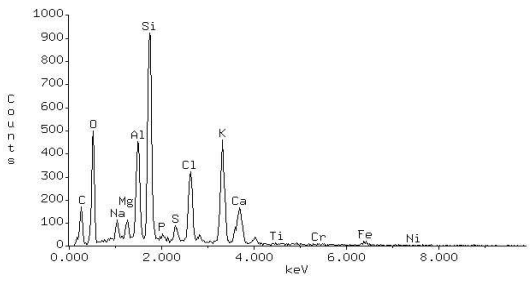


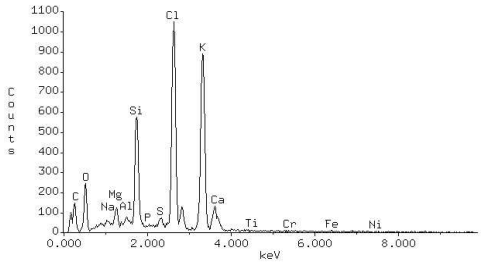
Figure 3.16: Filter ash - mixed fuels (spot a and spot b marked on the figure)

should be present if only mixing would play the role compared with the experimental data. This finding reveals an interesting behavior during co-combustion of straw and coal in the scope of the research requirements specified in chapter 2. It may be considered as of great importance on one side for utility operators and on another to understand the behavior of straw -coal system in Circulating Fluidized Beds. The co-combustion of biomass with coal should result in effective binding of alkalis with the clay minerals of the coal [Aho and Ferrer, 2004]. Here, it is believed that the high quantity of alumina-silicates in the coal shifts the equilibrium towards alkali alumina-silicate formation so the gaseous alkali species were not measured at the expected concentrations. In most recent works



Element	ZAF	Element Wt %	Atom %	Compound Formula	Compound Wt %
Na-K	2.07	1.83	1.86	Na2O	2.46
Mg-K	1.58	1.29	1.25	MgO	2.14
Al-K	1.38	7.35	6.38	Al2O3	13.88
Si-K	1.28	17.12	14.28	SiO2	36.61
K -K	1.17	14.81	8.88	K2O	17.84
Ca-K	1.18	7.17	4.19	CaO	10.04
S -K	1.23	1.71	1.25	SO3	4.26
Ti-K	1.25	0.12	0.06	TiO2	0.21
Fe-K	1.21	1.82	0.76	Fe2O3	2.61
P -K	1.38	0.49	0.37	P2O5	1.12
Cl-K	1.22	8.82	5.83	Cl	8.82
O -K	4.18	37.47 S	54.88	—	—
Total		100	100		100

Figure 3.17: EDS analysis of filter ash - mixed fuels, spot a (figure 3.16)



Element	ZAF	Element	Atom %	Compound	Compound
		Wt %		Formula	Wt %
Na-K	1.99	0.39	0.47	Na2O	0.52
Mg-K	1.5	1.56	1.8	MgO	2.59
Al-K	1.32	0.54	0.56	Al2O3	1.01
Si-K	1.15	9.13	9.11	SiO2	19.53
K -K	1.17	34.38	24.65	K2O	41.41
Ca-K	1.23	2.45	1.71	CaO	3.43
S -K	1.07	1.02	0.9	SO3	2.56
Ti-K	1.25	0	0	TiO2	0
Fe-K	1.19	0.45	0.22	Fe2O3	0.64
P -K	1.18	0.01	0.01	P2O5	0.03
Cl-K	1.1	28.28	22.37	Cl	28.28
O -K	5.86	21.79 S	38.19	---	---
Total		100	100		100

Figure 3.18: EDS analysis of filter ash - mixed fuels, spot b (figure 3.16)

concerning FB coal-biomass co-combustion importance of alumina and silica originating naturally from coal ash is emphasized [Furimsky and Zheng, 2003; Haÿrinen et al., 2004]. Therefore by mixing the coal with high alkali straw, at least part of the alkali metals released from the straw to the gas phase will interact with clay minerals in the coal to form alkali-alumina-silicates, for example Sanidine - $KAlSi_3O_8$ and/or Albite - $NaAlSi_3O_8$.

3.6.2 SEM/EDS analysis of the particles

SEM/EDS analysis of the CFBC measurements campaign originating samples of the bed material, fly ash and filter ash reveal new information about sequestering of alkali metals during combustion of high alkaline biofuels with coal in CFB systems. Investigation of the bed material (figure 3.9) shows that there is substantial difference between clean sand and the sand substracted from the reactor. It is visible that the sand from the reactor is covered with all kind of elements originating from combusted fuels. EDS analysis of the bed material

reveals presence of sulfur, calcium and alumina in higher concentrations than for clean sand (figure 3.10). It means that some compounds are adsorbed at the surface of the bed material but it means also that they may be released back to the system when the conditions inside the reactor change. Closer look at the fly ash particles reveals complicated, molten together structure of different fractions. At the figure 3.12 and figure 3.13 with proceeding EDS analysis the structure of the single fly ash particle with varying SEM magnification is shown. It is impossible to specify the exact composition of the particle because of the molten character and many interlaying constituents. The spot analysis reveals diversified origins of the particle. It also reveals how complicated the structure is. It is very difficult then to relate the structure and the composition to any particular fuel. The structure of the investigated flying ash is a composition of different forms of fly ash molten together. The situation is even more complicated with the filter ash (figure 3.18). It was impossible because of the system limitations to separate the filter ash originating from one fuel. The overall analysis reveals presence of multiple elements within the ash. Dominant presence of silica and alumina together with potassium and chlorine should be emphasized. These elements are expected taking into account the composition of the investigated fuels. The low temperature of the filter vessel (350°C) assures that all the gaseous alkali metals compounds are in solid state. The filter ash is then mixture of flying ash particles originating from all the sources in the reactor.

3.7 Conclusions

The chapter presents the unique measurements of gaseous alkali compounds performed on a CFB pilot scale combustor with specially selected high alkaline straw and coal. Very high concentrations of gaseous alkali metals have been observed during combustion of 100 % straw. Especially with HIAL 7 with very high potassium content and at high K/Si ratio the release was substantial. The measured values are still approximately one order of magnitude lower than the release values calculated based on the fuel composition. It is likely that part of the alkalis will condense on the bed material, flue gas pipe walls, fly ash particles or/and form aerosol particles in the flue gas. The co-combustion experiments lowered the measured values of K and Na species more than would have been expected only from the mass balance on the biomass-coal fuel fed to the reactor. This finding reveals an interesting behavior during the co-combustion of straw and coal in the scope of the research requirements specified in chapter 2. Blending then may be considered as of great importance on one side for utility operators and on another to understand the behavior of straw-coal systems. Mechanisms responsible for such substantial change in the measured values cannot be easily and straightforward concluded from the experiments. The sul-

fates were not measured by ELIF. The elements like Si and Cl were found to a play very important role in defining the system composition. Chlorine is believed as reported before by others researchers to be responsible for vaporization of alkali metals to the gas phase and silica for binding them in fly or/and bottom ash particles. This was observed during SEM/EDS investigation. Moreover SEM/EDS investigation of the bed material suggests a buffer like kind of behavior with the possibility to absorb and release some compounds. Alkalis bound into the minerals from the coal are not volatile, therefore the potentially harmful compounds will remain in the ash. Results of SEM/EDS provide additional information about the complexity of the system and make the picture more complete.

Chapter 4

Chemical equilibrium modelling of combustion system

4.1 Introduction to chemical equilibrium

4.1.1 Enthalpy

The enthalpy usually represented by H is defined as the energy released in a chemical reaction under constant pressure, H = Q_p. It is a property to evaluate the reactions taking place at constant pressure. Enthalpy differs from internal energy, U, as this is the energy input to a system at constant volume. The energy released in a chemical reaction raises the internal energy, U, and does work under constant pressure at the expense of energy stored in compounds. Thus

$$H = Q_p = U + PV \tag{4.1}$$

Change of enthalpy (ΔH) that accompanies a reaction is defined as the number of joules absorbed or released during the consumption of one mole of a reactant or the formation of one mole of product [Smith, 1982, Meites, 1981]. It has the units J·mol^{-1}. Reactions that absorb heat are called endothermic and have positive values of ΔH. Reactions that evolve heat are called exothermic and have negative values of ΔH. The enthalpy change (ΔH) of a chemical reaction depends on the amount of reactants, the temperature, and pressure.

4.1.2 Standard Enthalpy of Reaction

It is defined as the enthalpy change of reaction for at standard temperature and pressure (298.15K, 1bar). It can be expressed as follows:

$$\Delta H^0 = \sum_j n_j \left(H_f^0\right)_{j,products} - \sum_i n_i \left(H_f^0\right)_{i,reactants} \tag{4.2}$$

4.1.3 Standard Enthalpy of Formation

It is defined as the standard enthalpy change of a reaction that forms a compound from its basic elements, which are at also standard state. It is represented by ΔH^0_f and can be expressed for a reaction that involves n_i moles of the ith reactant and n_j mole of the jth product, as follows:

$$\Delta H^0_f = \sum_j n_j \left(H^0_f\right)_{j,products} - \sum_i n_i \left(H^0_f\right)_{i,reactants} \tag{4.3}$$

4.1.4 Activation Energy

It is defined as the minimum energy required to start a chemical reaction. Some elements and compounds react together just by bringing them into contact (spontaneous reaction). For others it is necessary to supply energy (heat, radiation, or electrical charge) in order to start the reaction, even if there is ultimately a net output of energy. This initial energy is the activation energy. The point at which the reaction begins is known as the energy barrier. When the energy barrier is reached, the chemical bonds in the reactants are broken, enabling them to proceed from reactants to products [Meites, 1981; Denbigh, 1981]. In some reactions, such as the combustion of fuels, the activation energy required for the chemical reaction to take place is very small, resulting in a rapid reaction. Other chemical reactions, such as the rusting of iron (a type of oxidation) have a very large energy barrier and take place slowly. A heat of reaction only describes the net energy of the reaction.

4.1.5 Spontaneous Reaction

Spontaneous reactions are defined as the reactions, which take place, by themselves, given enough time. These reactions are not necessarily fast, as speed is not a factor in defining the spontaneity of a reaction. For example explosions and many other spontaneous reactions are rapid, but other spontaneous processes, such as the precipitation of calcium carbonate require very long time. Factors that can influence the reaction rate are temperature, and a catalyst. A catalyst can accelerate the reaction if it is spontaneous. Similarly change in temperature , and pressure can influence for example the oxidation process.

4.1.6 Energy and Spontaneity

It has been observed that energy, or enthalpy drops in most of the chemical reactions. The energy that the chemical substances lose during reaction is given off as heat. This situation is alternatively expressed by saying that most of

the spontaneous chemical processes are exothermic. The combustion of gasoline, like all combustions, evolves heat; because the carbon dioxide and water molecules produced have lower energy than the gasoline and oxygen molecules from which they came. There are exceptions to the principle that all spontaneous reactions emit heat.

4.1.7 Entropy

Entropy is a measure of the degree of internal disorder of the system (or phase). The greater the degree of disorder, the higher the entropy. Increasing temperature always causes an increase of entropy. Entropy is measured in J/K·mole. The change in entropy of a system ΔS is given by:

$$\Delta S = \Delta S_{exchanged} + \Delta S_{internal} \tag{4.4}$$

For a reversible process,

$$\Delta S_{internal} = 0 \tag{4.5}$$

4.1.8 The Gibbs free energy

The second law of thermodynamics helps in identifying for a process whether it is reversible, irreversible, or impossible. If it is irreversible, then it is said to occur spontaneously, e.g. the spontaneous flow of heat at constant pressure or the sudden expansion of a gas into a low-pressure region. Entropy is also used for checking the spontaneity of a process, but problem with the entropy is that total entropy of the system and the surrounding is required to be known [Meites, 1981; Denbigh, 1981]. That's why a state function was defined for determining the spontaneity of a process, and termed free energy.

4.1.9 Entropy and Chemical Reactions

Energy or enthalpy alone has shown to be insufficient for determining the spontaneity of a reaction, and thus entropy is considered as a missing factor in this connection. For example a drop in enthalpy (ΔH negative) helps to make a process spontaneous, but is not enough by itself to be certain that it will be so. Simultaneously minimizing H and maximizing S, or minimizing H and -S favors spontaneity. So a new function was defined whose minimization combines both of the above requirements. This has been defined as the Gibbs free energy, G:

$$G = H - TS \tag{4.6}$$

The units of H ($Jmole^{-1}$) and S ($JK^{-1}mole^{-1}$) require that S be multiplied by the absolute temperature, T. For a reaction with the same initial and final temperature, the changes in enthalpy, entropy, and free energy are related by the

expression.

$$\Delta G = \Delta H - T\Delta S \tag{4.7}$$

This expression says that, at constant temperature, the change in free energy, ΔG, is the change in enthalpy, ΔH, minus the change in entropy multiplied by the absolute temperature, TΔS. Spontaneous reaction is defined as one in which the overall Gibbs free energy decreases, regardless of what happens to the enthalpy and entropy individually [Meites, 1981; Denbigh, 1981].

4.1.10 Temperature dependence of the Gibbs free energy

The Gibbs free energy is by definition a sensitive function of temperature. This is due to the relation between the enthalpic and entropic contributions to ΔG.

Some definite cases are defined as following:

1.ΔH < 0 and ΔS >0.

Then the reaction is always spontaneous at all temperatures.

2. ΔH > 0 and ΔS < 0.

Then the reaction is never spontaneous at all temperatures.
Other combinations depend more sensitively on temperature. There exists a special temperature T* at which ΔG is zero. This is written as

$$T^* = \Delta H/\Delta S \tag{4.8}$$

If both ΔH and ΔS are positive, then the reaction is spontaneous at temperatures higher than T*. If ΔH and ΔS are negative, then the reaction is spontaneous at temperatures below T*.

4.1.11 Standard-State Free Energy of Formation

The change in free energy that occurs when a compound is formed from its elements in their most thermodynamically stable states at standard-state conditions.In other words, it is the difference between the free energy of a substance and the free energies of its elements in their most thermodynamically stable states at standard-state conditions.
The standard-state free energy of reaction can be calculated from the standard-state free energies of formation as well.It is the sum of the free energies of formation of the products minus the sum of the free energies of formation of the reactants:

$$\Delta G^0 = \sum \left(G_f^0\right)_{products} - \sum \left(G_f^0\right)_{reactants} \tag{4.9}$$

4.2 Chemical Equilibrium Definitions

4.2.1 The Equilibrium Constant

For a general elementary chemical reaction,

$$aA + bB \leftrightarrow cC + dD \tag{4.10}$$

The concentrations of the reactants and products are related to each other according to

$$K_c = \frac{[C]^c [D]^d}{[A]^a [B]^b} \tag{4.11}$$

The number K_c is called the equilibrium constant, and is a function of temperature only (i.e., its numerical value doesn't change unless the temperature changes. The stoichiometric coefficients a, b, c and d show up as powers of the corresponding reactants and products.
The above definition is for the liquid phase reactions, another definition of the equilibrium constant is based on pressure rather than concentration for gas phase components. The ideal gas law gives

$$PV = nRT \tag{4.12}$$

Here P is the total pressure. In the case of several components, each has a partial pressure, all of which sum up to the total pressure:

$$P = P_A + P_B + P_C \tag{4.13}$$

For each component, the ideal gas law can be written in the form

$$P_A V = n_A RT \Rightarrow \frac{n_A}{V} = [A] = \frac{P_A}{RT} \tag{4.14}$$

4.2.2 Free Energy Changes and Equilibrium Constants

Free energy changes in chemical reactions are related to the reaction quotient Q of the reaction by the equation

$$\Delta G = \Delta G^0 + RTlnQ \tag{4.15}$$

The above equation will be used in the following section to describe chemical reactions quantitatively. The equation linking free energy changes and the reaction quotient can be used to describe a reaction, which is at chemical equilibrium. Chemical equilibrium is a condition in which the chemical activities or concentrations of all of the involved species are the equilibrium activities, so

Q = K. At equilibrium there is no net driving force for the reaction; the reaction will not proceed spontaneously either forward or backward, so ΔG is zero [de Nevers, 2002; Meites, 1981; Guenther, 1975]. A chemical equilibrium can therefore be described by a simpler equation linking the standard free energy change of the reaction, ΔG^0, to the equilibrium constant K of the reaction. This relationship is:

$$\Delta G^0 = -RTlnK \tag{4.16}$$

The information given by free energy values and equilibrium constant values is the same information, which is the position of chemical equilibrium for the chemical system to which the values refer. There is, therefore, a relationship between the numerical value for a free energy change and the numerical value for the equilibrium constant whose process corresponds to that change. It was shown earlier that value of ΔG, the standard free energy change of a chemical reaction, is negative if and only if the reaction occurs spontaneously. The value of the equilibrium constant is always positive and ranges between very large values (reaction proceeds spontaneously) and very small values (reaction proceeds in reverse). However, the logarithm of the equilibrium constant is positive when the value of the equilibrium constant is greater than one, and negative when the value of the equilibrium constant is less than one. It is not the equilibrium constant which is proportional to the free energy change, but the logarithm of the equilibrium constant. Because a positive logarithm of equilibrium constant and a negative free energy of reaction both correspond to a spontaneous reaction, a minus sign is shown in the equation.

4.2.3 A General Approach to Gibbs free energy

The Gibbs free energy is a function of pressure, temperature, and composition (i.e., the moles of the various components that are present, e.g., H_2O, CO_2, etc.). This functionality can be formally written as:

$$G = G\left(T, P, N_1, N_2, \ldots, N_{NS}\right) \tag{4.17}$$

Here, N_j is the number of moles of species j in the system, and the index NS is the total number of species in the system. Taking the total derivative of G gives:

$$dG = \left(\frac{\partial G}{\partial T}\right)_{P,N} dT + \left(\frac{\partial G}{\partial P}\right)_{T,N} dP + \sum_{j=1} \left(\frac{\partial G}{\partial N}\right)_{P,T,N_j} dN_j \tag{4.18}$$

Here the summation is over all the species present. Since T and P are constant, these terms drop out.This leaves equilibrium condition as:

$$dG = 0 = \sum_{j=1}^{NS} \mu_j dN_j \tag{4.19}$$

Here μ_j is chemical potential, which is defined as

$$\mu_j = \left(\frac{\partial G}{\partial N}\right)_{T,P,N_i} \tag{4.20}$$

The chemical potential can be thought of as the change of Gibbs free energy of a mixture caused by the addition of a differential amount of species j when the T, P, and other mole numbers are held constant.

$$G_j = u_j + Pv_j - Ts_j \tag{4.21}$$

Now we can expand h in terms of enthalpy of formation and also expand s to express the pressure correction for ideal gases:

$$G_j = h^0_{f,j} + (h_j - h_{f,j}) - T\left[s_j - Rln\left(\frac{P_j}{P_o}\right)\right] \tag{4.22}$$

Here $h^0_{f,j}$ is the enthalpy of formation at 298 K, h_j is the enthalpy at the target temperature, h^0_j is the enthalpy at 298 K, s_j is the 1 atm entropy at target temperature, T is the gas constant, P_j is the partial pressure of the component, and P_0 is 1atm. Properties that depend on just temperature can be separated:

$$G_j = u_j + Pv_j - Ts_j \tag{4.23}$$

Splitting up the terms gives:

$$ln\left(\frac{P_j}{P_o}\right) = ln\left(\frac{P_j}{P}\frac{P}{P_0}\right) = ln\left(\frac{N_j}{N}\frac{P}{P_0}\right) = ln\left(\frac{N_j}{N}\right) + ln\left(\frac{P}{P_0}\right) \tag{4.24}$$

Here, P is the system pressure and N is the total number of moles in the system. This leads us to an operational equation for calculating G_j:

$$G_j = G^* + RTN_j - RTlnN + RTln\left(\frac{P}{P_0}\right) \tag{4.25}$$

If we know T and P, we can get G^*, and the only unknowns are the mole numbers of species j and the total number of moles in the system. Substituting this into equation 4.19 gives us the operational equation for the minimization:

$$dG = 0 = \sum_{j=1}^{NS} G_j dN_j = \sum_{j=1}^{NS}\left[G^* + RTN_j - RTlnN + RTln\left(\frac{P}{P_0}\right)\right] dN_j \tag{4.26}$$

In this way the equilibrium constant approach has been defined. In that approach, an equilibrium reaction is hypothesized, and this is used to reduce all the dN_j to one variable. The resulting equation contains (within the G_j terms)

the variables N_j and N. Using algebraic manipulation and atom balances, the N_j and N terms are reduced to a single variable, which is solved (this approach is detailed in most standard thermodynamics texts). This approach becomes complicated for large systems so a general Gibbs minimization approach is adopted which is the base for all the equilibrium codes and can be found in literature e.g., [de Nevers, 2002; Smith, 1982; Meites, 1981].

4.2.4 Gibbs Energy Minimization

The total Gibbs energy of a system, which has to be minimized for a given temperature, pressure, and composition to establish equilibrium is often represented as

$$G = \sum_i n_i \mu_i \tag{4.27}$$

where n is amount, μ_i is chemical potential, and the sum extends over all chemically distinct entities (or species of the system). In order to differentiate between the chemical potential of species with that of an independent system component an alternative expression is given by,

$$G = \sum_\phi N^\phi G_m^\phi \tag{4.28}$$

where ϕ is a phase index and N^ϕ is the amount and $G^\phi{}_m$ is the integral molar Gibbs energy of the phase ϕ, provides better understanding , as there are phases of certain total amount of internal composition which coexist at equilibrium . The minimization of G in above equation at constant pressure and temperature is achieved with the constraints imposed by the mass balance equations. In terms of 'l' independent system components, these may be written as

$$G = \sum_\phi \sum_i n_i^\phi a_{ij}^\phi j = 1, 2, 3.., l \tag{4.29}$$

where $n^\phi{}_i$ is the amount of the ith constituent of phase ϕ, $a^\phi{}_{ij}$ is a coefficient of the stoichiometry matrix composed of the constituents of phase ϕ, and b_j is the total amount of the jth system component. At equilibrium , the following simple linear relation holds:

$$G = \sum_j b_j \mu_j \tag{4.30}$$

Here, the chemical potentials of the independent system components can be replaced by the Lagrangian multipliers that satisfy the minimum condition. In the equilibrium calculations , integral and partial molar Gibbs energy expressions are required. Generally , the integral expression is written as

$$G_m = G_m^0 + G_m^{id} + G_m^{xs} + G_m^p + G_m^{mo} \tag{4.31}$$

where G_m^0 and G_m^{id} are the Gibbs energy contributions from the pure phase components and from the ideal entropy term with respect to these components, respectively. The excess Gibbs energy contribution, G_m^{xs} , is often small or even negligible if proper phase components, and thus proper ideal state was chosen. However it should be noted that effects like immiscibility or chemical ordering cannot be modeled without G_m^{xs}, which therefore can be called chemical interaction term. The Gibbs energy contributions from changes in molar volumes, G_m^p, and magnetic ordering, G_m^{mo}, are of non-chemical nature and can normally be neglected.

4.3 Thermodynamic equilibrium calculations - approach

The thermodynamic equilibrium calculations have been performed for studying the behavior of chlorine-alkali-mineral interactions during the combustion of HIAL fuels. Figure 4.1 outlines the principle of global equilibrium analysis where the composition of the system at given temperature and pressure is calculated by minimizing the total Gibbs free energy of the system.

The calculations for chemical equilibrium have been carried out using the computer program Fact-Sage that minimizes the total Gibbs free energy of a system subjected to the restrictions of the mass balances [Eriksson and Hack, 1990]. The Equilib module is responsible for the Gibbs energy minimization in Fact-Sage. It calculates the concentrations of chemical species when specified elements or compounds react or partially react to reach a state of chemical equilibrium. Equilib employs the Gibbs energy minimization algorithm and thermochemical functions of ChemSage and offers considerable flexibility in the way the calculations may be performed [Bale, 2002]. For example, the following items are permitted: a choice of units (K, C, F, bar, atm, psi, J, cal, BTU, kWh, mol, ...); dormant phases in equilibrium; equilibrium constrained with respect to T, P, V, H, S, G, U or A or changes thereof; user-specified product activities (the reactant amounts are then computed); user-specified compound and solution data etc. For an exhaustive explanation of the FactSage features reference is made to manual of the program itself [Hack, 1995].

For the calculations the gas phase was taken as ideal, while the liquid, and solid phases are taken as pure. The input to the program was provided in the form of temperature, pressure, and composition of fuel and air. For all the equilibrium calculations, temperature was kept in the range of 350-1550^{o}C, while the pressure was maintained as atmospheric [Khan, 2004]. The input to the Fact-Sage is summarized as follows: elemental compositions of the fuel and the fuel ash

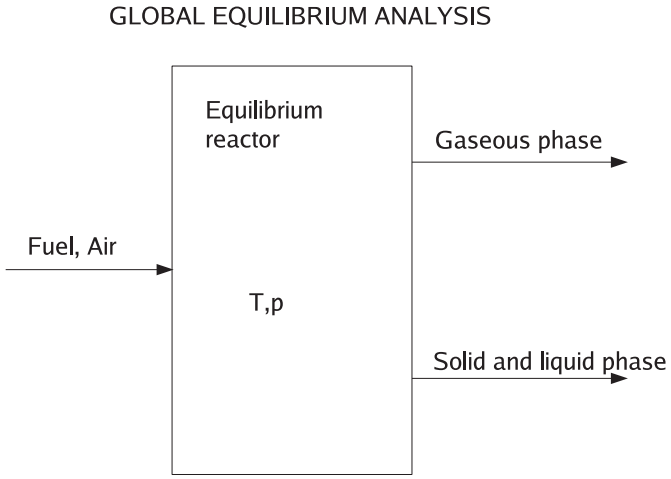


Figure 4.1: Global equilibrium analysis

with 20% excess air (α=1.2). In accordance with the literature in all the equilibrium calculations, besides the major elements of Cl, K, S all the minor elements e.g., Si, Ca, Al have also been considered to study the influence of mineral elements in ash on the behavior of chlorine and alkali metals. After getting input in the form of fuel composition, excess air, temperature, pressure, Fact-Sage looks for the thermodynamical data of these elements in the databases based on the existing literature data [i.e. Wagman, 1971; Barin, 1977; Stull, 1985]. Using theses species then thermodynamic equilibrium calculations are carried out. Species included in the thermodynamic calculations for all the cases of HIAL fuels, and HIAL-Coal co-combustion cases are given in the Table 4.1.

There are certain limitations in the use of thermodynamic equilibrium analysis for combustion applications. For instance in order to reach equilibrium either the temperature must be high enough or the species residence time should be long enough to reach the thermodynamic equilibrium [Dayton and Milne, 1995; Dayton et al., 1999a; Dayton et al., 1999b]. Composition and temperature gradients have also not been considered. In addition physical processes, such as particle nucleation, agglomeration and adsorption in the gas are not taken into consideration. Christensen and co-workers [Christensen and Livbjerg, 2000] in their paper described in detail a mathematical model called Plug Flow Aerosol Condenser for simulation of the formation and evolution of a multi-component aerosol during cooling of a flue gas with condensible vapors. Although there is

Category	Species
Combustion gas components	H_2,CO,CO_2,COS,N_2,HCl,SO_2,N_2O,Cl,NO_2,HS,Cl_2,NH_3,N_2H_2,H_2S_2,HNO,ClO,S, NO,N2O,O,O_2,SO_3,S,S_2,S_3,S_4,S_5,S_6,S_7,S_8,NaO,NO_2Cl,H_2S_2,H_2SO_4,H_2,CH_4,HNO_3, HCN,H_2CO,OH,$COCl_2$,K_2O,NaO,K,KO,Na,NaOH,HCO,HNO,$COCl_2$, HOOH ,HNCO,
Al-species	Al(g),AlCl(g),$AlCl_2$(g),$AlCl_3$(g),AlO(g),AlOH(g),AlO_2(g),AlS(g),OAlCl(g),Al_2(g), Al_2C_{l2}(g),Al_2O_2(g),Al_2O_3(s,l),Al_2O_3.CaO(s),Al_2O_3.CaO.SiO_2(s),$KAlO_2$(s),$KAlO_2$(s2), Al_2O_3(liq),$NaAlO_2$(liq),$MgAl_2O_4$(liq),KAl_9O_{14}(s),Al_2SiO_5(s,andalusite), Al_2SiO_5(s2,sillimanite),Al_2SiO_5(s3,kyanite),$(Al_2O_3)(SiO_2)_2$(s),$Al_6Si_2O_{13}$(s,mullite), $MgAlO_2$(s),Al_2O_3)$(SiO_2)_2(H_2O)_2$(s,kaolinite),Al_2O_3)$(SiO_2)2(H_2O)_2$(s2,halloysite), $Na_2Al_{12}O_{19}$(s),Al_2O_3)$(SiO_2)_2(H_2O)_2$(s3),$Al_2Si_4O_{10}(OH)_2$(s,pyrophyllite), $NaAlO_2$(s2),$NaAl_9O_{14}$(s),AlCH$_2$$NaO_5$(s,dawsonite),$MgAl_2O_4$(s,spinel),$NaAlSiO_4$(s,nepheline-a),$NaAlSiO_4$(s2,nepheline-b),$NaAlSiO_4$(s4,carnegieite),$NaAlSi_2O_6$(s,jadeite), $NaAlSi_3O_8$(s),$NaAlSi_3O_8$(s2,high),NaAlSi2O_6H_2O(s),$NaAl_3Si_3O_{12}H_2$(s,paragonite), $Mg_3A_{l2}Si_3O_{12}$(s,pyrope),$Mg_2Al_4Si_5O_{18}$(s,cordierite),$KalO_2$(s),$NaAlSiO_4$(s3,nepheline-c),$CaAl_2Si_2O_8$(s,hexagonal)$KFe_3AlSi_3O_{10}(OH)_2$(s,annite),$Mg_2Al_4Si_5O_{18}(H_2O)$(s,hydrous-cordi.),$KAlSi_3O_8$(s3,sanidine), ,$Mg_3Al_2Si_8O_{22}(OH)_2$(s,glaucophane), $KAlSiO_4$(s,kaliophyllit-a),$KAlSiO_4$(s2,kaliophyllit-b),$KAlSi_2O_6$(s,leucite(rhf)-a), $KAlSi_2O_6$(s2,leucite(rhf)-b),$KAlSi_3O_8$(s,microcline),$KAlSi_3O_8$(s2,k-feldspar), $KAl_3Si_3O_{10}(OH)_2$(s,muscovite),$KAl_7Si_{11}O_{30}(OH)_6$(s,kmont.nite), $Mg_3AlSi_3O_{10}(OH)_2$(s,phlogopite),$KAl(SO_4)_2$(s),$KAl(SO_4)_2(H_2O)_{12}$(s),$CaAl_2SiO_6$(s,ca-tschermak,$CaAl_2Si_2O_8$(s2,anorthite),$Ca_2Al_2SiO_7$(s,gehlenite),$Ca_3Al_2Si_3O_{12}$(s,grossular),$Ca_2Al_3Si_3O_{12}$(OH)(s2, zoisite), $Mg_5Al_2Si_3O_{10}(OH)_8$(s,clinochlorite) $CaAl_2Si_2O_7(OH)_2(H_2O)$(s,lawsonite),$CaAl_4Si_2O_{10}(OH)_2$(s,margarite), $CaAl_4Si_{22}O_{60}(OH)_{12}$(s), $Ca_2Al_3Si_3O_{12}(OH)$(s,clinozoisite),
K-species	KCl, KOH,$(KCl)_2$(g),K_2SO_4(s,l,g),K_2CO_3(s,s2),$K_2Si_4O_9$(s,l), $K_2Si_2O_5$(s,l) , $K_2Si_2O_5$(s)
Ca-species	CaO(g),$CaCl_2$(g),CaOH(g),$Ca(OH)_2$(g),$Ca_5HO_{13}P_3$(s,hydroxyapatite),$CaCl_2$(s), $K_2Ca(CO_3)_2$(s),$K_2Ca_2(CO_3)_3$(s),$MgOCaOSi_2O_4$(s),$MgOCaOSi_2O_4$(s),$Ca_3Fe_2Si_3O_{12}$(s), $Ca_2Mg_5Si_8O_{22}(OH)_2$(s)
Na-species	NaCl(s,l,g), Na_2SO_4(s,s2) , $Na_2Ca_3Si3O_{16}$(s), $Na_2Ca_2Si_3O_9$(s), $NaAlSi_3O_8$(s2),
PO_4, SO_4 species	Na_2SO_4(l),Na_2SO_4(solid,a-b),K_2SO_4(solid,alpha,beta),K_2SO_4(l),$Al(SO_4)_2$(s), $CaSO_4$(s,s2,s3),$MgSO_4$(s),$MgSO_4(H_2O)$(s,Kieserite), $Ca_3(PO_4)_2$,$K_2Ca_2(SO_4)_3$(s).
Si -species	SiC(g),$SiCl_2$(g),$SiCl_3$(g),$SiCl_4$,SiH(g),SiH_4(g),SiO(g),SiO_2(g),Si_2(g),Si_3(g),SiO_2(s) $MgSiO_3$(s,s2),Mg_2SiO_4(s)

Table 4.1: Main species obtained from thermodynamic equilibrium calculations

number of simplifications in the model the authors predict formation of aerosols especially in gases with high content of Na and K. Despite of all the limitations thermodynamic equilibrium analysis can be used to give equilibrium distribution of elements and reaction mechanism of various species at combustion conditions [Hald, 1994; Wei et al., 2002]. In this chapter the equilibrium calculations for HIAL1, HIAL3, HIAL4 and HIAL9 fuels have been included. Each fuel has been analyzed for the behavior of K, Cl, S, Na, Ca, and Al species. As Si is mostly bound with Ca,K, Na, or Al species, therefore it has not been described

separately.

4.4 Results

The results for the chemical equilibrium modeling are presented in figures 4.2 to 4.9, which show that variations in the fuel composition influence the behavior of the system very strongly. For HIAL 3 (figures 4.2 to figures 4.3) and HIAL 9 (figures 4.8 to figures 4.9), fuels with high silica content, silica-based compounds are present in substantial amounts for 100% biomass combustion. For 100% HIAL 7 (figures 4.6 to figures 4.7), characterized by high sulfur content, 40% of the total potassium is present as solid potassium sulfate. Co-combustion with coal changes the equilibrium system substantially. It can be seen that for co-combustion in both temperature ranges, the systems are composed mostly of one or two major compounds, which account for nearly all potassium and sodium at the temperature and fuel blend of interest. For both temperature ranges these compounds are alkali-alumina-silicates. The effect of M-Al-Si, where M stands in general for alkali metal atoms and means potassium or sodium is overwhelming. Especially for the lower biomass shares, namely the 20/80 cases, the equilibrium shifts towards formation of these compounds. Generally speaking, little difference was observed between the system at 750°C and at 850°C for lower biomass shares. The total amount of potassium or sodium included varies between particular blends, but in most cases the equilibrium composition is the same. However, as will be discussed below, the equilibrium components for the sodium system differ markedly from those obtained for potassium in pure biomass combustion.

4.5 Discussion

The calculations focus and present deeper insight on straw-coal system where alumina silicates are present. Following the research requirements defined in chapter 2 results of such defined system are presented. Analyzing the results of the equilibrium simulations, the very strong influence of the fuel mixing is evident. The calculations revealed that during co-combustion, the formation of M-Al-Si is thermodynamically favored. The effect is very strong, so that even a small share of coal promotes alkali sequestering. This mechanism may explain the substantial decrease in the measured values of gaseous alkalis during ELIF experiments. From the boiler operators' point of view, this kind of mechanism is desirable. The alkali-alumina-silicates remain then in the bottom ash and they have relatively high, safe melting temperatures. Part of the problems associated with deposit formation and corrosion can be avoided because less alkali compounds are volatilized.

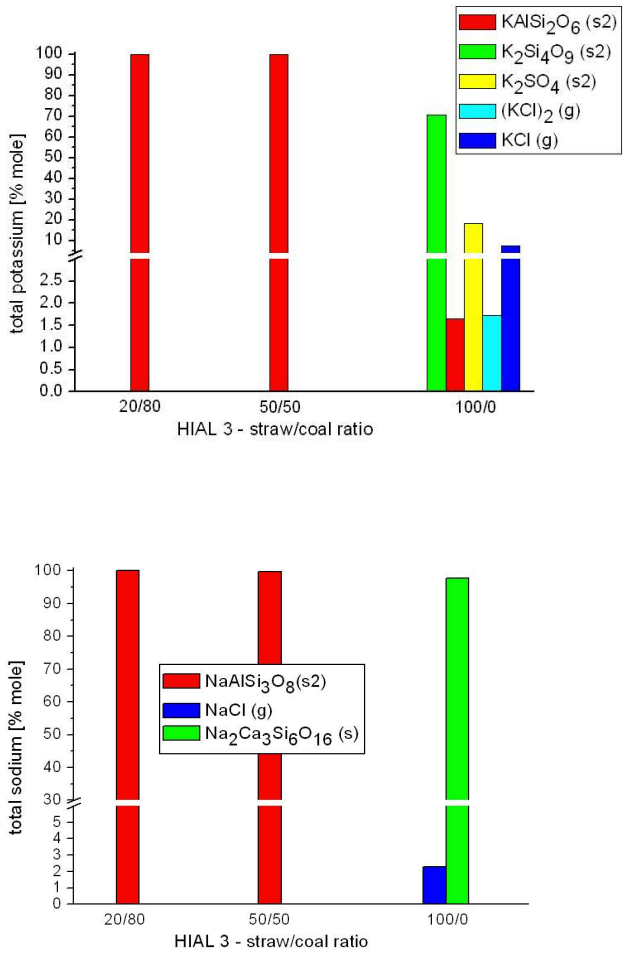


Figure 4.2: HIAL 3 - Thermodynamically stable compounds of K and Na at 750°C (average measuring point temperature) for combustion and co-combustion cases (ratios on energy basis, p=1bar)

The decrease in gas phase alkali cannot be explained only on the basis of mass balance due to mixing coal with biomass as already emphasized in chapter 3. Calculated, stable, solid compounds of all investigated fuels are mainly alumina silicates. Especially for 20% biomass - 80% coal the results are dominated by alkalis in the solid phase due to the formation of alkali alumina silicates.

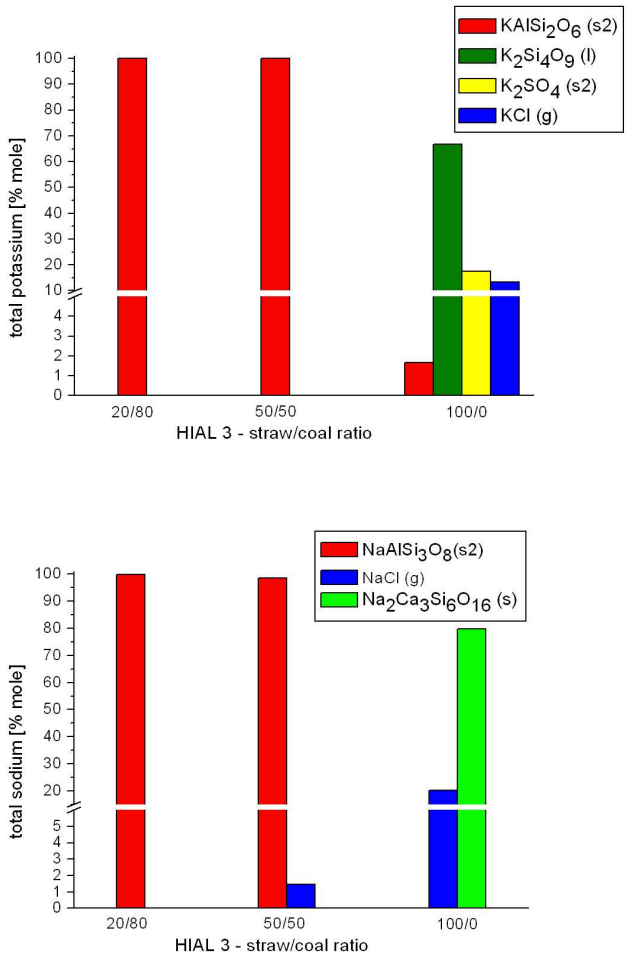


Figure 4.3: HIAL 3 - Thermodynamically stable compounds of K and Na at 850°C (average measuring point temperature) for combustion and co-combustion cases (ratios on energy basis, p=1bar)

This trend is visible either for potassium or for sodium and covers both temperature ranges. Similar findings were reported already by Wei and co-authors [Wei et al., 2002; Wei et al., 2005] and Aho and co-workers [Aho and Ferrer, 2005]. Wei and co-workers reported that for coal and straw co-combustion with less than 50% of straw most of the potassium is combined with aluminosilicates in the form of $KAlSi_2O_{6(s,s2)}$. The reduction in coal fraction increased the forma-

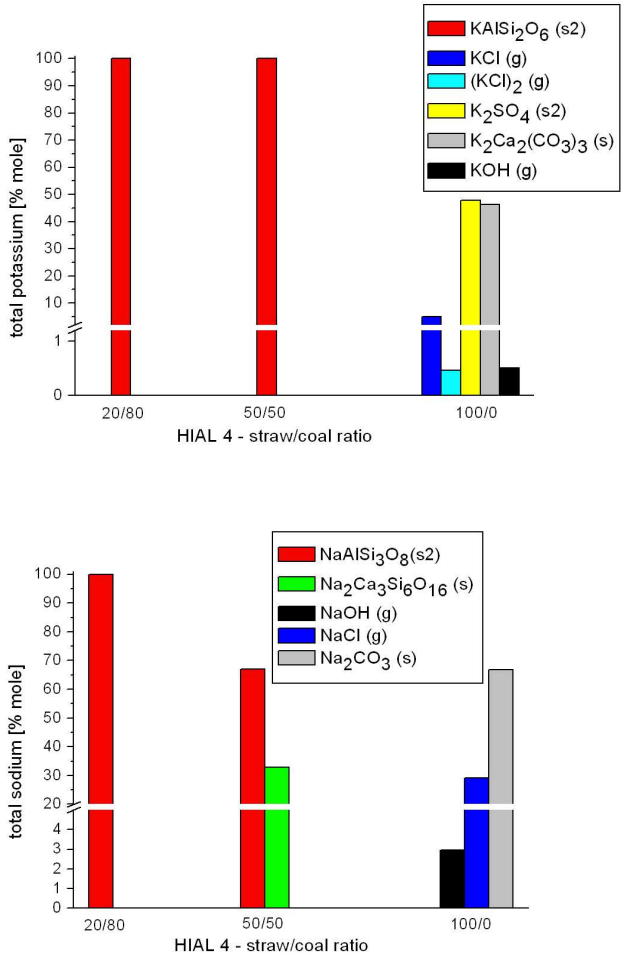


Figure 4.4: HIAL 4 - Thermodynamically stable compounds of K and Na at 750°C (average measuring point temperature) for combustion and co-combustion cases (ratios on energy basis, p=1bar)

tion of $K_2Si_4O_{9(liq)}$.
In the case of HIAL 7 (pure fuel), which is characterized by high potassium and sulfur but low chlorine, a substantial share of total potassium (40%) is predicted to be in sulfate form (figure 4.6 and figure 4.7). Refering to the table 3.4 in chapter 3 where ratios between some elements in the fuel are presented for HIAL 7 molar K/Cl and S/Cl are very high what explains the predicted high

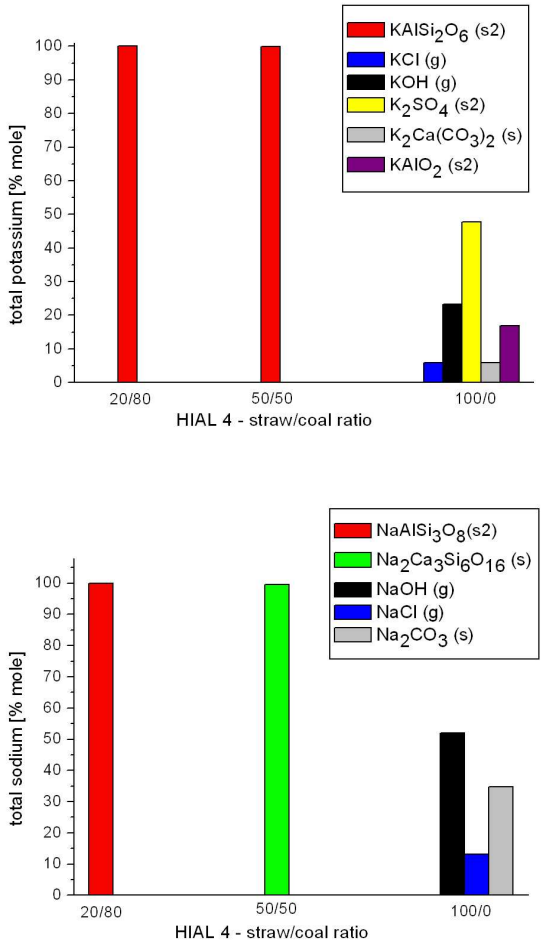


Figure 4.5: HIAL 4 - Thermodynamically stable compounds of K and Na at 850°C (average measuring point temperature) for combustion and co-combustion cases (ratios on energy basis, p=1bar)

formation of sulfates. For co-combustion with a 50/50 ratio, the corresponding proportion is 30% of total potassium. For sodium sulfate, however, the share is high only for 50/50 co-combustion cases. Sulfation of alkali species is possible as reported by Iisa and co-workers [Iisa et al., 1999] although those experiments were performed within a higher temperature range in a laminar flow reactor. The authors suggest that most of the sulfation will take place

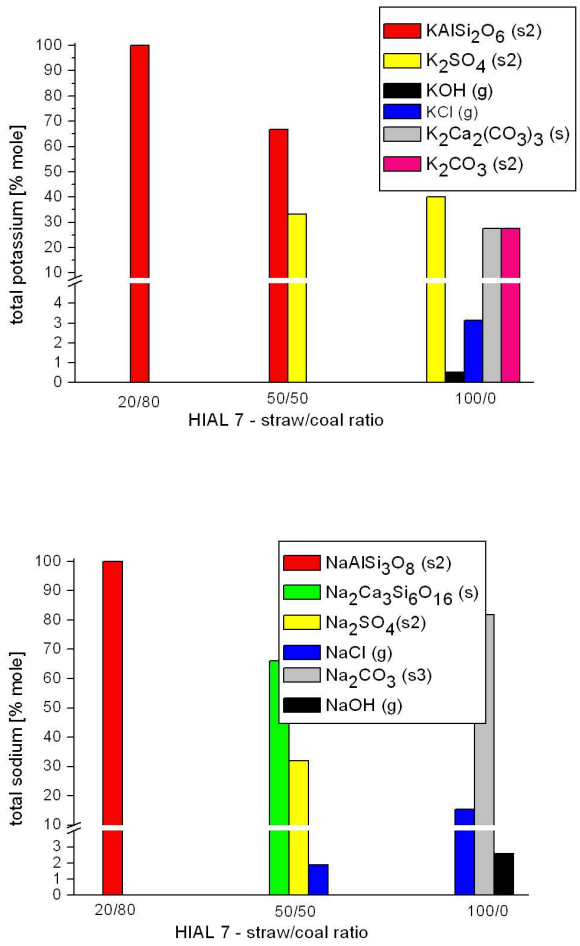


Figure 4.6: HIAL 7 - Thermodynamically stable compounds of K and Na at 750°C (average measuring point temperature) for combustion and co-combustion cases (ratios on energy basis, p=1bar)

in the gas phase because the process is much faster there than in the condensed phase. Jensen and co-workers [Jensen et al., 2000a] studied the nucleation of aerosols in the flue gases and in their study the alkali sulphates are formed by the sulphation of vapour phase and not solidified alkali chloride. The sulfation reaction is dependant on availability of SO_3 in the gas phase. It is possible that in case of CFB co-combustion part of the alkalis from straw

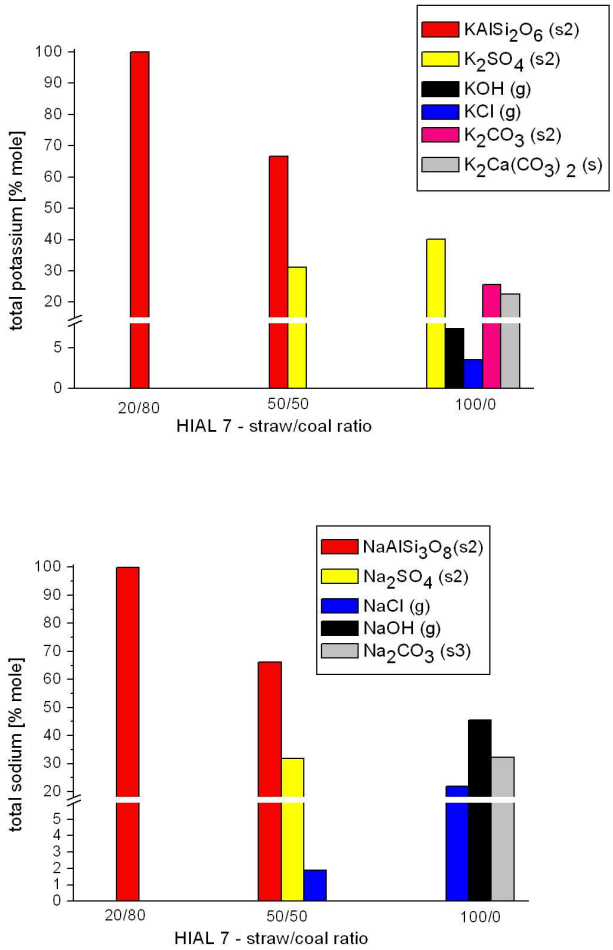


Figure 4.7: HIAL 7 - Thermodynamically stable compounds of K and Na at 850°C (average measuring point temperature) for combustion and co-combustion cases (ratios on energy basis, p=1bar)

sulfates are present in the gas phase but these were not detected by ELIF. Moreover, at the experimental conditions of this study alkali sulfates should be present only in condensed phase. Formation of potassium sulfates in condensed phase on for example ash particles can be kinetically inhibited as suggested by some authors [Furimsky and Zheng, 2003] and because of the residence time of particles in the CFB combustor this phenomena is not likely [Iisa et al., 1999;

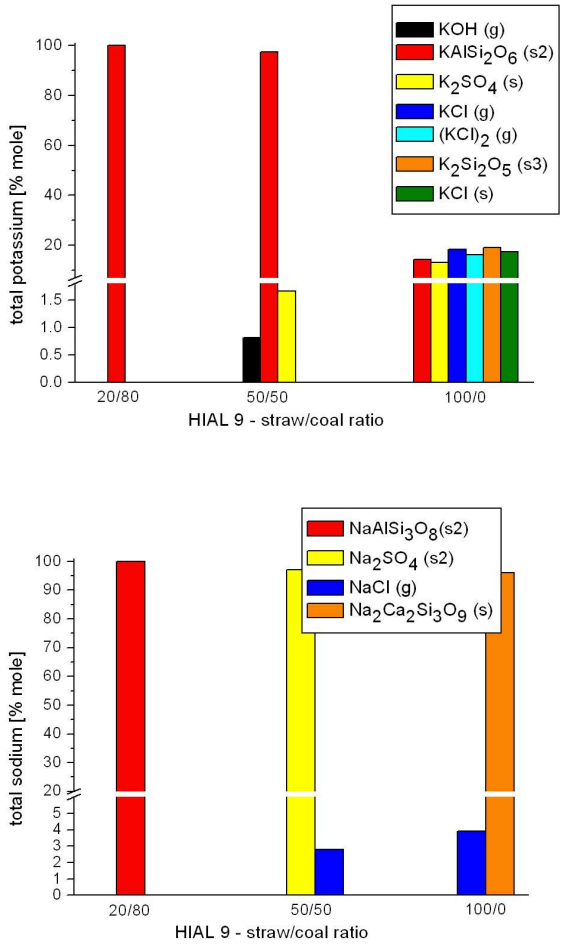


Figure 4.8: HIAL 9 - Thermodynamically stable compounds of K and Na at 750°C (average measuring point temperature) for combustion and co-combustion cases (ratios on energy basis, p=1bar)

Wolf et al., 2005]. However, it could be possible in downstream deposits.

The calculations were performed for two temperatures, in order to comply with the applied experimental conditions [Khan, 2004]. On average, the reactor operated at 850°C in the riser and downcomer, whereas the flue gases further downstream at the ELIF measuring position were at approx. 750°C. Tempera-

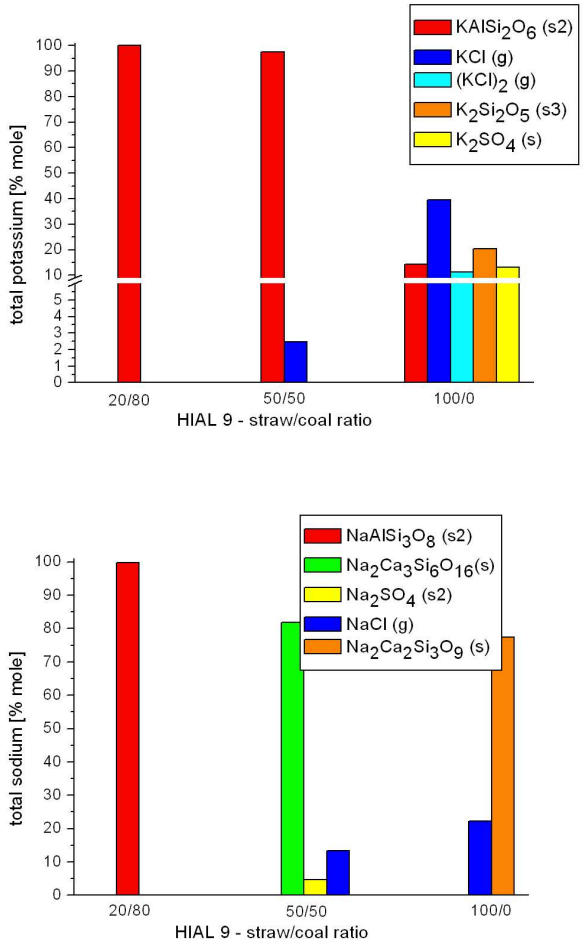


Figure 4.9: HIAL 9 - Thermodynamically stable compounds of K and Na at 850°C (average measuring point temperature) for combustion and co-combustion cases (ratios on energy basis, p=1bar)

ture is one of the most important parameters influencing the alkali release to the gas phase. It can be expected that KCl, for example, will volatilize more readily at 850°C because of the higher partial pressure. The bottom limiting temperature for gas alkali detection was 750°C. Below this temperature all most abundant alkali compounds are no longer in the gas phase. On the other hand, there is not much change in the calculated equilibrium composi-

tion between these two temperatures, even if some shift from one type of solid phase compound to another is observed. Kinetic hindrance of such a shift can be expected, namely the shift from potassium-calcium-carbonates $K_2Ca(CO_3)_2$(s) to $K_2Ca_2(CO_3)_2$(s) and formation of $KAlO_2$(s2) at the expense of KOH(g) and KCl(g) for HIAL 3 (Figure 4.2). In the case of HIAL 9, the fuel with the highest chlorine content and high potassium content (K/Cl = 1.84) but low low S/Cl ratio, the chemical equilibrium calculations predict the highest share of KCl in the system. In the case of 100% HIAL 9 combustion, at 750°C KCl (figure 4.8) and its dimer contribute more than 30% to the potassium in the system. In contrast, the corresponding calculations for sodium predicted compounds with calcium. For combustion of 100% HIAL 7, with even higher potassium content in the fuel but low chlorine (very high molar K/Cl ratio = 25.69), the gaseous potassium chloride contributes only as 3% of total potassium. Another gaseous compound, KOH is predicted below 1%. The rest of the compounds are solid. This seems to confirm the hypothesis about the importance of chlorine in forming the gas phase potassium compounds [Blander et al., 2001; Furimsky and Zheng, 2003 or Mojtahedi and Backman, 1989] but other mechanisms have to be responsible as well because in case of HIAL 7 the highest values of gaseous KCl were measured experimentally. The lowest experimentally measured values of potassium for HIAL 3 can be explained by formation of substantial amounts of $K_2Si_4O_9$ (l) at 850°C and $K_2Si_4O_9$ (s2) at 750°C. According to the calculations, these compounds account for up to 70% of total K at 750°C and their formation is also very undesirable for plant/boiler operators. These compounds have low melting temperatures and may contribute substantially to the growth of deposits. For sodium, sodium-calcium-silicates are formed instead.

4.6 Conclusions

The addition of coal to biomass changes the equilibrium of the combustion system. Under the scope of the defined in chapter 2 research requirements the performed calculations reveal that the formation of aluminosilicates is suggested with Al and Si originating from coal ash. This means that potassium from straw is bound into non-volatile, and much less harmful components which stay in the bottom ash. In general alkali metals bound into the minerals originating from the coal are not volatile, therefore the potentially harmful compounds will remain in the ash. Formation of aluminosilicates helps to explain the figure 3.8 in chapter 3 where synergy of coal-biomass co-combustion is clearly visible. Some influence of sulfur on alkali sequestering and formation of alkali sulfates was observed in the equilibrium calculations in case of HIAL 7 characterized with high sulfur content. However, in most cases for both temperature ranges the formation of aluminosilicates is the dominant process and appears to be responsible for lowering measured high concentrations of K and Na for 100% biomass

composition. As observed before by other researchers chlorine promoted potassium and sodium release from the fuel in form of KCl and NaCl. High level of K and Cl facilitates this process. The elements Si and Cl were found to a play very important role in defining the system composition and Cl is being mostly released as KCl according to the equilibrium calculations. For some fuels addition of coal promoted formation of Ca-sulfates because potassium was bound with alumina-silicates.

Chapter 5

Fundamental investigation of KCl - kaolin interactions

5.1 Introduction

Energy utilities encounter multiple difficulties when trying to increase the share of biofuels for energy conversion purposes. Especially biofuels like straw may cause operational problems because of their high contents of alkali metals and chlorine . During combustion of straw, KCl is released to the gas phase and may condense further downstream on heat exchangers. Deposit formation on relatively cold heat exchanging surfaces is a commonly recognized problem. High-temperature corrosion associated with biomass combustion is often being reported at most of the power plants using high chlorine and alkaline straw [Baxter et al., 1998]. Locally high concentrations of chlorine from chloride deposits on heat exchangers have been observed to substantially increase the corrosion rates of heat exchanging surfaces [John, 1984]. Therefore extensive research is needed to understand the mechanisms controlling the release of alkali metals and interactions with others components within combustion systems. It has been found that during co-combustion of straw with coal natural components in coal ash like alumina-silicates may provide synergy effects and bind gaseous potassium and sodium effectively in the less problematic form of alkali-alumina-silicates [Dayton et al., 1999a; Aho and Ferrer, 2005].

Kaolinite, which is a clay mineral, is a natural component in coal. Kaolinite is the main constituent of kaolin which is a common phyllosilicate mineral. The structure of kaolinite is composed of silicate sheets (Si_2O_5) bonded to aluminum oxide/hydroxide layers ($Al_2(OH)_4$) called gibbsite layers. Clay minerals are layered structures with the layers placed parallel to each other [Neimo, 1990; Kingery, 1976]. Between those interlayers voids exist. Because the layers often produce a negative charge the charge may need to be balanced by cations like Na^+ or K^+. In the interlayer voids water molecules can also be

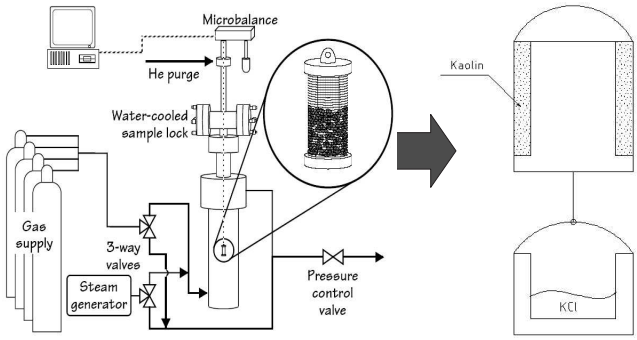


Figure 5.1: PTG reactor with the sample holder

situated. Alkali sorbing capabilities has been earlier reported in the literature [Turn et al., 1998b; Punjak and Shadman, 1988; Steenari, 1998]. It has been observed that K or Na atoms can be bound in those interlayer voids of kaolin under combustion conditions. Accordingly, kaolin might be added as an alkali getter to the combustion process. However, many factors concerning the alkali uptake are still unknown and to investigate the reaction between kaolin and KCl under various conditions, the experiments with a thermogravimetric (TGA) reactor were performed. The purpose of this work was to reveal information about the morphology and chemical compositions of kaolin both before and after contact with gaseous KCl.

5.2 Experimental

5.2.1 Thermogravimetric reactor

The experiments were performed with a TG reactor (Fig. 5.1) at atmospheric conditions. In the apparatus, the sample was suspended in a special sample holder from the balance above the reactor and the weight of the sample was registered as a function of time in a well defined gas environment at a certain temperature [Partanen, 2004]. The electrically heated reactor was lined with a quartz glass tube to prevent corrosion. The inner diameter of the quartz tube was 12 mm. The temperature of the reactor was measured by a thermocouple placed directly under the sample holder. The gas flow entered the reactor from the bottom. Multiple gas mixtures were used in the experiments. The dry part of the gas mixture was produced with a multi-component gas mixer. A separate steam generator provided some of the experiments with water vapor.

5.2.2 Sample holder

A special sample holder was designed for the experiments (Fig. 5.1). It consisted of two separate parts. In the lower one, a solid vaporable material is placed and in the upper, the cylindrical one, a solid sorbent can be placed. In this study the materials in the lower and upper sample holder were KCl and kaolin, respectively. In the experiments KCl was continuously evaporated and mixed with the gas mixture flowing upstream in the reactor. Thus the gaseous KCl was transported in to the vicinity of the kaolin, allowing a possible absorption reaction to take place. Two lower sample holders differing in size were designed and manufactured. By varying the size of the lower sample holder different evaporation rates may be obtained and thus also the concentration of the vaporable material in the gas phase will differ.

5.2.3 Samples and experimental conditions

As a preliminary investigation, pure kaolin and pure KCl were heated in a DTA-TGA to describe the behavior of the respective sample during heating. Following these tests, KCl evaporation experiments with the newly designed sample holders were performed. The purpose of these tests was to determine the evaporation rate of KCl specific for each of the two holder designs. Also, the effect of temperature was investigated. The main part of the test program consisted of an experimental investigation of the interactions between gaseous KCl and solid kaolin. Both sample holders, that were described above, were used in order to vary the evaporation rate, and thus also the concentration of gaseous KCl. For kaolin only one holder was used and approximately the same amount of kaolin was used in all experiments ($\sim$100 mg). The amount of KCl varied depending on the sample holder – with the bigger holder about 90 mg KCl was used, while in the experiments with the smaller one about 60 mg KCl was used. Runs were performed at two temperatures (800°C and 850°C). Also, the experimental times were varied to provide more information about the reaction progress. Accordingly, not only tests reaching complete, full evaporation of KCl (no KCl left in the sample holder) but also tests lasting for shorter periods, i.e. 10 and 20 minutes, were done. The countdown of the experimental time was initiated at the point when the reactor reached the desired temperature (800°C or 850°C). Most of the experiments were performed in a pure N_2 atmosphere. The nitrogen used in the tests was high purity, laboratory class dry gas. Apart from the pure nitrogen runs, some additional runs were made in a steam-N_2 and a steam-O_2-CO_2-N_2 atmosphere.

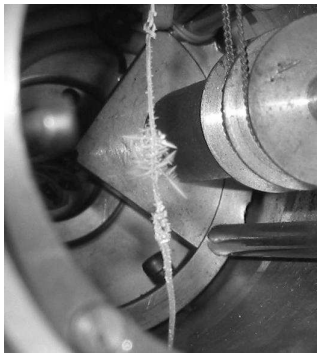


Figure 5.2: Condensation of KCl on the platinum wire inside the PTG reactor

Table 5.1: Average complete evaporation time (atmospheric pressure)

Run	Time	Water	Nitrogen	Temp.
	[s]	[%]	[%]	[°C]
6353	3200	0	100	850
6354	4100	0	100	850
6361	6100	0	100	800
6367	5200	0	100	850
6375	2100	15	85	850

5.3 Results and discussion

5.3.1 Evaporation of KCl

KCl evaporation tests were done at two different temperatures (800°C and 850°C) using both the bigger and the smaller KCl sample holder. A comparison of the approximate times is presented in table 5.1. It has to be stressed that the times for complete evaporation differed from test to test. even though the same holder, amount of reactants and atmosphere were used, which in turn means that it is difficult to repeat experiments with exactly the same KCl concentration in the gas, i.e. every experiment is unique. It has to be pointed out that the weight signal during evaporation was influenced by condensation of KCl on the colder platinum wire further upstream the reactor. This may have influenced on the calculated evaporation rate, however, the time for total evaporation should nevertheless be correct, since at that point no weight change took place anymore. An image of the platinum wire covered with KCl crystals is presented in Fig. 5.2.

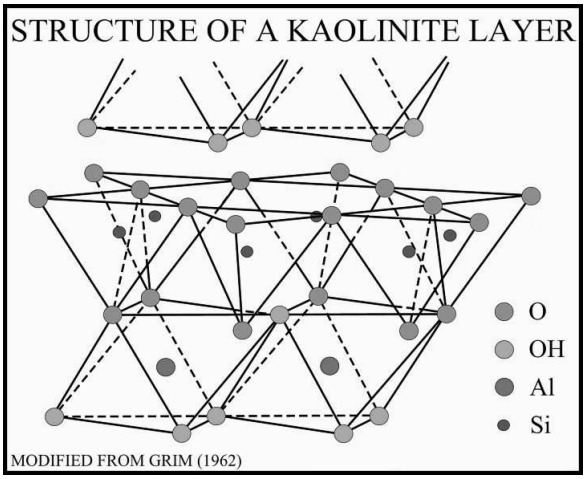


Figure 5.3: Structure of kaolinite (adapted from Grim, 1962)

5.3.2 Morphology investigation with SEM

Kaolin clay has been selected as a possible alkali getter. Kaolin is described as a highly porous, plate like material. The plates consists of layers of silica rings joined to a layer of alumina octahedral through shared oxygen atoms (Fig. 5.3). The morphology of kaolin was investigated with a SEM apparatus (Fig. 5.4), Fig. 5.5, Fig. 5.6). The aim of this investigation was to reveal information about the structure of kaolin before and after thermal treatment. Moreover possible morphological changes after reaction with KCl were under scope.

The investigation revealed a complicated, highly porous, layered structure of this clay. No visual changes were observed in the structure of kaolin after thermal treatment in 100% N_2 atmosphere (Fig. 5.4, Fig. 5.5). Similarly the structure did not seem to change after runs with KCl present in the gas phase (Fig. 5.6). A stack of multiple plates within a kaolin particle is clearly visible from Fig. 5.4 and Fig. 5.5. The porous structure together with a surface charge originating in non-ideality of the Al-Si matrix indicate that the material may be a promising agent for capturing K and Na atoms as suggested in the literature [Neimo, 1990].

Agglomeration of the bed and fuel ash may cause problems during fluidized bed combustion of biomass fuels. Previous research showed that the bed material particle was covered with a sticky coating which covered the original bed particle and consisted mostly of Ca-K-silicates. The stickiness of these de-

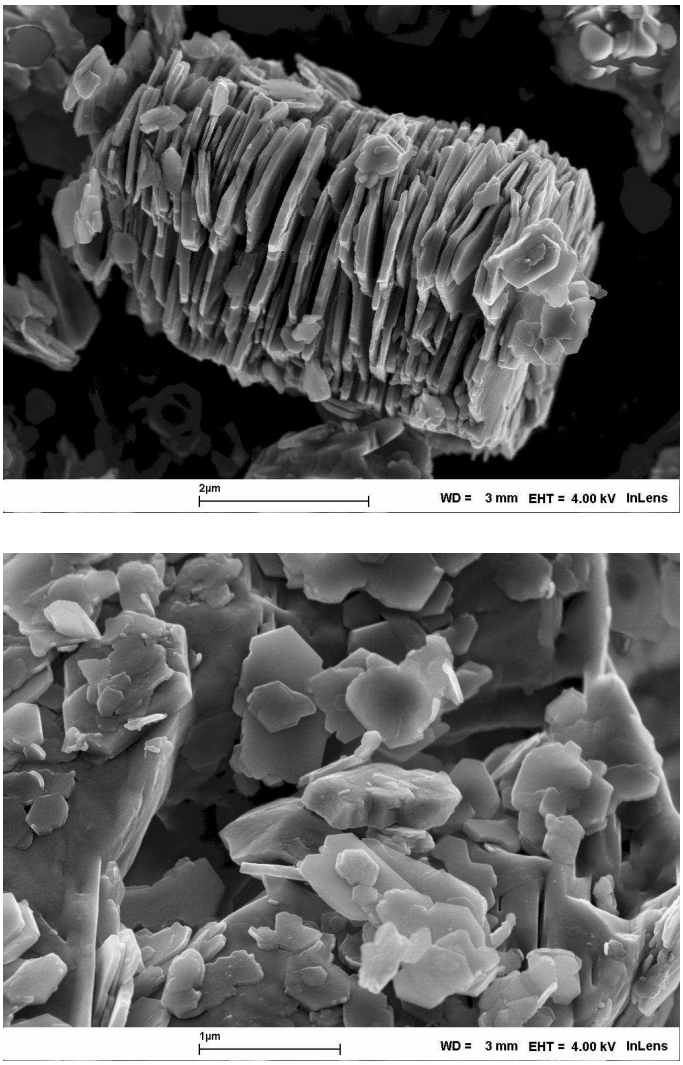


Figure 5.4: Structure of thermally untreated kaolin

posits was directly related to the potassium content. When kaolin was added to the system kaolin was transformed to meta-koalin absorbing potassium species [Ohmann and Nordin, 2000]. The investigation of the mechanisms responsible for the alkali uptake reveals that during heating of kaolin the water bound within the structure is being released at temperatures between 500°C and 600°C leading to kaolin dehydration and possible changes in overall charge balance

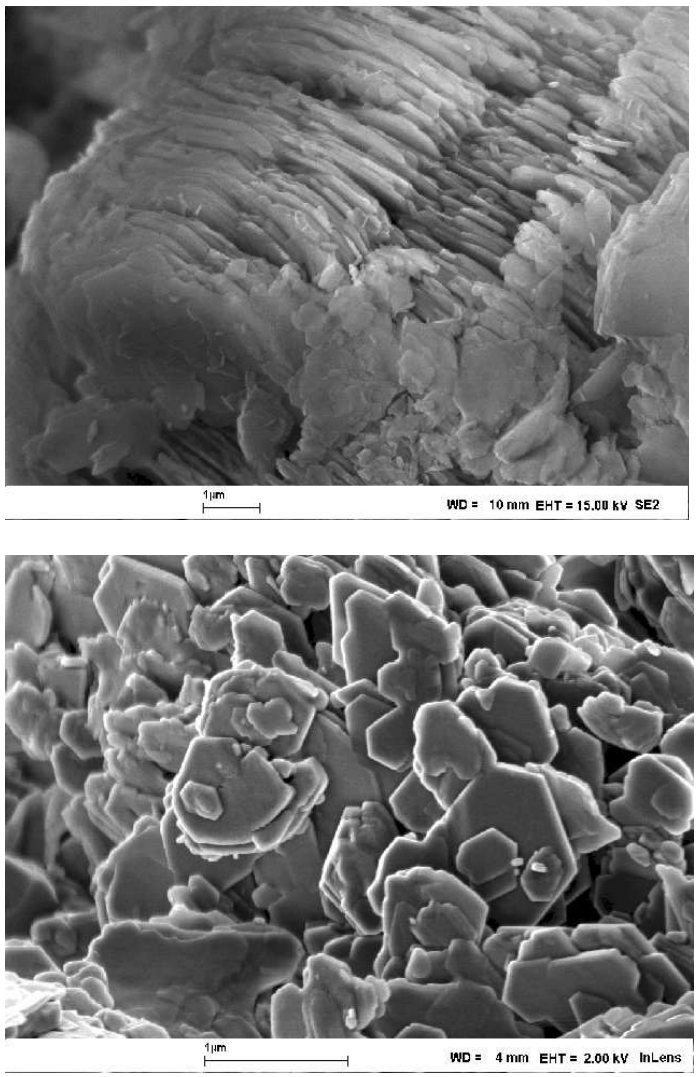


Figure 5.5: Structure of kaolin after thermal treatment (p=atm., t=850°C)

within the particles. The structure of the thermally untreated particles is presented in Fig. 5.4. The structure of kaolin after thermal treatment (Fig. 5.5) is very similar. Investigation of kaolin that has reacted with KCl showed a similar structure as unreacted kaolin. Similarly we can observe that the structure of kaolin that reacted with KCl with the steam present remained the same (Fig. 5.6).

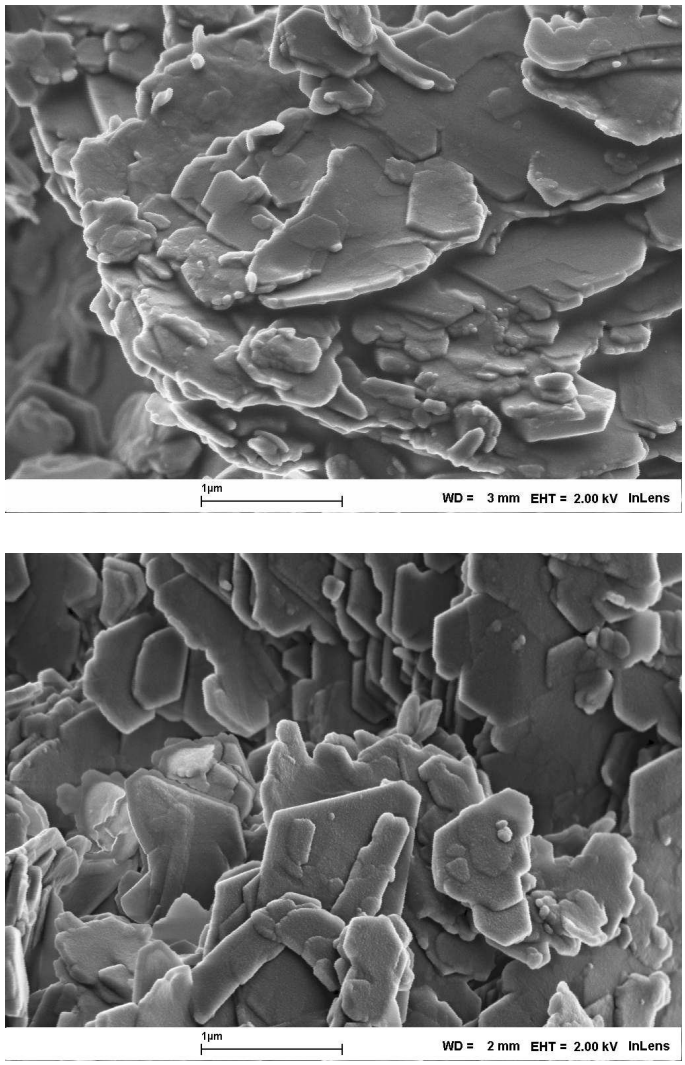


Figure 5.6: Structure of kaolin after reaction with KCl, upper - nitrogen atmosphere, lower - nitrogen+steam atmosphere (p=atm., t=850°C)

5.3.3 Elemental composition of samples

The elemental compositions of the samples were determined with a SEM/EDS apparatus. The composition of the kaolin used in the tests is presented in table 5.2. The amount of potassium present in the kaolin before the experi-

Table 5.2: Elemental composition of kaolin, SEM/EDS, as received as determined with the SEM/EDS.

Element	wt [%]	Element	wt [%]
Na	0.18	Ti	0.07
Mg	0.02	Fe	0.87
Al	21.22	P	0.16
Si	25.65	Cl	0.06
K	2.41	O (by diff.)	49.31
Ca	0.03		

Table 5.3: Chemical analysis of the samples, the total amount of absorbed potassium per kilogram of kaolin - comparison between wet analysis and EDS

ELEMENT	**SAMPLE**	**6353**	**6357**	**6361**	**6359**
		big holder	big holder	big holder	big holder
		KCl + kaolin	KCl + kaolin	KCl + kaolin	KCl + kaolin
		full time, 850oC	10 min. - 850oC	full time - 800oC	10 min. - 800oC
K - w.a.	mg/kg TS	55300	34300	54500	28300
K – EDS	mg/kg	60997	47200	67100	30800
ELEMENT	**SAMPLE**	**6367**	**6363**	**6365**	
		small holder	small holder	small holder	
		KCl - kaolin	KCl - kaolin	KCl - kaolin	
		full time, 850oC	10min. - 850oC	10min. - 800oC	
K - w.a.	mg/kg TS	46800	27300	25300	
K – EDS	mg/kg	57100	21000	26800	

ments was subtracted from the total amount analyzed after the experiments. The potassium detected in the kaolin can be considered as natural impurities. The used potassium chloride was a high purity material delivered by Merck. Furthermore, a number of selected samples were sent for wet chemical analysis. The results are shown in table 5.3 and represent the total amount of absorbed potassium per kilogram of kaolin. The literature findings for the kaolin indicating the maximum alkali metals sorbing capacity (no water in the gas stream) are shown in table 5.4 together with the comparison for other sorbing compounds like Emathlite and Diatomaceous Earth. The maximum values reported were at the level of 266 mg/g. For the performed TG tests the maximum values (table 5.3) were at the level of 60 mg K/mg of kaolin for the full time tests. For the 10 minutes tests they varied between 21 mg K/g to 41 mg K/g

Table 5.4: Amount of alkali metals absorbed per g of sorbent [Turn et al., 1998a]

	Absorbed amount in mg/g of the getter
Emathlite	150-190
Diatomaceous	18
Kaolinite	max. 266

of kaolin. It has to be pointed out that the kaolin particles were not fully saturated after the full time tests. It was found in the literature [Punjak et al., 1989; Scandrett and Clift, 1984] that after saturation no desorption was observed for kaolin. That means that the measured values of the full time tests do not represent the maximum sorbing capacity of kaolin. The compositions of the kaolin samples after the TGA runs in 100% N_2 are given in Fig. 5.7. It can be seen that the longer the time of reaction the higher the potassium content in the analyzed samples. The influence of the temperature on the potassium capture is less visible. The concentration of potassium in the kaolin from tests in 100% N_2 varied from about 6%, when the test lasted for ten minutes, to almost 17% for the complete evaporation runs. Large variations can be observed when comparing the potassium capture efficiencies under different operational conditions. First of all, as expected, the shortest runs within 10 minutes time frame are characterized with the lowest concentration of K. For runs 6363 and 6365 (10 minutes runs, small holder) values of detected potassium within the kaolin sample were at the level of approx. 2.5%. It is only slightly higher than the level of potassium as impurities in pure kaolin (Fig. 5.8). The differences for the total amount of the absorbed potassium observed between two sample holder geometries for 10 minutes runs and the investigated temperatures range don't let to conclude any definite trends. For 850°C, the bigger sample holder is in favor, the ten minutes run (6357) is finished with total amount of absorbed potassium at the level of 4.72%. On the contrary for lower temperatures the test with the smaller sample holder had more of potassium absorbed. Run 6365 ended with 0.72% as the total K absorbed. In general ten minutes runs in lower temperatures ended with lower absorption rates. This can be expected because of the reaction kinetics. The results from the runs with steam (Fig. 5.9) present showed a large increase of potassium absorption compared to the tests with no water (Fig. 5.8). The improvement was the highest in the runs with 15% H_2O and 85% N_2, with no CO_2 or O_2 present (for example run 6375). In this case the total potassium absorption (as percentage of the input of the potassium to the system) was more than 23%. The influence of water on the effectiveness of the absorption reaction has also been reported in the literature [Turn et al., 1998b; Punjak and Shadman, 1988; Tran et al., 2005] but

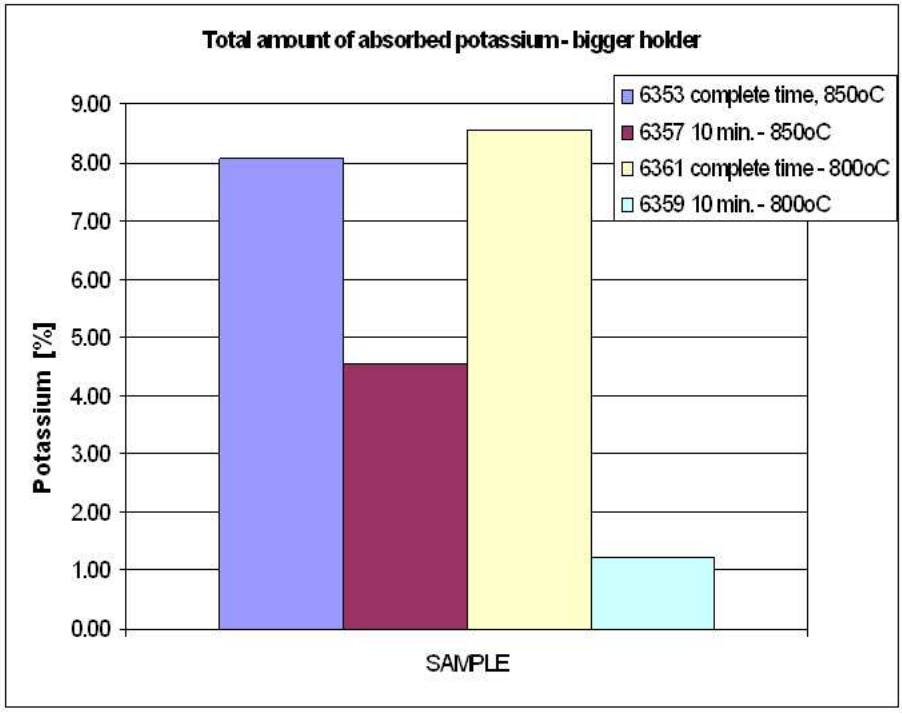


Figure 5.7: Potassium absorption (as percentage of the input potassium) in the kaolin samples based on EDS analysis (100% N_2atmosphere) - bigger holder

experimental data are scarce. The available literature reports that water may help potassium to penetrate the matrix of the clay [McLaughin, 1990]. Tran et al. [Tran et al., 2005] suggested the following mechanism with water present, splitting the overall reaction into two steps with different reaction rates.

$2KCl_{(g)} + A \rightleftharpoons A*2KCl$ *slow (rate limiting) (1)*

$A*2KCl + H_2O_{(g)} \rightleftharpoons K_2O*A + 2HCl_{(g)}$ *rapid (2)*

Where A stands for a vacant active site on meta-kaolin surface and

$K_2O*S = K_2O*Al_2O_3*2SiO_2 = 2KAlSiO_4$

The experimental findings confirm that water present in the gas phase may substantially increase the production of gaseous HCl and help to release potas-

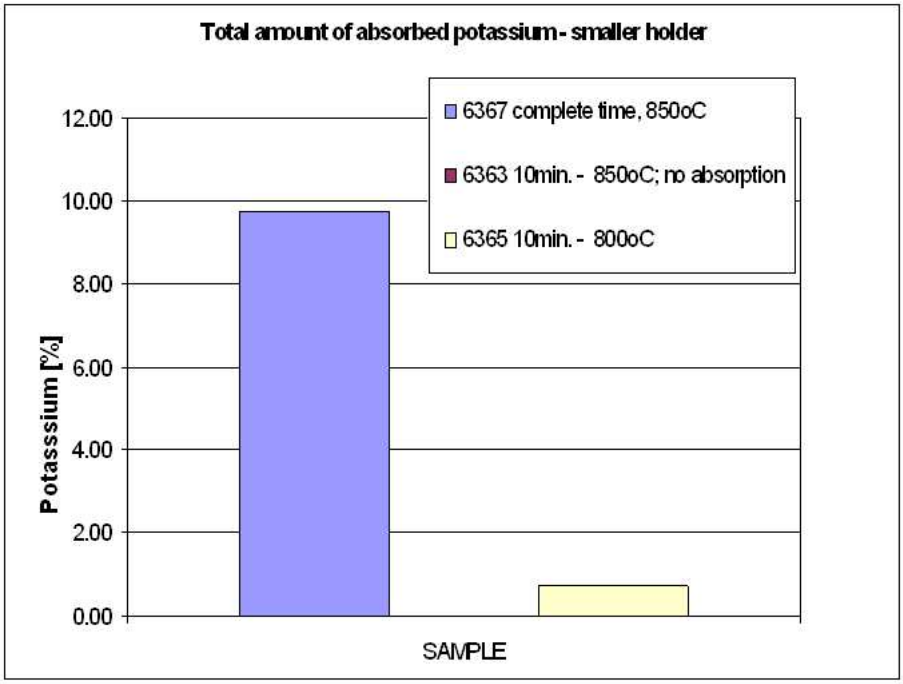


Figure 5.8: Potassium absorption (as percentage of the input potassium) in the kaolin samples based on EDS analysis (100% N_2 atmosphere) - smaller holder

sium making it available for reaction with kaolin (Fig. 5.9). In the tests with steam, oxygen and carbon dioxide in the gas (6379) the potassium values were lower than with only water and nitrogen but still reaching almost 15%. The competition for available potassium between oxygen and aluminum-silicates within kaolin particle can be the reason for lower values. In the case with complete evaporation the EDS elemental analysis of the whole surface is comparable with the cross section values (Fig. 5.10). In both cases (for instance sample 6353), more than 8% of total potassium input was absorbed. For the short 10 minutes runs the situation looks different. In sample 6357 the surface concentration of potassium was about 4%, excluding the kaolin background potassium, while in the cross section investigation after correcting with amount of the background potassium values are close to zero. For sample 6359 it is 0.72% for the cross-section (Fig. 5.10). Reason for this can be that kaolin particles in the sample holder may not be in contact with KCl gas within the time of experiment.

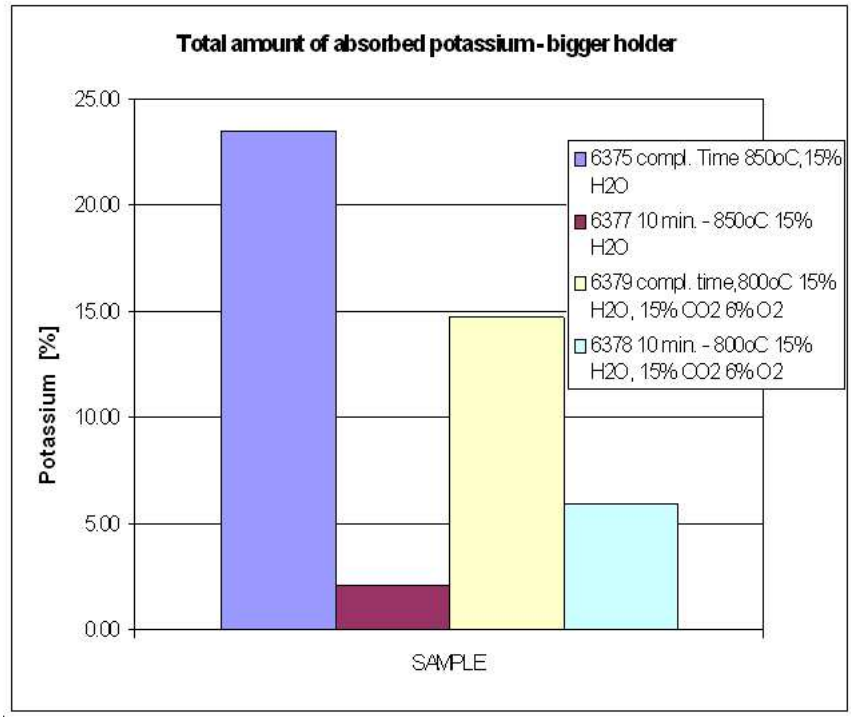


Figure 5.9: Potassium absorption (as percentage of the input potassium) in the kaolin samples based on EDS analysis (tests with steam)

5.3.4 Cross section investigation with SEM/EDS and X-ray mapping

Cross section cuts of the kaolin samples were prepared to investigate whether the reaction between gaseous KCl and kaolin took place only on the surface of the particles or/and within the whole volume of the kaolin particles. The sample preparation was done by casting the reacted kaolin particles into epoxy and then cutting the sample to get cross sections of the particles. The cutting and the sample preparation was performed without any contact with water to prevent leaching. The cut particles were then studied with SEM. An X-ray map from a test with complete KCl evaporation time (approx. 3200 sec.) at 850°C is presented in Fig. 5.11 (6353), while an X-ray map of a 10 minute sample reacted under the same operational conditions is shown in Fig. 5.12 (6357). Focusing on the phenomena responsible for potassium capture we would expect that if there were only physical adsorption, KCl should be found on the surface of the kaolin particle. Physical adsorption is characterized by van der Waals

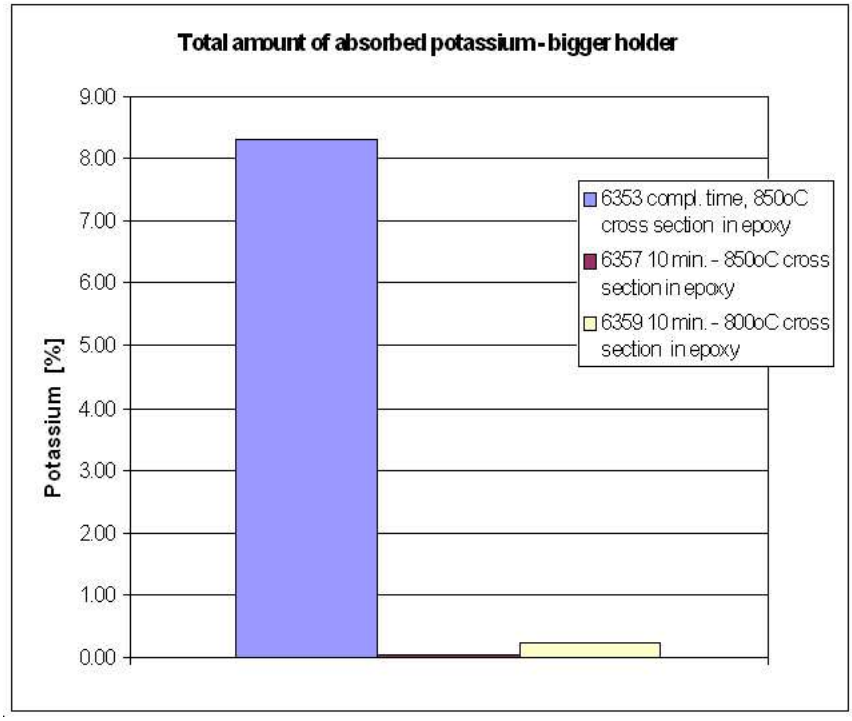


Figure 5.10: Potassium absorption (as percentage of the input potassium) - bigger holder, cross section in epoxy

or dispersion forces and it reaches equilibrium very fast. During the process several layers of KCl can be formed on a particle. Opposite to physical adsorption where the adsorbed component can be released when its partial pressure decreases, the chemisorption binds molecules more firmly [Turn et al., 1998b]. We can see from Fig. 5.11 that the whole cross section area for sample 6353 is characterized with the same concentration of K regardless the position on the kaolin particle. Furthermore only atomic potassium was detected without chlorine present although the potassium was introduced as a chloride. It means that not only adsorption of KCl (g) on the kaolin particle takes place, but also that a reaction takes place step by step within the whole porous kaolin particle. It can be stated that there is chemisorptive interaction between the solid and the potassium. For run 6357 with no steam the X-ray mapping revealed a reaction front inside the particle. Approximately 5μm of particle was reacted within 10 min. run which gives approx. 0.5 μm/min of reaction speed for the operational conditions used in the experiment. Comparing these results with

the X-ray mapping of sample 6378 (Fig. 5.13 with steam) it can be observed that the rate was much faster, approx. 100 to 50 μm of the particle was reacted in the same time, which means that the rate was ten times higher. However, as a cause of the experimental setup, it is not clear whether the kaolin particles really were in contact with the gas during the entire test. To check the above and also the calculated reaction rates, experiments with a mono-layer of kaolin particles in KCl gas should be performed. Thus the problem with the KCl diffusion to the inner kaolin particles in the sample holder would be omitted

5.4 Conclusions

The experiments have been performed in order to investigate whether kaolin can be used as an alkali absorbent. The aim was to obtain a deeper understanding of the mechanisms and characterize its dependence of different experimental parameters e.g. temperature, water. The results confirmed that kaolin can be successfully used as an absorbent of alkali metals under combustion conditions. The unique and new images of SEM/EDS elemental analysis of the reacted kaolin samples showed that the capture of alkali is not only, if at all, an adsorption phenomena but also, or only, a chemical reaction, since potassium could be found within the whole structure of the kaolin particle and not only on the surface. This was furthermore supported by the fact that no chlorine was present within the kaolin particles after the tests, although the potassium was introduced as a chloride. The investigation of the kaolin particles morphology showed that the particle was highly porous consisting of interlaying aluminum oxide – silica oxide sheet. Even though the kaolin particles were highly porous the reaction seemed to be controlled by diffusion within the particle. The investigation revealed the novel images of X-ray mapping showing clearly the front of reaction moving within the kaolin particle. As could be seen from the results, the amount of absorbed alkali was dependant on the experimental conditions. Under the scope of the in chapter 2 defined research goals the chapter 5 presents novel findings about KCl capture. Especially, the composition of the gas phase played an important role, e.g. by introducing steam to the gas phase the final potassium content was much higher than without steam. X-ray mapping confirmed that water present in the gas phase promoted the absorption process. The research revealed the absorption rate which was approx. 10 times higher with steam present in the gas phase. In the runs where all KCl was allowed to evaporate the effect of temperature within the tested range (800-850°C) was not so strong. However, in the runs that were interrupted after 10 minutes the temperature effect was more pronounced.

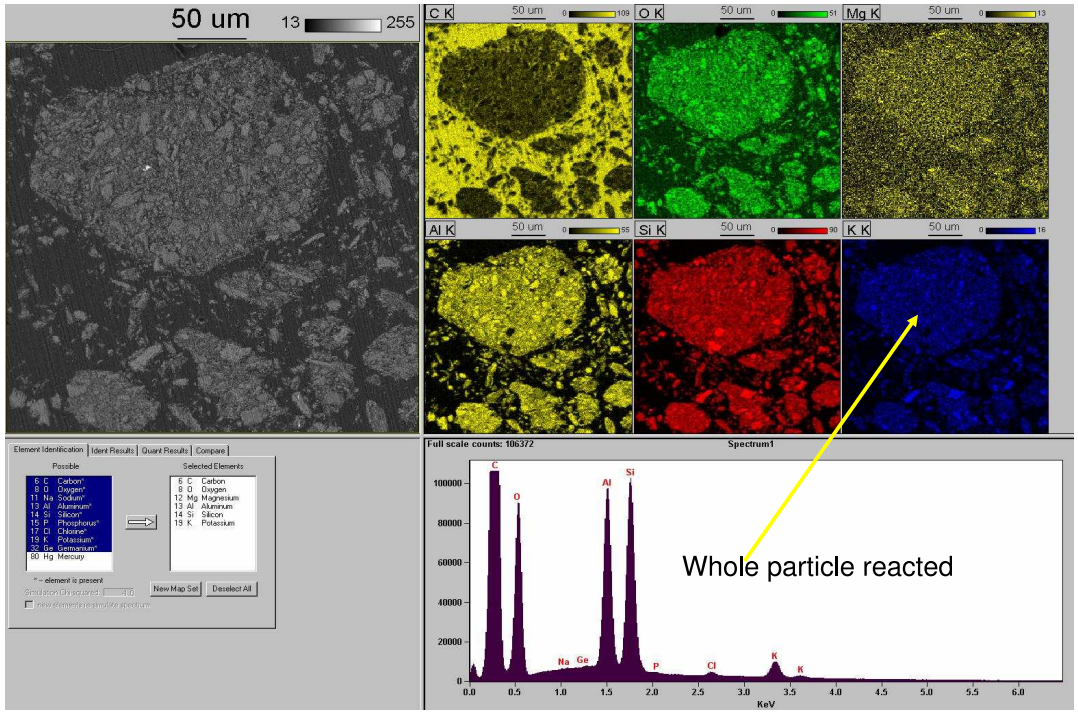


Figure 5.11: X-ray mapping of kaolin particles, full evaporation time, sample 6353

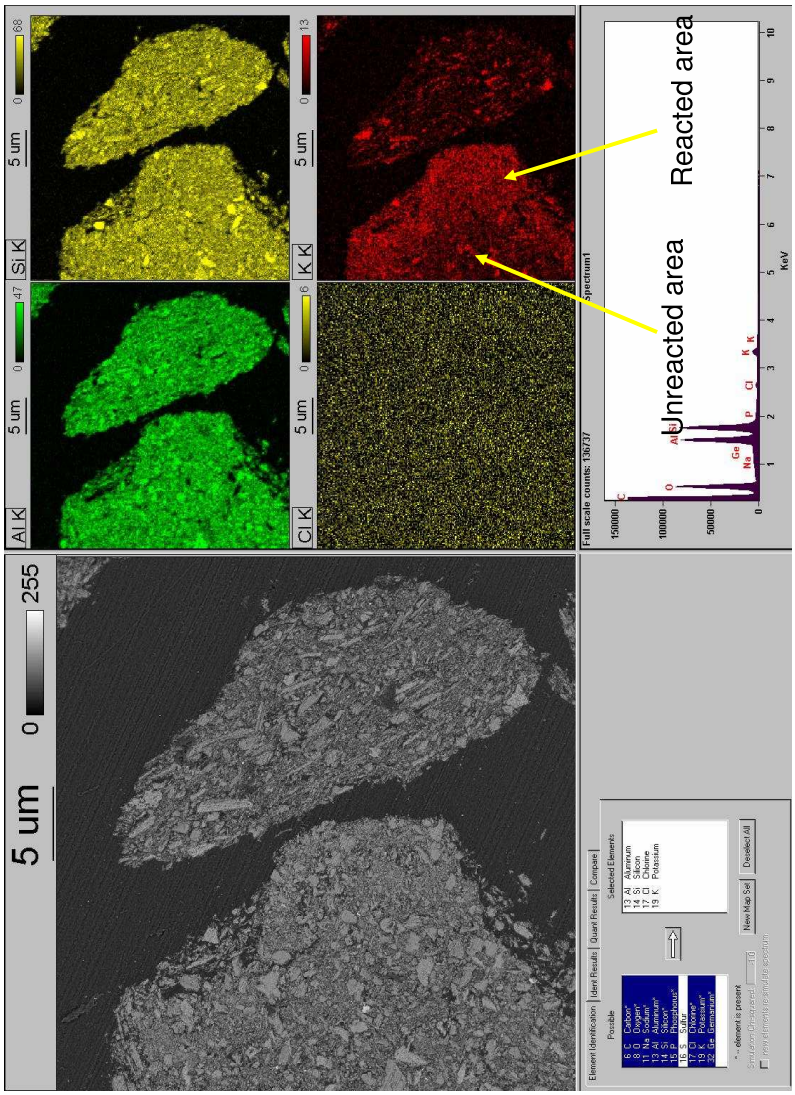


Figure 5.12: X-ray mapping of kaolin particles, 10 min run, sample 6357, front of reaction visible for K, N_2 atmosphere

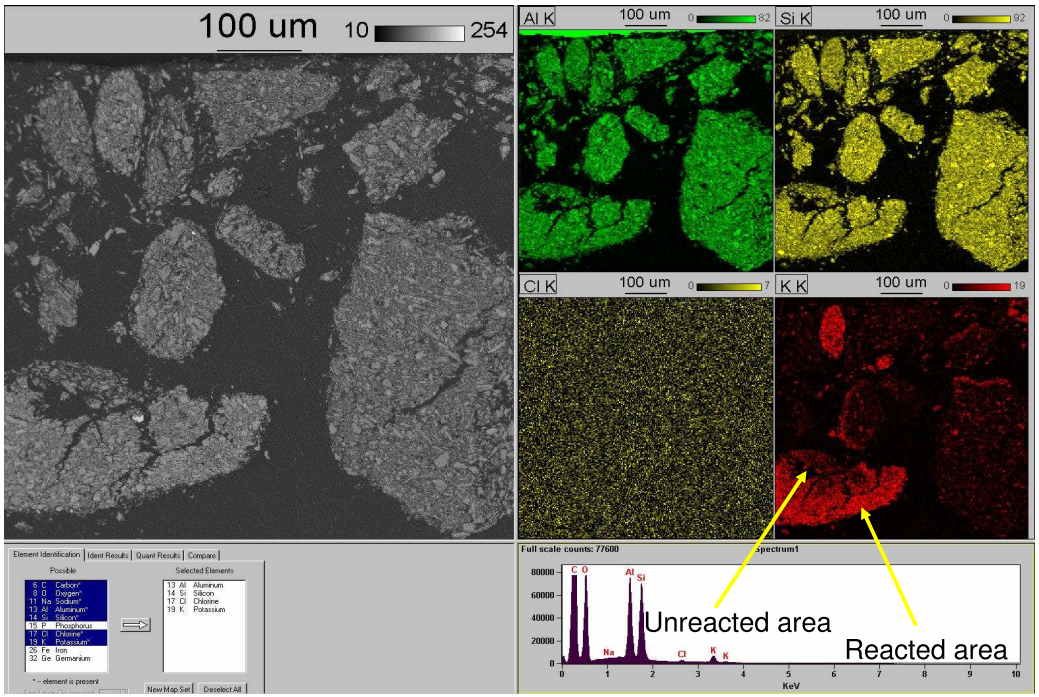


Figure 5.13: X-ray mapping of kaolin particles, c) 10 min. run, 15% steam, 6% O_2, 15% CO_2 and N_2 atmosphere, sample 6378

Chapter 6

Final conclusions and recommendations

6.1 Conclusions

The final conclusions presented in this chapter summarize the performed work in view of the research requirements presented at the end of chapter 2.

6.1.1 Experimental work

The experimental work included the combustion experiments performed on the CFB combustor available in the Section Energy Technology and the fundamental investigation of KCl - kaolin interactions. Moreover, some preliminary studies on the heated grid reactor were performed and are included in Appendix A.

The experimental work on the CFB reactor with help of ELIF measuring technique extended the scarce knowledge about straw-coal co-combustion in CFB systems and revealed very high concentrations of gaseous alkali metals in combustion gases of the specially selected HIAL straws. The values in the order of several ppmv were measured and in case of HIAL 7 even above 200 ppmv, such high values would cause operational problems (like corrosion or/and deposit formation) to the down-stream equipment in power producing units.

Proceeding further with the in chapter 2 defined research requirements, the co-combustion tests revealed that the addition of coal lowered the measured values of the alkali metals and blending can be considered as positive. The decrease of the measured values was not only the effect of the lower alkali input but also, as shown in chapter 4, an effect of the chemical interaction between the coal and the alkali metals originating from straw.

The detailed study of kaolin, a promising alkali getter and common clay mineral, revealed the porous, plate-like structure of the mineral. SEM/EDS anal-

ysis revealed multiple silica alumina layers within the structure of kaolin. Because of this composition, the porous structure and previously reported in literature most promising alkali capturing capabilities, kaolin was chosen for further investigation revealing more information about the absorption process.

Unique and new images of SEM/EDS elemental analysis of the reacted kaolin samples showed that the capture of alkali is not only an adsorption phenomena but also and predominately a chemical reaction, since potassium could be found within the whole structure of the kaolin particle and not only on the surface. The conclusion about the reacting KCl-kaolin system was supported by the fact that no chlorine was found within the particle. Moreover the potassium content was depending on the reaction time. It was concluded that the reaction was diffusion controlled. The investigation revealed the novel images of X-ray mapping showing clearly the front of reaction moving within the kaolin particle.

Promising for further applications was the fact that the gas phase composition played an important role in the process. Introduction of steam to the gas phase increased the potassium absorption. Steam, present in the gas phase promoted the absorption of potassium within the kaolin particle. It was proved in this thesis that water in the gas phase resulted in the increased final potassium content. The speed of the reaction was approx. ten times higher.

The synergy effect experienced during blending of coal with straw can help to minimize the negative impact of high alkali metals content in straw, can be beneficial for power operators promoting a broader implementation of herbaceous fuels for energy production. Alumina silicates minerals present in coal ash were proved to bind alkali metals effectively and lower the alkali emissions. Especially the blending can be beneficial for CFB operating plants characterized with greater fuel flexibility.

6.1.2 Modelling work

The modelling work included chemical equilibrium modelling using the commercially available FactSage program. The main findings confirm and provide more explanation to the experimental observations.

The fuels differed in composition. HIAL 3 and HIAL 9 were rich in silica and chlorine, while HIAL 7 was characterized with a very high potassium level. HIAL 4 contained relatively big amounts of calcium. For HIAL 3 and HIAL 9 with relatively high content of K and chlorine KCl release to the gas phase was according to equilibrium calculations higher than for other fuels. Potassium to silica ratio was varying for the fuels, being extreme in case of HIAL

7. Alkali metals if bound with alumina-silicates originating from coal and/or from additives are not volatile under CFB combustion conditions and stay in the solid phase, mainly in the form of bottom or fly ash. It means they are not so troublesome like the ones present in the gaseous form. In the simulations the formation of alumina-silicates was found to be dominant in the defined system. Formation of alkali sulfates was present, especially with higher shares of coal but the formation of alumina-silicates was found to be more important. Mixing with coal strengthened the formation of alkali alumina silicates and for different coal shares formation of these compounds was dominant. Hence the blending had a positive effect on alkali sequestering. The positive effect is not only the result of dilution but mainly chemical reaction between coal originating alumina-silicates and alkali metals from straw.

6.2 Recommendations

Taking into account the findings of this research the following recommendations are proposed.

6.2.1 Experimental work

Alkali concentration measurements using a wet trapping technique should be avoided as these are very prone to errors. They should not be taken as reference to further tests. It is very difficult to avoid or/and estimate quantitatively the error in measurements.

It is recommended to improve the ELIF resistance to the optical access window contamination. The very high particulate content originating from HIAL 9 blocked the optical access window. Better gas purging should be applied. Moreover it is recommended to improve the particle sampling over the system. Especially the fly and filter ash sampling should be improved. Implementation of a particle impactor for the fly ash sampling would allow better physical and chemical resolution of the fine particles and help with the mass balance closure.

It would be recommended to continue the investigation of alkali sorbing additives like kaolin on pilot plant scale CFB combustors. Tests with the kaolin and HIAL straw-coal co-combustion at different experimental conditions should be performed with detailed measurements of the gaseous alkali metals content together with investigation of the fly and bottom ash. The experimental techniques should be improved by means of better bottom and fly ash sampling.

The fundamental studies of kaolin-alkali metals interaction presented in the chapter 5 are being continued. The group at Åbo Akademi, Finland decided to

continue with the initiated tests. The researchers there are trying to understand in more details the capture process inside the kaolin particle and influence of additional parameters on it. The promising studies with water addition should be extended to investigate the phenomenon of the increased alkali absorption. The phenomena where water present in the flue gases promotes the absorption reaction may be of great importance for the system where fuels with high water content like straw are burned.

6.2.2 Modelling work

Taking into account the chemical equilibrium modelling part of the thesis it would be recommended to model the influence of water for the equilibrium system. It would be interesting to focus on a sensitivity analysis for water. It is also advised to perform a sensitivity analysis for the alumina-silicates content in the system. In this work the chemical equilibrium modelling was focused on the selected fuels and their interactions but from a scientific point of view investigating the maximal sorbing capacities of different clays and mechanisms responsible for that would provide new, interesting information about the system behavior.

The results of the equilibrium calculations included in this thesis should be expanded with the equilibrium calculations taking into account the kinetics and in particular the sulfation kinetics in order to present more complete model of the system.

In order to simulate the reactor conditions as realistic as possible the influence of silica sand may be an interesting issue. It would be recommended to address this issue in further research. Because of the time limitations this research was not done but it is still an open discussion which part of the silica rich bed material take into account in the simulations.

The sensitivity analysis for some parameters like chlorine or sulfur would provide in the end some additional scientific value to the research presented in thesis. The burden of work to model each of the system is big enough to provide fruitful material for further research.

References

Aho, M. and Ferrer, E. (2004). Preventing chlorine deposition on heat transfer surfaces with aluminium-silicon rich biomass residue and additives. *Fuel*, 83:1299–1305.

Aho, M. and Ferrer, E. (2005). Importance of coal ash composition in protecting the boiler against chlorine deposition during combustion of chlorine-rich biomass. *Fuel*, 84(2–3):201–212.

Andersen, K. (1998). *Deposit formation during coal-straw co-combustion in a utility PF-boiler*. PhD thesis, Technical University of Denmark.

Bale, C. (2002). Factsage thermochemical software and databases. *Calphad*, 26(2):189–229.

Barin, I. (1977). *Thermochemical Properties of Inorganic Substances*. Springer-Verlag, Berlin.

Basu, P. (1999). Combustion of coal in circulating fluidized-bed boilers: a review. *Chemical Engineering Science*, 54:5547–5557.

Basu, P. and Fraser, S. (1991). *Circulating Fluidized Bed boilers, design and operation*. Butterworth-Heinemann.

Baxter, L. (1993). Ash deposition during biomass and coal combustion - a mechanistic approach. *Biomass & Bioenergy*, 4(2):85 – 102.

Baxter, L. L., Miles, T. R., Miles, T. R., Jenkins, B. M., Milne, T., Dayton, D., Bryers, R. W., and Oden, L. L. (1998). The behavior of inorganic material in biomass-fired power boilers: field and laboratory experiences. *Fuel Process. Technol.*, 54:47–78.

Blander, M. (1997). The inorganic chemistry of the combustion of aspen wood with added sulfur. *Biomass & Bioenergy*, 12(4):289 – 293.

Blander, M., Milne, T., Dayton, D., Backman, R., Blake, D., Kuhnel, V., Linak, W., Nordin, A., and Ljung, A. (2001). Equilibrium chemistry of biomass combustion: A round-robin set of calculations using available computer programs and databases. *Energy & Fuels*, 15(2):344 – 349.

Brem, G., editor (2003). *Advanced waste incineration concepts*, Waste Symposium.

Chadwick, B., Ashman, R., Campisi, A., Crofts, G., Godfrey, P., Griffin, P., Ottrey, A., and Morrison, R. (1996). Development of techniques for monitoring gas-phase sodium species formed during coal combustion and gasification. *International Journal of Coal Geology*, 32(1-4):241 – 253.

Chadwick, B., Griffin, P., and Morrison, R. (1997). Quantitative detection of gas-phase naoh using 355-nm multiple-photon absorption and photofragment fluorescence. *Applied Spectroskopy*, 51(7):990 – 993.

Chirone, R., Salatino, P., and Scala, F. (2000). The relevance of attrition to the fate of ashes during fluidized-bed combustion of a biomass. *Proc. Combust. Inst.*, 28:2279–2286.

Christensen, K. and Livbjerg, H. (2000). A plug flow model for chemical reactions and aerosol nucleation and growth in an alkali-containing flue gas. *Aerosol Science and Technology*, 33(6):470–489.

Christensen, K., Stenholm, M., and Livbjerg, H. (1998). The formation of submicron aerosol particles, HCl and SO_2 in straw-fired boilers. *J. Aerosol Sci.*, 29(4):421–444.

Cleve, K. (1999). Latest developments and status of long term experience in cfb technology. In *Proc. 15th ASME Conference on Fluidized Bed Combustion*.

Coda, B., Aho, M., Berger, R., and Hein, K. R. G. (2001). Behavior off chlorine and enrichment of risky elements in bubbling fluidized bed combustion of biomass and waste assisted by additives. *Energy&Fuels*, 15:680–690.

Davidsson, K. O., Engvall, K., Hagstrom, M., Korsgren, J. G., Lonn, B., and Pettersson, J. B. C. (2002a). A surface ionization instrument for on-line measurements of alkali metal components in combustion: Instrument description and applications. *Energy&Fuels*, 16:1369–1377.

Davidsson, K. O., Korsgren, J. G., Pettersson, J. B. C., and Jaglid, U. (2002b). The effects of fuel washing techniques on alkali release from biomass. *Fuel*, 81:137–142.

Davidsson, K. O., Stojkova, B. J., and Pettersson, J. B. C. (2002c). Alkali emission from birchwood particles during rapid pyrolysis. *Energy&Fuels*, 16:1033–1039.

Dayton, D. C., Belle-Oudry, D., and Nordin, A. (1999a). Effect of coal minerals on chlorine and alkali metals released during biomass/coal cofiring. *Energy&Fuels*, 13:1203–1211.

Dayton, D. C., Jenkins, B. M., Turn, S. Q., Bakker, R. R., Williams, R. B., Belle-Oudry, D., and Hill, L. M. (1999b). Release of inorganic constituents from leached biomass during thermal conversion. *Energy&Fuels*, 13:860–870.

Dayton, D. C. and Milne, T. A. (1995). Mechanisms of alkali-metal release during biomass combustion. *Abstr. Pap. Am. Chem. Soc.*, 210:87–FUEL.

de Jong, W. (2005). *Nitrogen compounds in pressurized fluidised bed gasification of biomass and fossil fuels*. PhD thesis, Delft University of Technology.

de Nevers, N. (2002). *Physical and chemical equilibrium for chemical engineers*. John Wiley & Sons.

Denbigh, K. (1981). *The prnciples of chemical equilibrium; with applications in chemistry and chemical engineering*. Cambridge University Press.

Dou, B., Shen, W., Gao, J., and Sha, X. (2003). Adsorption of alkali metals vapors from high-temperature coal-derived gas by solid sorbents. *Fuel Processing Technology*, 82:51–60.

Drury, T., Roberts, G., and Roberts, J. (1962). *Advancess in Glass Technology*. Plenum Press.

Edgecombe, L. (1956). The state of combination of chlorine in coal. Extraction of coal with water. *Fuel*, 35.

EHN (2004). 25mw straw-fired, high efficiency power plant. Technical report, EU information booklet.

Eriksson, G. and Hack, K. (1990). Chemsage - a computer program for the calculation of complex chemical equilibria. *Metalurgical Transactions B*, 21B:1013.

European Commission (1998a). Biomass heat.

European Commission (1998b). EU study funded by the altener programme in 1998/9.

European Renewable Energy Council (2000). Renewable Energy Target for Europe.

Fallgren, T. (1991). Gasanalyse in der zementindustrie. *Zement-Kalk-Gips*, 44:309–315.

Fisher, J. (1977). *The resistance of ceramics to chemical corrosion*. The Chemical Society, London.

Freihaut, J. and Proscia, W. (1989). Tar evolution in heated-grid apparatus. *Energy & Fuels*, 3:625–635.

Furimsky, E. and Zheng, L. (2003). Qualification of chlorine and alkali emissions from fluid bed combsution of coal by equilibrium calculation. *Fuel Processing Technology*, 83:7–21.

Gabra, M., Nordin, A., Öhman, M., and Kjellström, B. (2001). Alkali retention/separation during bagasse gasification: a comparison between a fluidised bed and a cyclone gasifier. *Biomass & Bioenergy*, 21:461–476.

Gibbins-Matham, J. and Kandiyoti, R. (1988). Coal pyrolysis yields from fast and slow heating in a wire-mesh apparatus with a gas swept. *Energy & Fuels*, 2:505–511.

Glarborg, P. and Marshall, M. (2005). Mechanism and modelling of the formation of gaseous alkali sulfates. *Combustion and Flame*, 141:22–39.

Gottwald, U., Monkhouse, P., and Bonn, B. (2001). Dependence of alkali emissions in PFB combustion on coal composition. *Fuel*, 80:1893–1899.

Gottwald, U., Monkhouse, P., Wulgaris, N., and Bonn, B. (2002a). In-situ study of the effect of operating conditions and additives on alkali emissions in fluidised bed combustion. *Fuel Process. Technol.*, 75:215–226.

Gottwald, U., Monkhouse, P., Wulgaris, N., and Bonn, B. (2002b). In-situ study of the effect of operating conditions and additives on alkali emissions in fluidised bed combustion. *Fuel Process. Technol.*, 75:215–226.

Grim, R., editor (1962). *The kaolin deposits of Georgia and South Carolina*, volume 14 of *23rd International Geological Congres*.

Guenther, W. B. (1975). *Chemical equilibrium; a practical introduction for the physical and life sciences*. Plenum.

Hack, K. (1995). *FactSage, program for chemical equilibrium modelling - manual*.

Hald, P. (1994). *Alkali Metals at Combustion and Gasification Equlibrium Calculations and Gas Phase Measurements*. PhD thesis, Technical University of Denmark.

Hansen, L., Frandsen, F., and Dam-Johansen, K. (1999). Characterization of ashes and deposits from high temperature coal-straw co-firing. *Energy & Fuels*, 13:803–816.

Hansen, P., Bank, L., and Dam-Johansen, K. (1995). In-situ measurements in fluidized bed combustors: design and evaluation of four sample probes. In *Fluidized Bed Combustion - Volume 1*.

Haÿrinen, V., Hernberg, R., and Aho, M. (2004). Demonstration of plasma excited atomic resonance line spectroscopy for on-line measurement of alkali metals in a 20 kW bubbling fluidized bed. *Fuel*, 83:791–797.

Heikinnen, J. (2005). *Characterisation of supplementary fuels for co-combustion with pulverised coal*. PhD thesis, Delft University of Technology.

Hein, K. and Bemtgen, J. (1998). EU clean coal technology - co-combustion of coal and biomass. *Fuel Processing Technology*, 54:159–166.

Huffaman, G., Huggins, F., Shah, N., and Shah, P. (1990). Behaviour of basic elements during coal combustion. *Prog. Energy Combust. Science*, 16:243–251.

Iisa, K., Salmenoja, K., and Baxter, L. (1999). Sulfation of potassium at combustion conditions. *Energy&Fuels*, 13:1184–1190.

Jacobs, J. (1999). The future of fluidized-bed combustion. *Chemical Ebgineering Science*, 54:5559–5563.

Jenkins, B. M., Bakker, R. R., and Wei, J. B. (1996). On the properties of washed straw. *Biomass Bioenerg.*, 10:177–200.

Jensen, J., Nielsen, L., Schultz-Moller, C., Wedel, S., and Livbjerg, H. (2000a). The nucleation of aerosols in flue gases with a high content of alkali - a laboratory study. *Aerosol Science and Technology*, 33(6):490 – 509.

Jensen, P., Frandsen, F., Dam-Johansen, K., and Sander, B. (2000b). Experimental investigation of the transformation and release to gas phase of potassium and chlorine during straw pyrolysis. *Energy & Fuels*, 14:1280–1285.

Jensen, P., Stenholm, M., and Hald, P. (1997). Deposition investigation in straw-fired boilers. *Energy & Fuels*, 11(5):1048 – 1055.

John, R. (1984). *High Temperature corrosion in Energy Systems*, chapter High temperature condensation of deposits based on Na, Cl, S, Fe and O and the corrosion of Fe. AIME.

Kassman, H., Abul-Milh, M., and Amand, L. (1995). Measuerements of NH_3 and HCN concentrations in a CFB boiler, a comparison between a conventional absorption and FTIR technique. *Fluidized Bed Combustion - ASME*, 2.

Kassman, H. and Amand, L. (2001). Secondary effects in sampling ammonia in the combustion chamber of a cfb boiler. *42nd IEA-Fluidized Bed Conversion meeting*.

Kaufmann, H. (1997). *Chlorine compounds in emissions and residues of herbaceous biomass*. PhD thesis, Swiss Federal Institute of Technology, Zurich.

Khan, N. (2004). Thermodynamic equilibrium modeling of high alkali (HIAL) fuels and co-combustion of coal-HIAL fuels for CFB. Master's thesis, Delft University of Technology.

Kingery, W. (1976). *Introduction to ceramics*. John Wiley & Sons.

Lee, S. and Johnson, I. (1980). Removal of gaseous alkali metal compounds from hot flue gas by particulate sorbents. *Journal of Engineering for Power*, 102:397–402.

Lee, S., Teats, F., Swift, W., and Banerjee, D. (1992). Alkali-vapor emission from PFBC of Illinois coals. *Combust. Sci. and Tech.*, 86:327–336.

Lin, W., Dam-Johansen, K., and Frandsen, F. (2003). Agglomeartion in bio-fuel fluidized bed combustors. *Chemical Engineering Journal*, 96:171–185.

Lind, T. (1999). *Ash formation in circulating fluidized bed combsution of coal and solid biomass*. PhD thesis, Technical Research Centre of Finland, VTT.

Mann, M. and Spath, P. (2001). A life cycle assesment of biomass cofiring in a coal-fired power plant. *Clean Products and Processes*, 3:81–91.

Manzoori, A. and Agarwal, P. (1992). The fate of organically bound inorganic elements and sodium-chloride during fluidized-bed combustion of high sodium, high sulfur low rank coals. *Fuel*, 71(5):513 – 522.

McLaughin, J. (1990). *The removal of volatile alkali salt vapours from hot coal-derived gases*. PhD thesis, Univeristy of Surrey, Guildford.

McMullan, J. (2004). Fossil fuel power generation. state-of-the-art. Technical report, PowerClean Thematic Network.

Meites, L. (1981). *An introduction to chemical equilibrium and kinetics*. Oxford:Pergamon.

Miles, T. R. (1996). Alkali deposits found in biomass boilers the behaviour of inorganic material in biomass fired power boilers field and laboratory experiments. Technical report, Sandia National Laboratory.

Miles, T. R., Miles, T. R., Baxter, L. L., Bryers, R. W., Jenkins, B. M., and Oden, L. L. (1996). Boiler deposits from firing biomass fuels. *Biomass Bioenerg.*, 10:125–138.

Mojtahedi, W. and Backman, R. (1989). The fate of sodium and potassium in the pressurised fluidised-bed combustion and gasification of peat. *Journal of the Institute of Energy*, pages 189–196.

Monkhouse, P. (2002). On-line diagnostic methods for metal species in industrial process gas. *Progres in energy and combustion science*, 28(4):331 – 381.

Monkhouse, P. and Glazer, M. (2006). Personal communications.

Mühlen, H. and Sowa, F. (1995). Factors influencing the ignition of coal particles, studies with a pressurized heated-grid apparatus. *Fuel*, 74:1551–1554.

Mukherjee, S. and Borthakur, P. (2003). Effects af alkali treatment on ash and sulphur removal from assam coal. *Fuel Processing Technology*, 82:51–60.

Mulik, P., Alvin, M., and Bachovchin, D. (1983). Simultaneous high-temperature removal of alkali and particulates in a pressurized gasification system. Technical Report DoE/MC/16372-8, Westinghouse Research and Development Center, Chemical Sciences Division, Pittsburgh, PA.

Neimo, L. (1990). Paper making chemistry. Technical report, Paper making science and technology.

Nielsen, H., Frandsen, F., Dam-Johansen, K., and Baxter, L. (2000a). Deposition of potassium salts on heat transfer surfaces in straw-fired boilers: pilot-scale study. *Fuel*, 79:131–139.

Nielsen, H. P., Frandsen, F. J., Dam-Johansen, K., and Baxter, L. L. (2000b). The implications of chlorine-associated corrosion on the operation of biomass-fired boilers. *Prog. Energy Combust. Sci.*, 26:283–298.

Nielsen, P. (1998). *Deposition and High-Temperature Corrosion in Biomass-Fired Boilers*. PhD thesis, Technical University of Denmark.

Nikolaisen, L. (1998). Straw for energy production. Technical report, The Centre for Biomass Technology.

Obernberger, I. (1998). Decentralized biomass combustion: State of the art and future developments. *Biomass & Bioenergy*, 14(1):33–56.

Ohmann, M. and Nordin, A. (2000). The role of kaolin in prevention of bed agglomeration during fluidized bed combustion of biomass fuels. *Energy&Fuels*, 14:618–624.

Olsson, J. G., Jaglid, U., and Pettersson, J. B. C. (1997). Alkali metal emission during pyrolysis of biomass. *Energy&Fuels*, 11:779–784.

Olsson, J. G., Pettersson, J. B. C., Padban, N., and Bjerle, I. (1998). Alkali metal emission from filter ash and fluidized bed material from PFB gasification of biomass. *Energy&Fuels*, 12:626–630.

Oniszk-Poplawska, A., Rogulska, M., and Wisniewski, G. (2003). Renewable energy developments in poland to 2020. *Applied Energy*, 76:803–816.

Partanen, J. (2004). *Chemistry of HCl and Limestone in Fluidised Bed Combustion*. PhD thesis, Abo Akademi.

PowerTechnology (2006). Lagisza power plant Supercritical Circulating Fluidised Bed. Internet Resources.

Punjak, W. and Shadman, F. (1988). Aluminosilicate sorbents for control of alkali vapors during coal combustion and gasification. *Energy&Fuels*, 2:702–708.

Punjak, W., Uberoi, M., and Shadman, F. (1989). High-temperature adsorption of alkali vapors on solid sorbents. *AIChE Journal*, 35(7):1186–1194.

Raask, E. (1985). *Mineral impurities in coal combustion, behaviour, problems and remedial measures*. Springer Verlag.

Robinson, A. L., Junker, H., and Baxter, L. L. (2002). Pilot-scale investigation of the influence of coal-biomass cofiring on ash deposition. *Energy&Fuels*, 16:343–355.

Sander, B. and Henriksen, N. (2000). Emissions, corrosion and alkali chemistry in straw-fired combined heat and power plants. In *1st World Conference on Biomass for Energy and Industry, Sevilla, Spain*, pages 775–778.

Scandrett, L. and Clift, R. (1984). The thermodynamic of alkali removal from coal-derived gases. *Journal of the Institute of Energy*.

Scherpenzeel, J. (1999). Economic comparison between costs of energy crops and costs of biomass residues and fossil fuels in the netherlands.

Schoen, J. (1956). Effects of temperature on the liberation of Cl and alkalis from coal. *British Coal Utilization Research Association*.

Schultz, G. (1998). Securing in supply in short and longer term of wood and straw - iea report.

Schurmann, H., Unterberger, S., Hein, K. R. G., Monkhouse, P. B., and Gottwald, U. (2001). The influence of fuel additives on the behaviour of gaseous alkali-metal compounds during pulverised coal combustion. *Faraday Discussusions*, 119:433–444.

Siedlecki, M. (2003). Alkali measurements: start-up of the cfb combustor and the development of gas sampling procedure. Master's thesis, Delft University of Technology.

Smith, W. R. (1982). *Chemical reaction equilibrium analysis; theory and algorithms*. John Wiley & Sons.

Spliethoff, H., Unterberger, S., and Hein, K. (2001). Status of co-combustion of coal and biomass in Europe. In *Proceedings of the Sixth International Conference on Technologies and Combustion for a Clean Environment, Porto, Portugal, 2001*.

Steenari, B. M. (1998). High-temperature reactions of straw ash and the anti-sintering additives kaolin and dolomite. *Biomass Bioenergy*, 14:67–76.

Stull, D. (1985). *JANAF Thermochemical Tables*. U.S. Department of Commerce, Washington.

Sun, C. and Kozinski, J. (2000). Ignition behaviour of pulp and paper combustible wastes. *Fuel*, 79:1587–1593.

Thompson, D. and Argent, B. (1999). The mobilisation of sodium and potassium during coal combustion and gasification. *Fuel*, 78:1679–1689.

Tillman, D. (2000). Biomass cofiring: the technology, the experience, the combustion consequences. *Biomass&Bioenergy*, 19(6):365 – 384.

Tran, K. Q., Iisa, K., Steenari, B. M., and Lindqvist, O. (2005). A kinetic study of gaseous alkali capture by kaolin in the fixed bed reactor equipped with an alkali detector. *Fuel*, 84(2–3):169–175.

Turn, S., Kinoshita, C., Ishimura, D., Hiraki, T., Zhou, J., and Masutani, S. M. (2001). An experimental investigation of alkali removal from biomass producer gas using a fixed bed of solid sorbents. *Ind. Eng. Chem. Res.*, pages 1960–1967.

Turn, S., Kinoshita, C., Ishimura, D., and Zhou, J. (1998a). The fate of inorganic constituents of biomass in fluidized bed gasification. *Fuel*, 77(3):135–146.

Turn, S. Q., Kinoshita, C. M., Ishimura, D. M., Zhou, J., Hiraki, T. T., and Masutani, S. M. (1998b). A review of sorbent materials for fixed bed alkali getter systems in biomass gasifier combined cycle power generation applications. *J. Inst. Energy*, 71:163–177.

United Nations (1997). United nations framework convention on climate change - Kyoto Protocol.

Valmari, T., Lind, T. M., Kauppinen, E. I., Sfiris, G., Nilsson, K., and Maenhaut, W. (1999a). Field study on ash behavior during circulating fluidized-bed combustion of biomass. 1. Ash formation. *Energy&Fuels*, 13:379–389.

Valmari, T., Lind, T. M., Kauppinen, E. I., Sfiris, G., Nilsson, K., and Maenhaut, W. (1999b). Field study on ash behavior during circulating fluidized-bed combustion of biomass. 2. Ash deposition and alkali vapor condensation. *Energy&Fuels*, 13:390–395.

van Loo, S. and Koppejan, J. (2002). *Handbook of biomass combustion and co-firing*. Twente University Press.

Veijonen, K. (2005). European biomass CHP in practice. In *Biomass Conference Paris*.

Wagman, B. (1971). *Selected Values of Chemical Thermodynamic Properties*. U.S. Department of Commerce, Washington.

Wei, X. L., Lopez, C., von Puttkamer, T., Schnell, U., Unterberger, S., and Hein, K. R. G. (2002). Assessment of chlorine-alkali-mineral interactions during cocombustion of coal and straw. *Energy&Fuels*, 16:1095–1108.

Wei, X. L., Schnell, U., and Hein, K. R. G. (2005). Behaviour of gaseous chlorine and alkali metals during biomass thermal utilisation. *Fuel*, 84:841–848.

Wolf, K., Smeda, A., Müller, M., and Hilpert, K. (2005). Investigation on the influence of additives for sulfur dioxide reduction during high alkaline biomass combustion. *Energy & Fuels*, 19:820–824.

World Energy Council (2004). Sourvey of energy resources. internet resources.

Wornat, M., Hurt, R., Yang, N., and Headley, T. (1995). Structural and compositional transformations of biomass chars during combustion. *Combustion and Flame*, 100(1-2):133 – 145.

Zevenhoven-Onderwater, M., Backman, R., Skrifvars, B. J., and Hupa, M. (2001). The ash chemistry in fluidised bed gasification of biomass fuels. Part I: predicting the chemistry of melting ashes and ash-bed material interaction. *Fuel*, 80:1489–1502.

Appendix A

Structural changes during rapid devolatilization of high alkali bio-fuels

A.1 Introduction

The present work presents rapid devolatilization and char burn out results with a bench scale heated grid apparatus for three different biomass fuels. The heated grid apparatus was used for this preliminary research to simulate and investigate the behavior of the fuel in the first moments of the combustion process in a large scale CFB installation to help in understanding the release of alkali metals, S, Cl release from the fuel particle. The influence of the temperature and the heating up rate on the structure of the particles was investigated. The morphological changes were analyzed with a microscope, moreover the combustion process was recorded with a CCD camera. The TGA analysis of the fuel was performed to emphasize the differences in the structure of the samples.

A.2 Experimental apparatus

The experiments have been performed on a heated grid apparatus also called heated wire mesh. The device can be used for characterization of solid fuels at high heating rates in order to simulate conditions in large scale applications. The reactor consists of a stainless steel mesh mounted between two copper electrodes. The size of the stainless steel mesh is about 1 square centimeter. The reaction zone can be closed and sealed with a cylindrical shape chamber for experiments in pressurized or modified atmosphere. The chamber is equipped with CaF_2 windows for observation purposes. The current and heating up rate is controlled through a PC. The measured temperature as a

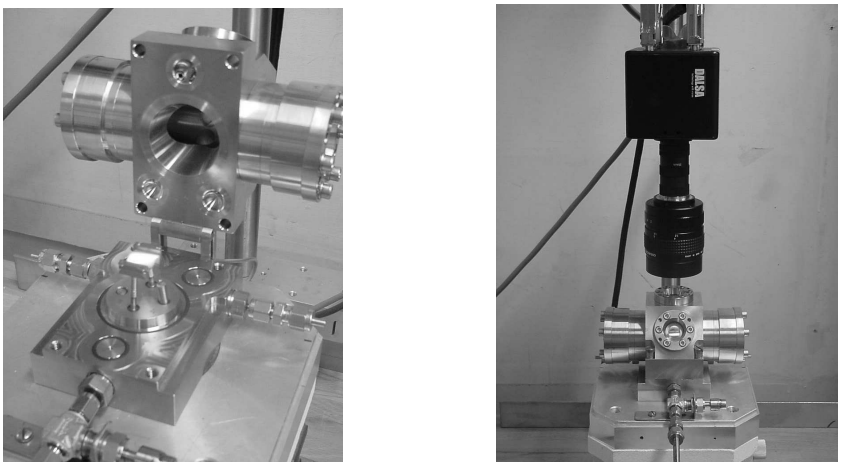


Figure A.1: Heated Grid apparatus, left - electrically heated grid, right - closed grid with CCD camera

function of time are stored with high temporal resolution using a fast data acquisition card. Values of heating rate up to 10^3 K/s can be reached. The temperature of the grid is measured with 0.1 mm S-type thermocouple with 0.2 mm junction. The thermocouple is placed below the grid. The maximum temperature of the grid is restricted with properties of the metal mesh. During the experiments reported in this paper a stainless steel mesh was used. The combustion process has been recorded with a high speed CCD camera coupled with the heated grid apparatus and controlled with a PC. The samples have been investigated for structure diversities and morphological transformations with a microscope with magnification of 220 times. The microscope was coupled with a PC with frame grabber software. It has to be pointed out that the temperature measured by the thermocouple is not the temperature of the particle itself. The junction measures the temperature of the grid. The problem of the temperature measurement with thermocouple is known for heated grid devices and was already reported in the literature [Freihaut and Proscia, 1989; Gibbins-Matham and Kandiyoti, 1988; Mühlen and Sowa, 1995]. Moreover the heat capacity of the thermocouple junction is larger than single stainless steel wire of the mesh. That means that the thermocouple will cause a cold spot on the grid, which will lower the temperature readings. The thermocouple heat capacity, not direct contact with the fuel particle and heat transfer limitations within the particle itself for high heating up rates impose inaccurate temperature readings. Differences up to 100K were reported by some authors [Freihaut and Proscia, 1989; Gibbins-Matham and Kandiyoti, 1988]. For the same

Table A.1: Biomass fuels

		HIAL 2 – Spanish Oat	HIAL 5 – Spanish Barley	HIAL 7 – Bras. Carinata
Moisture	%	17.2	13.6	10.6
Ash	% dry	3.9	7.2	5.1
C	% dry	48	45	45
H	% dry	6.3	6	6
N	% dry	0.93	0.76	1.1
S	% dry	0.16	0.19	0.28
Cl	% dry	0.06	1.1	0.06
Si	% dry	0.29	0.82	0.06
Al	% dry	0.01	0.01	0.01
Fe	% dry	0.01	0.01	0.01
Ca	% dry	0.8	0.39	0.74
Mg	% dry	0.08	0.1	0.07
Na	% dry	0.14	0.3	0.01
K	% dry	0.61	2.5	1.7
P	% dry	0.1	0.05	0.17
LHV dry	MJ/kg	17.4	16.5	16.7
LHV daf	MJ/kg	18.1	17.8	17.6

reason the calculated heating rate is in practice the heating up rate of the stainless steel mesh. Moreover the fuels were characterized with SDT 2960 thermogravimetric analyzer (TGA) manufactured by TA Instruments. The maximum temperature of the TGA analyzer is 1500°C. The device is characterized with a balance sensitivity of 1μg, the maximum adjustable heating rate can be set at 100 °C/min. The experiments have been performed at two temperature levels and with two heating up rates. The first one was characterized with the average grid temperature of 500°C and the grid heating up rate of 180 K/s and the second one with the average grid temperature of 1000°C and grid heating up rate of 770 K/s. Prior to the experiments 5 mm long straw particles with approx. weight of 2 mg have been prepared. For the experiments, in most cases the single particle was placed on the grid.

A.3 Results and discussion

The heated grid apparatus has been used for the rapid devolatilization experiments in order to simulate high heating rates experienced by a fuel particle in the large scale CFBC. Moreover the behavior of the particle during the combustion process, especially the very first moments of the particle transformation were investigated. The morphological changes of the samples were recorded with a camera coupled with the system. Ashes were investigated with the microscope. For the experiments three kinds of straw have been selected (table A.1). HIAL 2, HIAL 5, HIAL 7 are characterized with different chemical composition. Spanish oat is relatively low in K, Cl, Si, but the ratio K/Cl is

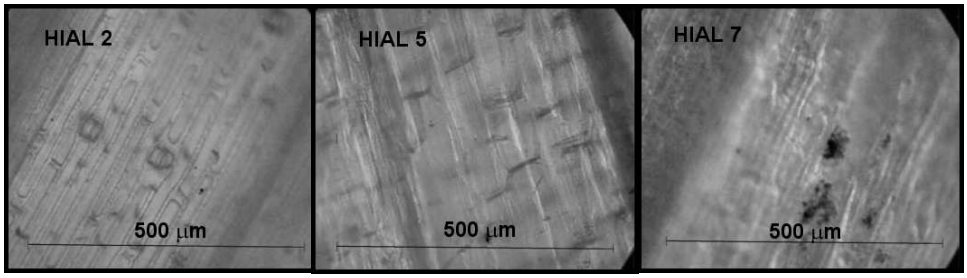


Figure A.2: Structure - biomass fuels HIAL2, HIAL5, HIAL7

high. Spanish Barley is characterized with high K, Cl content. Spanish Brasica Carinata presents high content of K and S, moreover it is low in Cl and Si. The K/Cl ratio for Brasica Carinata is very high comparing to other analyzed fuels. Samples of HIAL 2, HIAL 5, and HIAL 7 have been prepared and the structure investigated (Fig. A.2). It was observed that HIAL 2, HIAL 5, HIAL 7 are characterized by different structure of the fibres. Moreover the structure is inhomogeneous with some flaw visible as in case of HIAL 7. The flaw is supposed to be mineral inclusion. Following the analysis with the microscope the combustion experiments have been performed. The combustion process has been recorded with a CCD camera. Images of the particle at different steps of the combustion process have been selected (Fig. A.3). Figure A.3 presents the combustion process for HIAL 2 straw characterized with a mean grid temperature of 550°C and a combustion time of approx. 5 sec. Shrinking of fibres in the particle was observed during the volatile matter release (Fig. A.3). Similar effect was reported by Sun and co-workers [Sun and Kozinski, 2000] during combustion of the fibrous paper sludge. The char combustion overlapped the combustion of volatiles (Fig. A.3). A decrease in the size of the particle and fragile, loose structure was observed at the end of the experiment (Fig. A.3). Similar transformations decreasing the particle aspect ratio and development of lace-like structure as burning proceeded were reported during biomass char combustion in the work of Wornat and co-workers [Wornat et al., 1995] The experiments were performed with a heating up rate approx. of 770 K/s and the residence time on the grid of 10s. The mean grid temperature was about 1000°C. The particle experienced severe morphological transformations. We suppose that in case of HIAL 2 and HIAL 7 the ash is mainly silica skeleton of the particle. In case of HIAL 5 investigation of the stainless steel mesh revealed that ash melted and covered the mesh with a layer of deposit. HIAL 5 is a high K and Si containing straw, straws like that were reported to cause deposits with molten character [Sander and Henriksen, 2000]. Formation of low-melting alkali silicates seems to the most propable mechanism. Wornat and co-workers [Wornat et al., 1995]

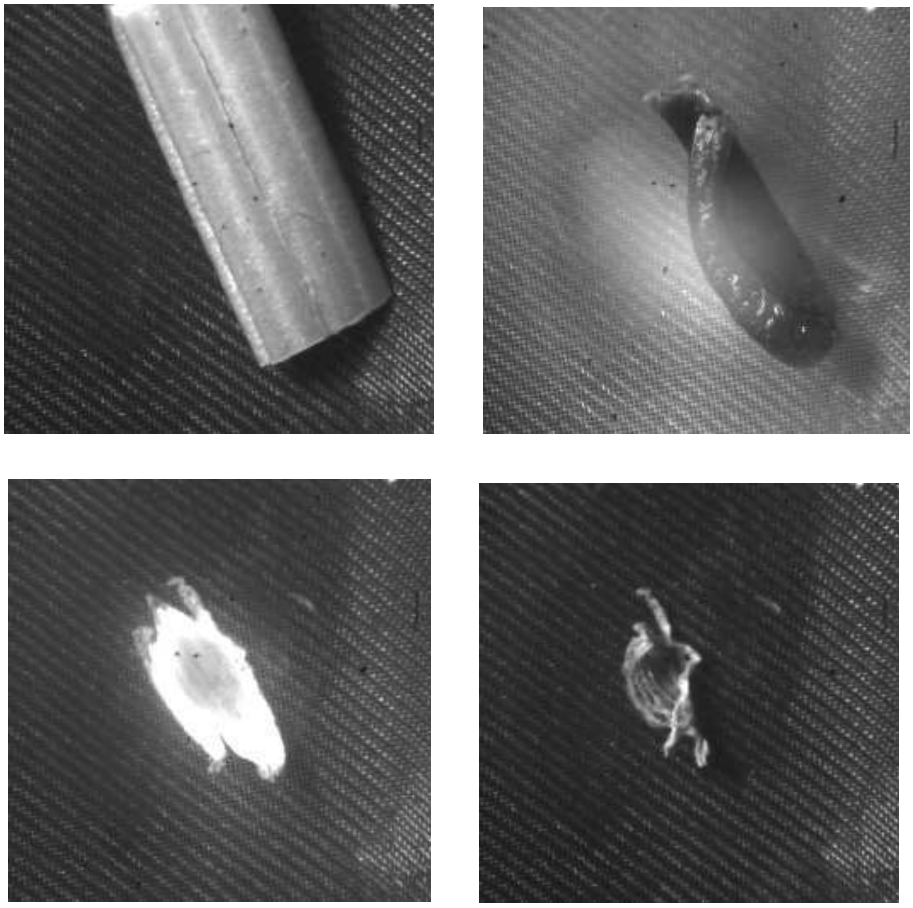


Figure A.3: Four stages of HIAL 2 combustion, combustion time approx. 5 sec., the mean grid temp. 550°C

reported formation of silica rich droplets on the surface of the biomass chars. In case of HIAL 5 there were droplets observed on the deposit surface (figure 4c). To specify the exact chemical composition of the droplets further chemical analysis is necessary. In case of fluidized bed combustion a high share of HIAL 5 fuel may cause operational problems because of bed agglomeration phenomena. The grid was exposed to a high temperature, high alkali combustion conditions after particle devolatilization. Interesting is a comparison between a image of the new stainless steel mesh and one after the tests with HIAL 5 and HIAL 7 (Fig. A.4). The high concentration of K, Si and Cl in HIAL 5 seems to be re-

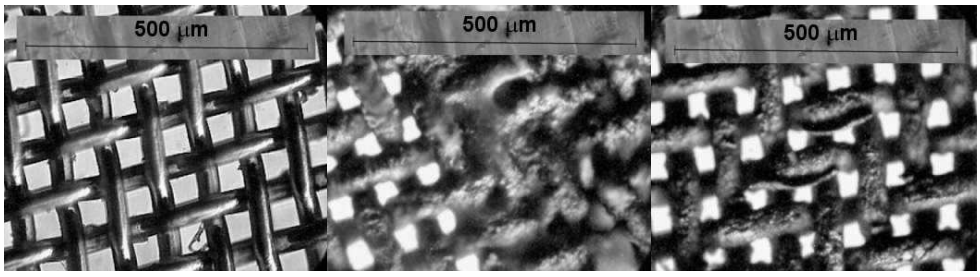


Figure A.4: Biomass fuels, left - clean mesh, center - after combustion of HIAL5, right - after combustion of HIAL7

sponsible for molten deposits probably of alkali-silicates on the surface of the grid (Fig. A.4). The experiments were done in temperature of 1000°C, which is high enough to melt ash material with high alkali-Si composition and close the porous structure of the mesh. In case of HIAL 7 corrosion was observed on the mesh surface. Fig. A.4 portrays the surface of the mesh after combustion experiments with HIAL 7, cracks and pores are visible on the surface. It can be concluded that high temperature alkali environment acts destructively on the smooth cylindrical surface of the stainless steel wires.

A.4 Conclusions

The structural changes during rapid devolatilization of three different high alkali bio-fuels have been investigated. The bio-fuels vary in chemical composition and are characterized with different content of alkali metals and Cl, S and Si. The microscope investigation revealed inhomogeneous nature of HIAL 2, HIAL 5, HIAL 7. One can expect that three types of straw will be characterized with behavior at combustion conditions during full scale CFB experiments. Considering future fuel characterization for CHP because of inhomogeneous structure precise chemical analysis over large quantities of straw can be difficult and the results may vary. Within one type of straw substantial differences may be experiences. This will intensify or retard corrosion attack and slagging/fouling propensity of HIAL biomass. Moreover it will result in variation during in situ alkali measurements. The combustion experiments on the heated grid with the high heating up rates revealed rapid and severe decomposition of the straw particles. Decomposition of the fibers led to twisting within the particle and resulted in fragile, lace-like structure of the ash after char burn-out. The ash that remained on the grid is supposed to be silica skeleton of the straw. For HIAL 5 deposits were observed on the surface of the grid, probably of molten alkali-silicates. HIAL 5 is high in potassium and silica may cause problems

with bed agglomeration and deposits formation during following CFBC experiments. Moreover high temperature corrosion and destruction of outer surface of the stainless steel mesh after few combustion experiments with HIAL 7 and HIAL 5 were noticed. Rapid twisting of the particles was observed especially with the high heating rates. It is expected that already during devolatilization phase migration of alkalis to the particle surface and most likely partial release took place. This will probably influence the alkali metal release to the gas phase within CFBC.

Appendix B

Alkali sampling on pilot scale CFB

B.1 Introduction

Circulating Fluidized Bed technology was proven to be able to handle different kind of fuels coal, wood but also more problematic ones like straw or waste [Basu, 1999; Jacobs, 1999]. As an agricultural residue straw is available in large quantities in Europe. The almost zero net CO_2 emissions make it an attractive, sustainable bio-fuel particularly for small, decentralized Combined Heat and Power (CHP) plants. Widespread use of straw for energy generation is being retarded because of the operational problems caused by its chemical composition. Especially the high alkali metals content together with Si and Cl are responsible for bed agglomeration, slagging, fouling and alkali induced corrosion attack in boiler walls, heat exchangers and other down-stream equipment [Hansen et al., 1995; Hald, 1994]. To prevent the above-mentioned operational problems clear understanding of the complex behavior of the alkali metals within combustion systems is required. To study the relationships between the reacting elements effective sampling of the alkali metals out of combustions systems is needed. During the combustion tests with the gaseous alkali metals sampling problems with extraction of the particle free flue gas from the riser of CFB were encountered. The tip of the gas extracting probe was extremely fast entirely blocked with a mixture of the bed material and flying ash. The sampling time was not long enough to extract the amount of gas required. The literature survey performed to find a solution for this problem unfortunately did not give satisfactory results. Because of the high dust load the particle free gas extraction is a very challenging task. A flow in a riser is described as non-uniform suspension of solid particles moving up and down in an up-flowing gas-solid continuum [Basu and Fraser, 1991]. Some data on gas extraction with difficult sampling conditions, namely very high temperature and high dust load was reported for cement kilns [Fallgren, 1991]. Moreover design of a probe for

ammonia sampling operating in similar conditions in the combustion chamber of the CFBC was found [Kassman et al., 1995; Kassman and Amand, 2001]. Moreover work by Lind and Valmari describe the particles sampling on CFB combustors [Lind, 1999; Valmari et al., 1999a]. A dedicated article, purely describing particle free gas extraction from a CFB boiler in such specific conditions could not be found. The work presented in this appendix presents the practical experience gained during screening for the optimal solids free flue gas extraction method. The different tips and sampling approaches are described and their usefulness discussed.

B.2 Problem outline

Gas sampling from the operating CFB combustor appeared to be problematic. The gas sampling was necessary to investigate composition of bed material, fly ash. The substraction of the fly ash was critical to understand behavior of alkali metals and their sequestering in the system. A probe was designed and build. During the testing stage various sampling tips attached to the probe were proposed.

B.3 Problem solving

The tip T1 (figure B.1) was proposed during the design stage. The tip T1 consisted of 5 mm. alumina tube opening and two ceramic silica quartz filtering disks. Two quartz glass filtering disks 4 mm thick each placed inside the tip was supposed to filter the gas. The probe was introduced to the reactor and the gas extracting pomp started. After few minutes of sampling there was no gas flow observed. The experiment was stopped and the probe investigated for possible reasons. When the probe was removed from the system the opening of the tip had been blocked. The blockage causing solids were removed and investigated. They were mixture of the bed material and fly ash closely packed in the small alumina oxide tube of the tip T1 (figure B.2). One of the quartz glass disk filters was covered with a thin layer of dusty material, probably products of bed material abrasion. To prevent the collection of relatively coarse bed material in the narrow alumina tube, the tip was modified. The tip T2 was manufactured. The opening protected with the stainless steel mesh was proposed (figure B.3). The new test was started and the probe was introduced into the reactor. The tip T2 enabled approx. 2 minutes of effective sampling. The probe with the tip T2 was removed from the reactor and examined. The examination revealed that the openings in the stainless steel mesh were entirely blocked. The material was very fine fly ash and products of sand abrasion. Likely some of the sticky ash particles impacted the mesh and started to build a layer of deposits around

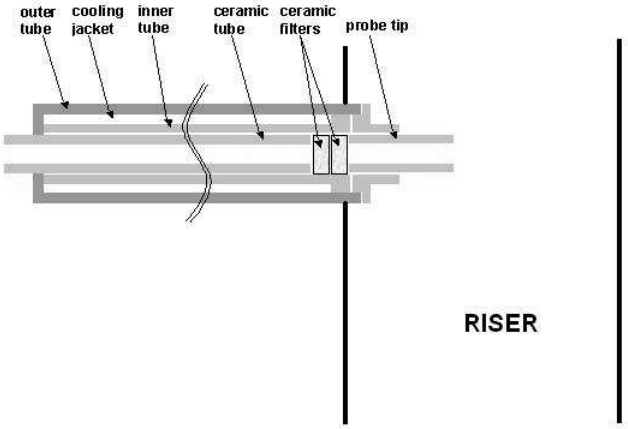


Figure B.1: Probe with tip T1 mounted on the riser



Figure B.2: Tip T1 blocked with bed material and fly ash

it. The process continued and finally the openings were blocked. The concentration of fine particles in the riser is significant so the process was additionally accelerated. The gas flow was completely stopped. Inside the tip no coarse sand was found. Before the steel mesh was blocked, some of the fines penetrated into

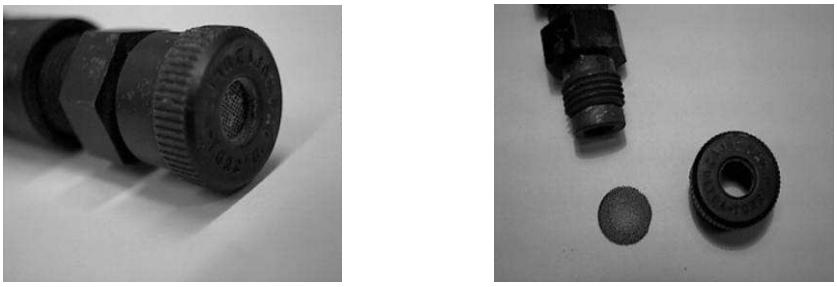


Figure B.3: Tip 2 - assembled on the probe (left), disassembled (right)

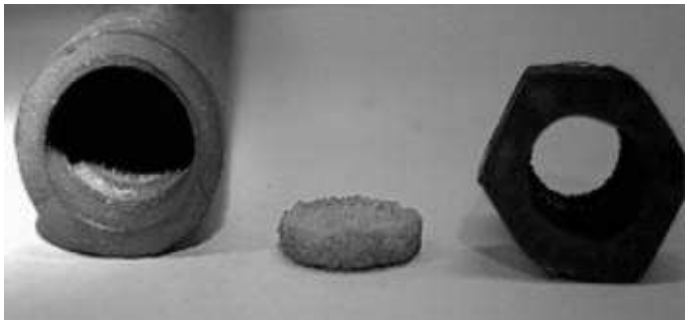


Figure B.4: Tip T3 configuration; the tip with the filter disassembled from the probe

the quartz glass filter disks and deposited there. Parallel with the tip T2 the tip T3 was developed with the idea behind it to make the opening of the tip much bigger so the coarse sand can freely get in and out. The tip T3 was ordered (figure B.4), installed on the probe and together with the probe inserted in the riser. For the tip T3 the coarse sand did not block the opening of the tip as it was in case of the tip T1 but large amounts of fines present in the extracted gas blocked entirely the first of two filtering discs (figure B.5). After approx. 3 minutes the flow steadily decreased and finally totally congested. The probe had to be removed. Unfortunately the extracted amount of gas was not high enough. The front disk was entirely covered with a layer of fines. The new filter disks had to be ordered and replaced. Trials to remove the filtered material from the porous surface of the quartz glass by means of the opposite gas flow were not successful. The tests continued and the sintered steel filters with various pore size were implemented (figure B.6 - left). For the tip T4 the 60μm sintered steel filter was welded to the tip. The probe was inserted to the combustor and the gas extraction initiated. Unfortunately also this idea failed, the pores of the sin-

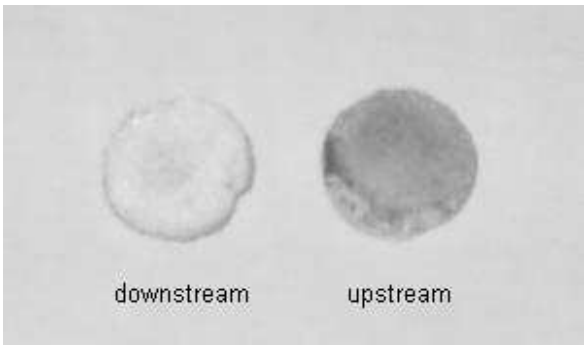


Figure B.5: Quartz glass filtering disks after the experiments with T3, the upstream disk is entirely blocked

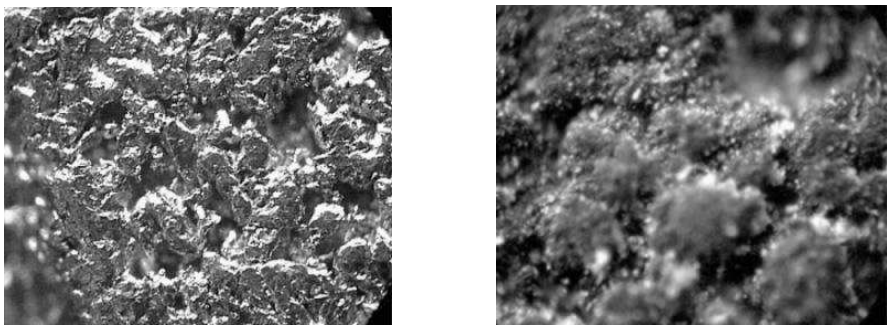


Figure B.6: Sintered steel material used for tip T4, 60μ pore size (left), the tip blocked after the experiments (right)

tered steel filter were blocked extremely fast. The abrasion effect from the bed material was expected to clean the filter continuously but it was not the case. After removal and cooling down the surface of the steel filter was investigated with an optical microscope (figure B.6 - right). As it can be seen the pores were filled with the fines and the gas sampling was not possible. The modification of the tip T4 resulted in the tip T5. Instead of the fine 60μm sintered steel the 130μm steel mesh filter element (figure B.7 - left) from the same manufacturer as the first stage filter was used. It was welded to the tip. The stainless steel mesh was supposed to filter the coarse sand. Inside the tip then the second stage filtering element was placed. In this case the 60μm sintered steel filter was used, the same material as for the tip T4. The sampling time for the tip T5 was extended by factor 4 comparing to previous tests. The flue gas flow was

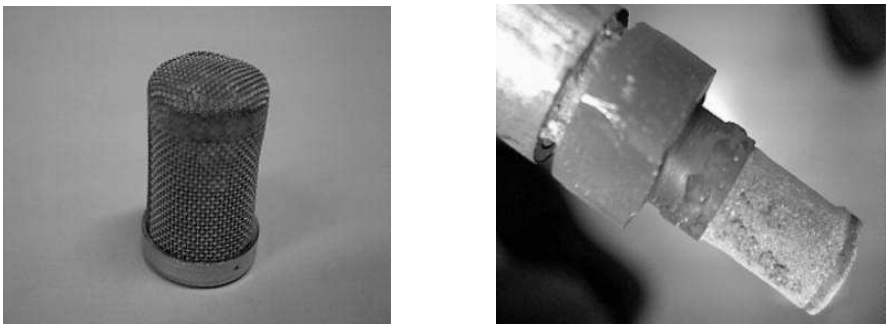


Figure B.7: Steel mesh filter tip T5 (left); as a probe tip after tests (right)

detected for several minutes probably due to enlarged filtering surface. In the end also the tip T5 was blocked. The investigation revealed that the blocking of the coarse filter was the reason (figure B.1 - right). Proceeding with the tests with different tips it became clear, that some mechanism of the filter cleaning would be desirable. Similar approach had to used by Fallgren and co-workers [Fallgren, 1991] in the cement kiln. For cleaning purposes flow of compressed nitrogen in opposite direction was the easiest to use. The solids accumulated on the filters and in the pores were expected to be forced back and the pores freed. Pressurized, 4 bars nitrogen was applied in 1-2 second long shots in the direction opposite to the normal gas flow in the probe. A simple system consisting of a three-way manual valve was built. When cleaning was necessary the valve was open and nitrogen pushed into the probe. During normal operation the valve was set for gas sampling. Every probe design except the tip T1 and T6 was tested with the nitrogen cleaning. Summarizing observations are as follows:

- Nitrogen cleaning applied to the already blocked filter gave no satisfactory results;
- Cleaning was the most effective on the steel mesh filters; on the porous filters (ceramic, sintered steel) the effect was less visible, because it was almost impossible to remove the particles once they entered the pores;
- cleaning would probably be most effective if done on a regular basis (e.g. every 1 minute) even before the start of the gas sampling. A small flow in the opposite direction for no sampling periods should keep the filter clean. However, this approach was not tested.

The experienced problems resulted in moving the measuring position downstream the cyclone. The new tip T6 with the modified shape (figure B.8 - left)

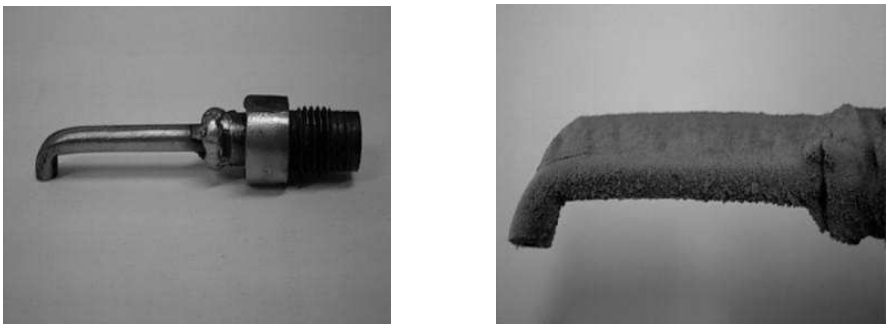


Figure B.8: Steel mesh filter tip T6 (left); after few hours of operation cover with fly ash (right)

was proposed. In this way the substantial part of the solid material, mainly coarse particles separated by the cyclone, was avoided. Downstream the cyclone the concentration of solids, mostly fines was still substantial (figure B.8 - right). The curved tip with the opening in the direction of flow prevents at least some part of the solid from being entrained to the tip. Moreover the filtering quartz glass disks were exchanged with much cheaper ceramic fiber wool. The ceramic fiber wool was removed and replaced after every experiment. With the tip T6 successful particle free flue gas extraction without nitrogen cleaning was possible. The operation times of up to 2 hours were reached. With time, slight decrease in the gas flow was observed sometimes. It depended on amount of the ceramic fiber material placed in the tip.

B.4 Conclusions

Screening for the most suitable method in particle free flue gas sampling in high temperature, high dust load conditions was performed. The tests revealed that the gas extraction on the riser of CFB facilities is a very challenging task; many tip configurations didn't provide satisfactory results. The sampling time was too short according to the specific requirements needed. A system for cleaning applied to the blocked filters blocked was not successful. The back pulsing applied to the steel mesh filters was more effective. Moving the sampling position, designing a new tip shape together with applying another filter material resulted in substantial improvement.

Appendix C

Wet gas trapping measurement protocol

This measurement protocol describes how the impingers, used in the wet trapping of the gaseous trace elements, should be handled. Two different protocols can be distinguished, one for trace elements and one for fly ash. This protocol deals with the trace element measurements.

Preparation:

1. Let 10+1 borosilicate glass impingers and 10+1 teflon bottles soak in a 5% HNO_3 pro analysis solution for 48 h.
2. Rinse the bottles and impingers with ultra pure water and let them dry in an oven at 105°C for 24 h.

Measurement:

1. Weigh the impingers before the actual measurement.
2. Fill 4+1 impingers with 200 ml a 5% HNO_3 pro analysis solution
3. Set 1 impinger with solution aside as a blank
4. Place the impingers in the ice bad. Connect them together and to the probe with teflon tubing. The first impinger being an empty one.
5. Write down the volume meters start position
6. Open the ball valve carefully and slowly when the main part of the probe is running
7. Let the gasflow run for as long as possible, preferably more than 4 hours
8. Close the ball valve slowly and carefully

9. Write down the volume meters end position

Finalizing:

1. Disconnect the impingers and rinse the unheated part of the probe with as little as possible 5% HNO_3 pro analysis solution into the first impinger.
2. Rinse the teflon tubing with as little as possible 5% HNO_3 pro analysis solution into the respective impingers.
3. Weigh the impingers again
4. Empty the impingers, including the blank into labeled and numbered teflon bottles.

Do not rinse the impingers or bottles!!!

Appendix D

Alkali measurements with batch techniques

D.1 Wet trapping method - principles and experimental setup

Wet trapping method of alkali sampling is a batch technique. The certain amount of alkali metals containing gas is extracted from a reactor and analyzed. The sampled gas is led through a train of bubblers containing a solution of 5%wt nitric acid. The gaseous alkali compunds present in the gas stream dissolve in the solution. The solution is then analysed. The sampling train consists of:

- sampling probe
- connecting silicon tubes
- set of bubblers with nitric acid solution immersed in ice-water bath
- gas meter
- pump

The pump creates a slight underpressure in the sample train. This forces the gas sampled in the reactor through a sampling train with the acid solution (Fig. D.1). The alkali compounds present in the flue gas dissolve in there and the clean gas is led through the gas clock to determine the volume of the sampled flue gas. After the experiment the solutions from every flask is analyzed the amount of the gaseous alkali compounds in the sampled flue gas. Using the wet gas trapping the preparations phase and the sampling procedure must be carried out very carefully as the results are easily altered. Accuracy is required when setting up the experiment and during the gas sampling. Knowing then operational conditions (temperature, flow, amount of the sampled gas etc.) and

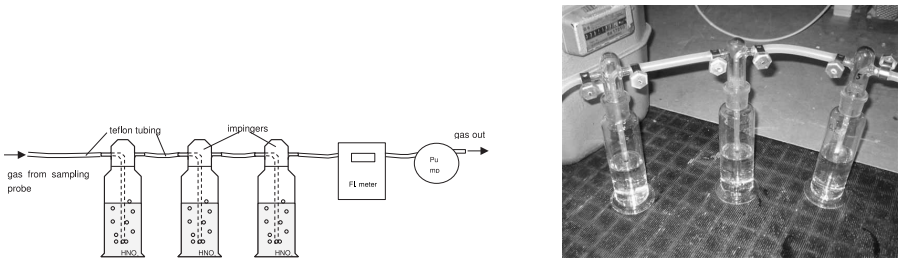


Figure D.1: Wet trapping method, sampling train - bubblers

the chemical composition of the nitric acid it is possible to calculate the amount of alkali metals present in the gas phase. The overview of the experiments is presented in table D.1

Measurements of the gaseous alkali metals compounds during combustion or gasification processes with batch, intrusive technique is difficult and challenging task. The very first and basic problem arise because of the condensation temperature of alkali compounds. In practice there is no gaseous alkali present below 750°C. This requires that all sampling lines are kept at least above 750°C If this is not the case the alkali metals are removed from these sampling lines and taken into account in the whole mass balance (see Hansen et al., 1995). In case of the experiments described here the sampled gas was cooled down below 750°C. After the experiments the connecting silicon tubes and the sampling probe were washed out with nitric acid 5% wt pro-analysis to include the condensed alkali metals compounds in overal mass balance. Moreover the sampled gas must be cleaned of all particulate matter before entering the sampling system. If some fly ash particles reach the sampling line and dissolve in acid solution they alter the results substantially (see results). Alkali measurements are very vulnerable to particle contamination. The influence of undesired fly ash particles on the results is shown in the section with the experimental results. Following with the list of requirements it has to be mentioned that all surfaces of the sampling system have to be alkali resistant. They musn't react with or release alkali metals. Moreover the sampling line should be constructed in in careful way that no alkalis are allowed to pass the samling train and leave the system. The system for the measurments used was fully detachable. It was necessary to wash out the condensed alkali metals. The sampling probe was made of high purity alumina because of its resistance to alkali metals compounds. The sampled gas was filtered with ceramic fiber, in-house developed kind of filter

The expertise gained during the alkali metals compounds sampling on the CFBC

Date	Fuel	T reactor [oC]	T sampling [oC]	Test number	Fuel Ratio	Remarks
8-10-2004	HIAL 9	850	750	1	100.00%	
8-10-2004	HIAL 9	850	750	2	100.00%	
8-10-2004	HIAL 9	850	750	3	100.00%	
22-10-2004	HIAL 3	850	750	1	100.00%	
22-10-2004	HIAL 3	850	750	2	100.00%	
12-11-2004	HIAL 3	850	750	1	50\50%	
12-11-2004	HIAL 3	850	750	2	50\50%	
12-11-2004	HIAL 3	850	750	3	50\50%	
21-10-2004	HIAL 9	850	750	1	50\50%	
21-10-2004	HIAL 9	850	750	2	50\50%	
21-10-2004	HIAL 9	850	750	3	50\50%	
13-10-2004	HIAL 9	850	750	1	50\50%	fly ash contaminated
13-10-2004	HIAL 9	850	750	2	50\50%	fly ash contaminated
13-10-2004	HIAL 9	850	750	3	50\50%	fly ash contaminated
03/02/05	HIAL 4	850	750	1	50\50%	
03/02/05	HIAL 4	850	750	2	50\50%	
03/02/05	HIAL 4	850	750	3	50\50%	
03/02/05	HIAL 4	850	750	1	100.00%	
03/02/05	HIAL 4	850	750	2	100.00%	
03/02/05	HIAL 4	850	750	3	100.00%	

Table D.1: Wet chemical method - overview of the experiments

are described in details in Appendix B.

D.2 Results

The results of the wet trapping measurements are presented in figure D.2. Different fuels has been tested. HIAL 3, HIAL 4 and HIAL 9 were selected for multiple tests. Two basic fuels shares has been investigated. The experiments were done for 50% biomass - 50% coal and 100% biomass combustion. Great variation in the results was observed. Some of the results for the 50% biomass combustion show values higher than for 100% biomass combustion. Some of the values are also unexpectedly low. As mentioned before the wet trapping technique is very sensitive to contamination. Apart of the regular data for 100% and 50% tests results for the sampling train contaminated with fly ash are shown. More information about how the gas was substracted from the reactor can be found in appendix under the tittle "Alkali sampling on pilot scale CFB".

D.3 Discussion

The experimental findings of the wet trapping measurements are quite inconsistent and difficult to compare with other method like ELIF. For combustion of HIAL 4 50% produced very low values (figure D.2). Comparing the results for HIAL 4 50% and HIAL 100 % as expected the difference is visible but the trend is opposite because the 50% combustion values are one order of magni-

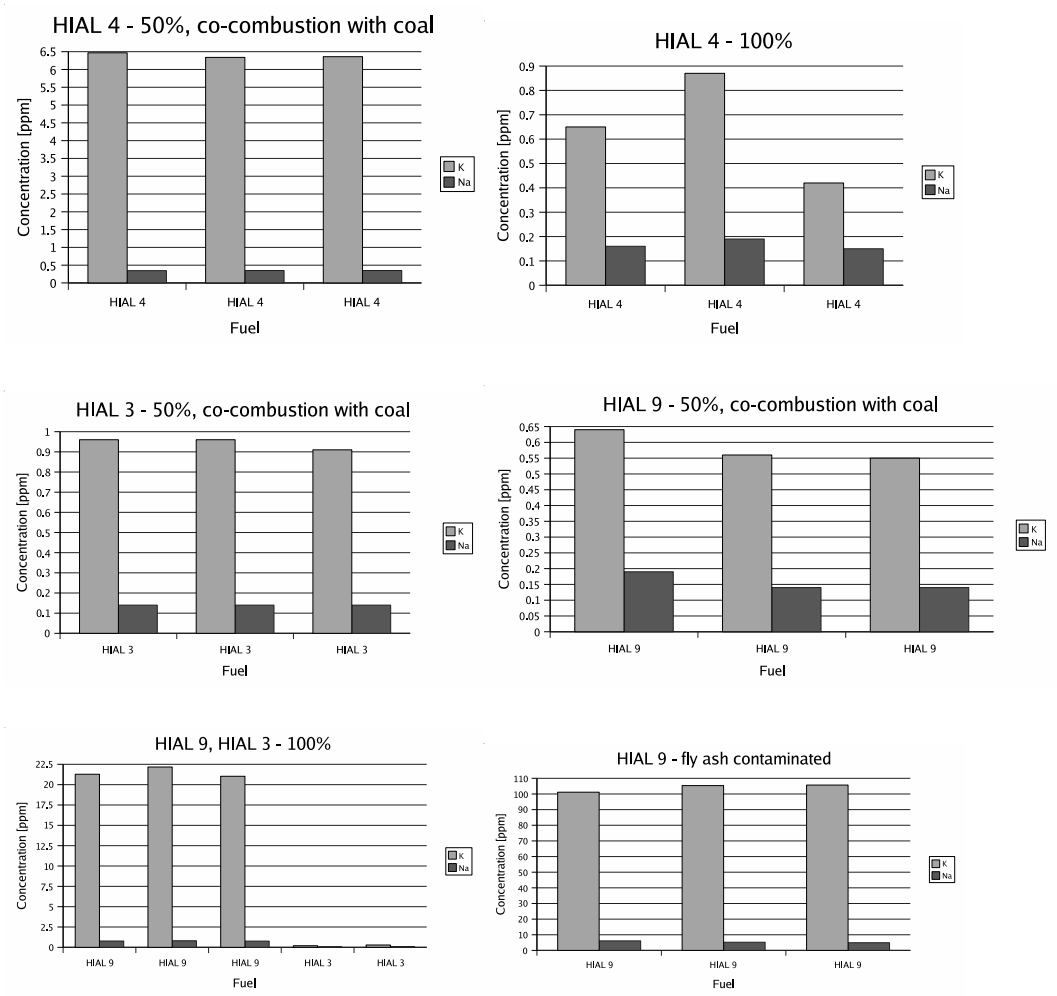


Figure D.2: Wet trapping method - results

tude higher than predicted for pure HIAL 4 combustion. It was observed in all experiments including ELIF measurments that mixing with coal first of all lowers the values because of dillution but second of all also because of reaction between coal ash elements and alkalis originating from straw. The reaction is described further on in the section with the experiemental findigs of ELIF and in the chapter 4 with the chemical equlibrium modelling. The literature findings also confirm this trend [Blander, 1997; Aho and Ferrer, 2004]. The values

for HIAL 4 100% are below 1ppm. It has to be stressed that the way the gas is samppled may influence a lot the results. Beacuse the sampling line was kept below the condensation temperature for the gaseous alkali metals after every experiment the sampling line was washed with 5% nitric acid pro analysis to remove all condensed alkalis. This was very difficult process and propable source of errors. The reason for that is during the washing process not all syrfaces to be washed are in contact with the acid. Wetting of the inner surface of alumina sampling tube is extremelly difficult. It means that it has massive consequences for the final results and interpreting the trends. Not only the values can be substantailly lower because of the sampling efficiency but also the trends are difficult to interpret because the after experiments processing (washing) is not reproductible and prone to errors. It is impossible to wash the sampling line in the same way as in preceeding experiment to compare the tests. During the experiments at the same operational conditions and for the same fuel (HIAL 7) differences in order of magnitude were observed (1.794 and 10.624 mg/nm^3 at 850^{o}C normalized for 6% oxygen). In general values above 20 ppm level were measured for 100% HIAL 9 combustion, for 50% and the same fuel they were substantially lowered below 1 ppm. It is difficult to rely on the data below 1 ppm because 1 ppm is the detection limit for the analyzing hardware. For HIAL 3 the both cases (100% combustion and 50% mixed with coal) are below ppm level.

One graph has been included where the results of particle contaminated experiment are presented. Some of the flying ash particles were found in the sampling train after the experiment. Propably originating in the leakage in the filter of the probe. The alkali metal compounds condensated on the particles dissolved in the nitric acid solution and altered substantially the results. It has to be stressed that the results of the wet trapping method are discussed in order to address disadvantages of the method. This means that they are too much inaccurate to be take into consideration and for comparison with the ELIF measurements.

Appendix E

SEM/EDS analysis of the CFBC samples

Certain amount of samples originating in the combustion experiments was selected for further analysis with SEM/EDS. In general the results are presented in chapter 3. Here some additional data has been presented. The appendix include the table with overview of the tested samples and the fulfilling SEM images together with corresponding EDS scans.

Sample number	Type	Date	Fuel	Analysis	Remarks
1	bed mat.	05/05/04	coal	SEM/EDS	
2	bed mat.	05/05/04	coal	SEM/EDS	
3	fly ash	08/10/04	HIAL 9 – 100%	SEM/EDS	
4	filter ash	10/04/04	-	SEM/EDS	
5	clean sand	-	-	SEM/EDS	
6	filter ash	26/01/04	-	SEM/EDS	
7	filter ash	01/03/04	-	SEM/EDS	
8	fly ash	13/10/04	HIAL 9 – 50%	SEM/EDS	
9	FTIR port ash	03/02/04	HIAL 4 – 100%	SEM/EDS	
10	fly ash	03/02/05	HIAL 4 – 100%	SEM/EDS	

Figure E.1: Overview of the samples

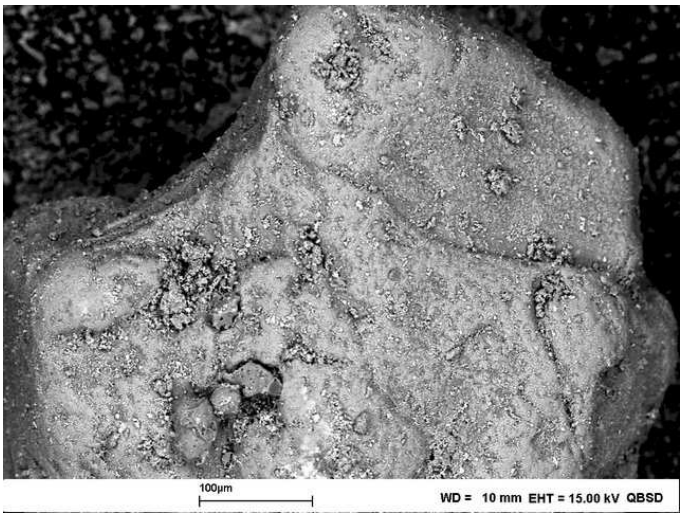


Figure E.2: Sample 2 - bed material after the experiments, magnification 200x

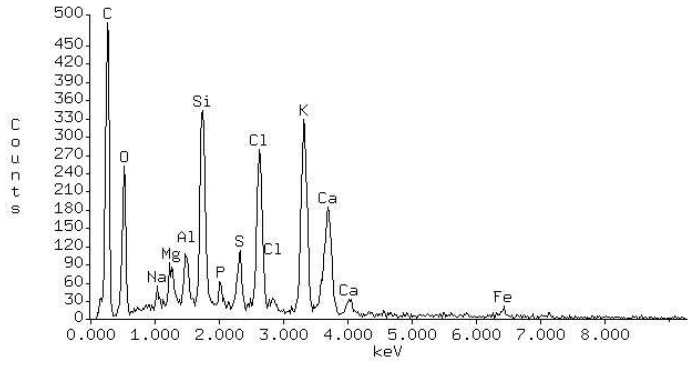


Figure E.3: Sample 2 - bed material after the experiments, magnification 200x, composition

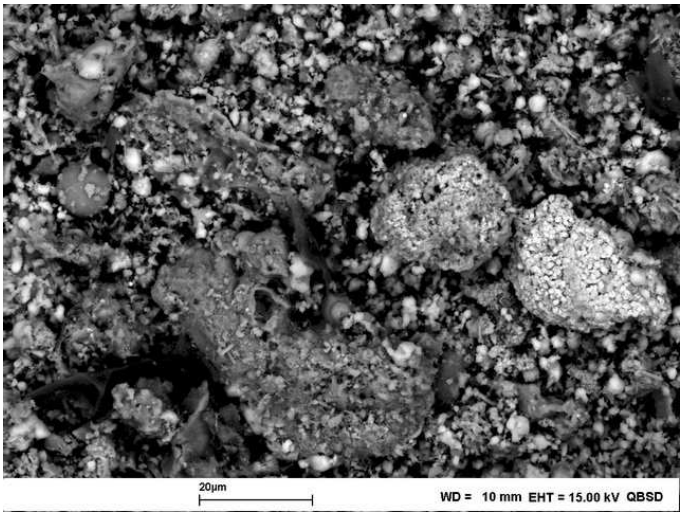


Figure E.4: Sample 7 - filter ash, magnification 1k

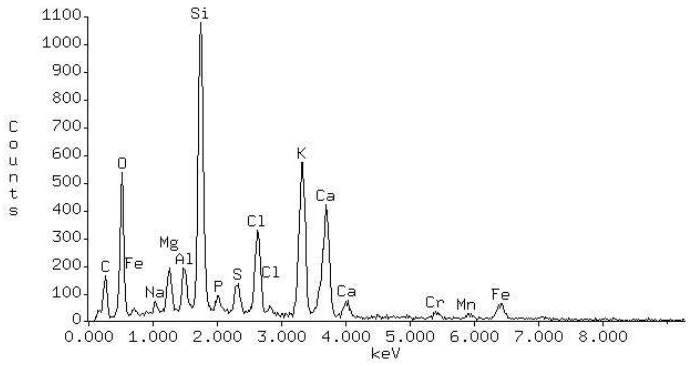


Figure E.5: Sample 7 - filter ash, magnification 1k, composition

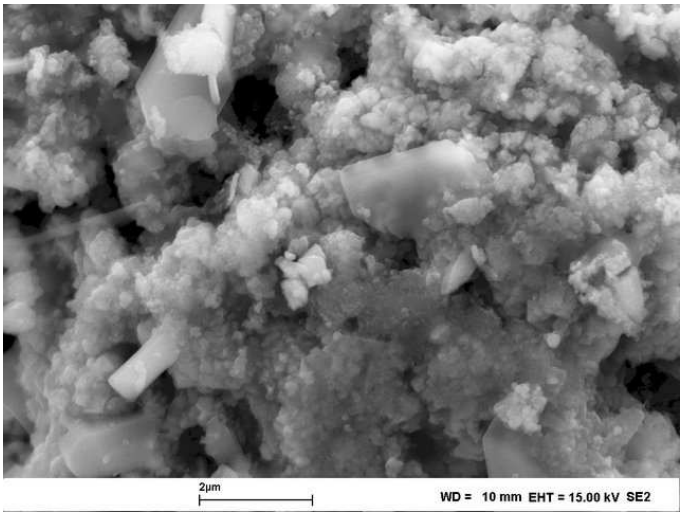


Figure E.6: Sample extracted from filter ash, magnification 10k

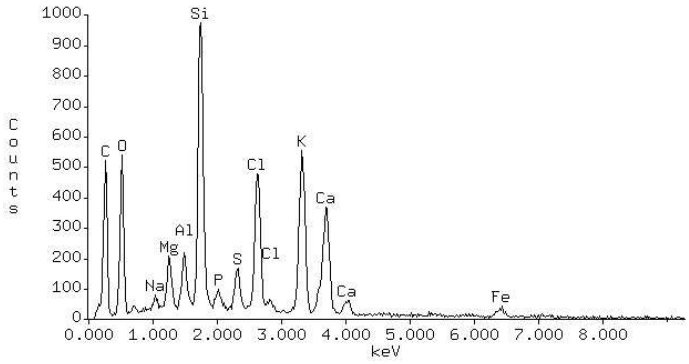


Figure E.7: Sample extracted from filter ash, magnification 10k, composition

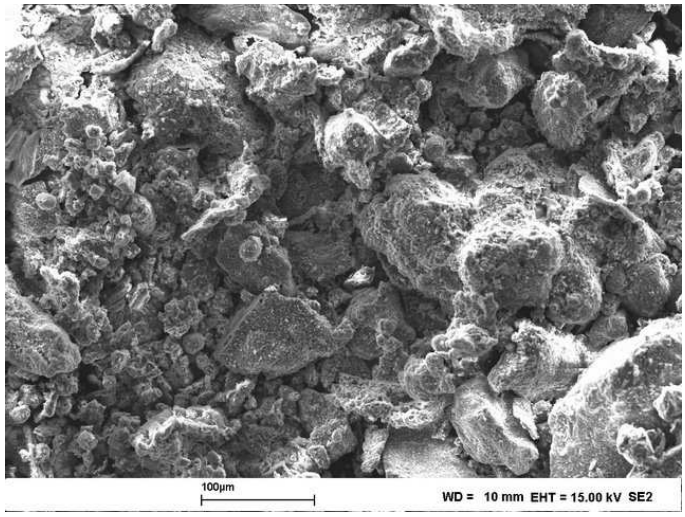


Figure E.8: Fly ash sample, magnification 200x

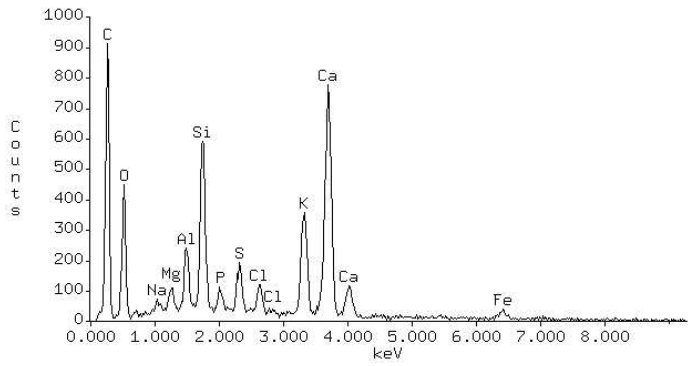


Figure E.9: Fly ash sample, magnification 200x, composition

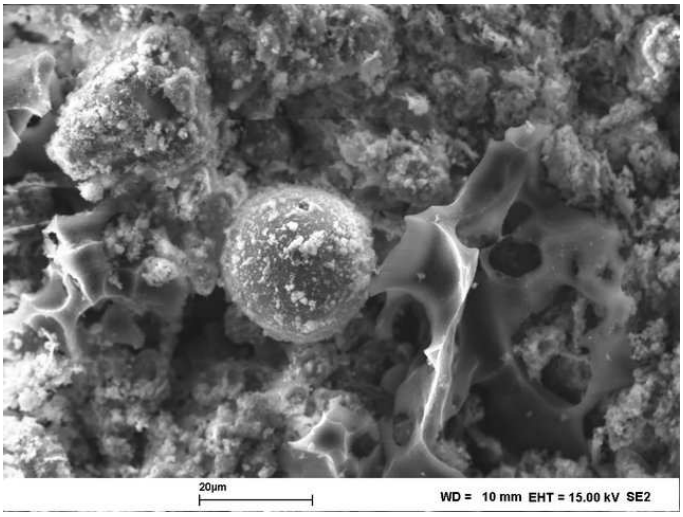


Figure E.10: Fly ash sample with Si, Ca reach spherical structure, magnification 1k

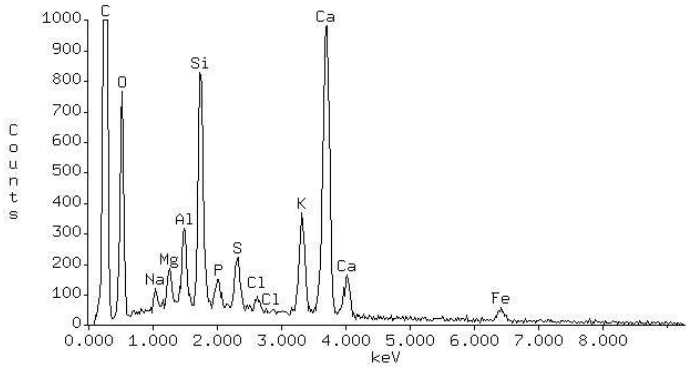


Figure E.11: Fly ash sample with Si, Ca reach spherical structure, magnification 1k, composition

Appendix F

SEM/EDS analysis of kaolin samples

A certain amount of samples originating from the PTG kaolin-KCl interaction measurements were selected for further analysis with SEM/EDS. In general the results are presented in chapter 5. Here some additional data is presented. The appendix includes EDS scans of the samples and the description of the experiments is given in tables F.1 to F.2.

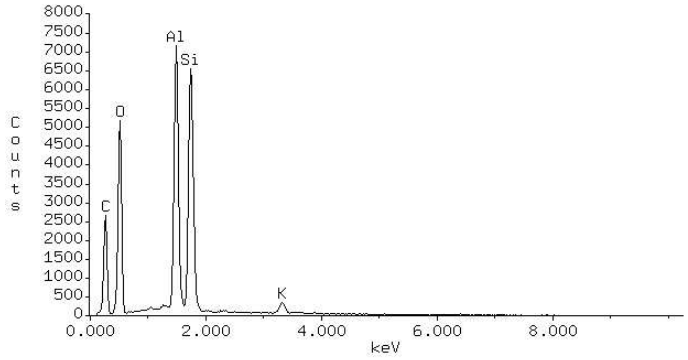


Figure F.1: EDS analysis - sample 6355

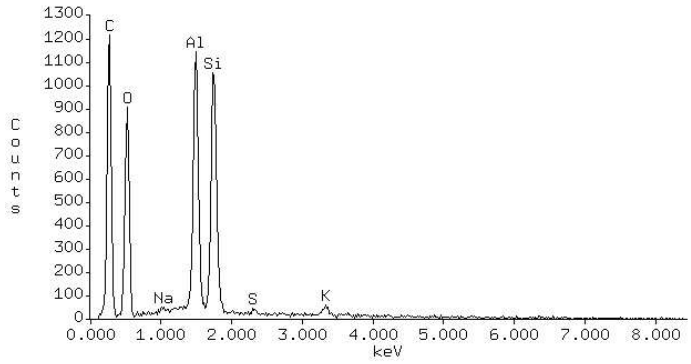


Figure F.2: EDS analysis - sample 6356

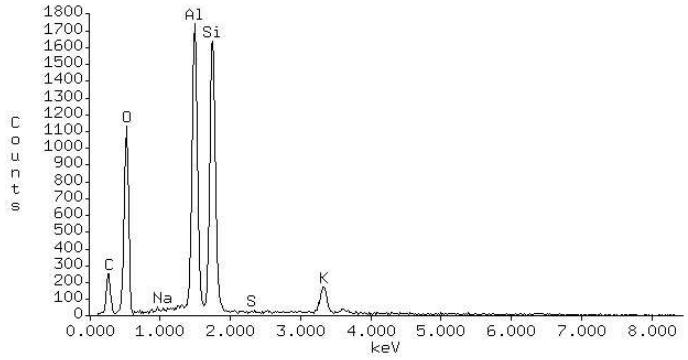


Figure F.3: EDS analysis - sample 6357

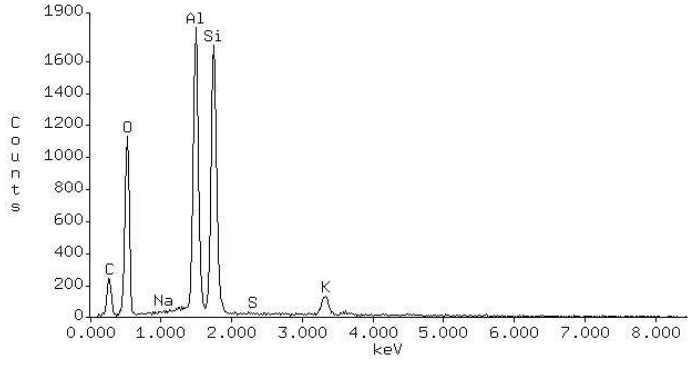


Figure F.4: EDS analysis - sample 6358a

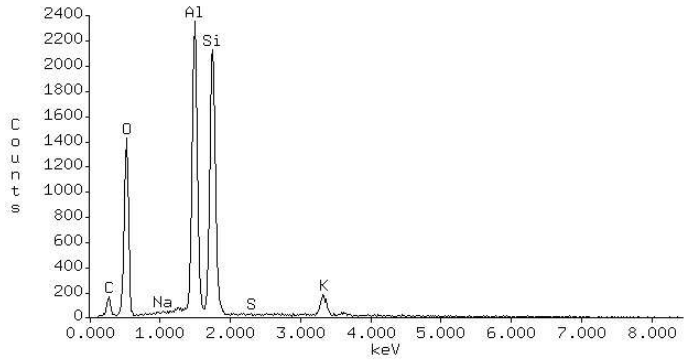


Figure F.5: EDS analysis - sample 6358b

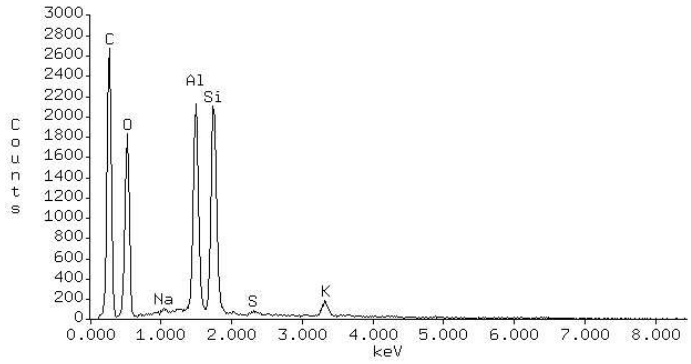


Figure F.6: EDS analysis - sample 6359

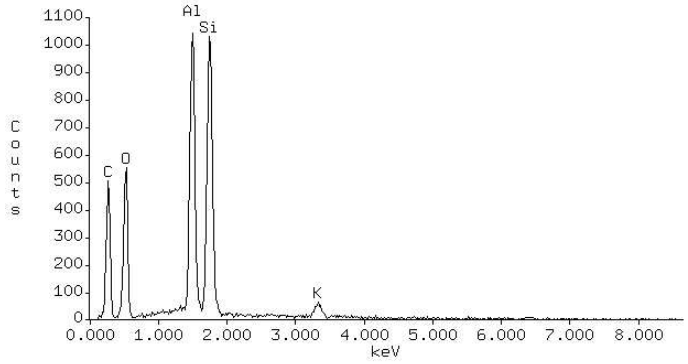


Figure F.7: EDS analysis - sample 6359 overall

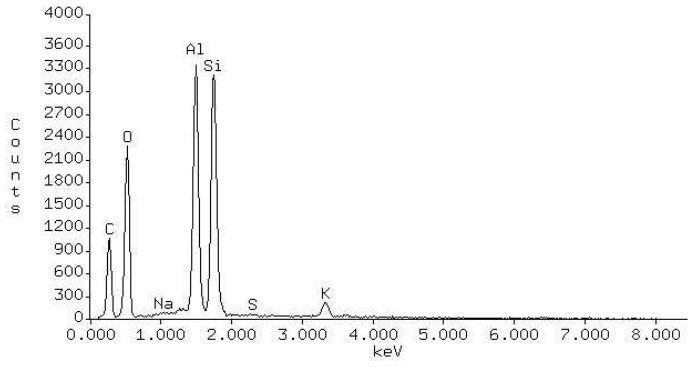


Figure F.8: EDS analysis - sample 6360

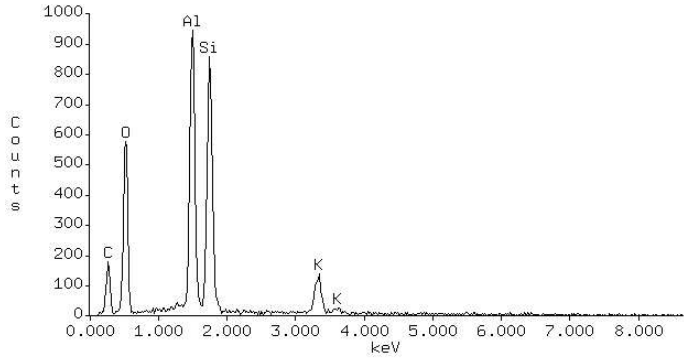


Figure F.9: EDS analysis - sample 6361

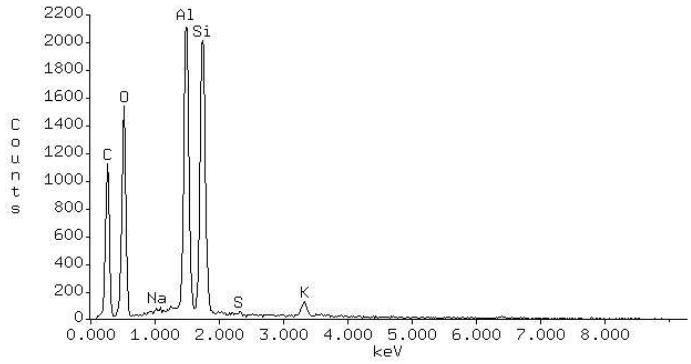


Figure F.10: EDS analysis - sample 6363

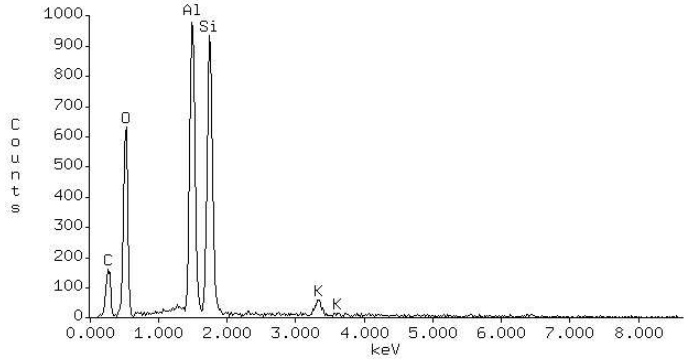


Figure F.11: EDS analysis - sample 6365

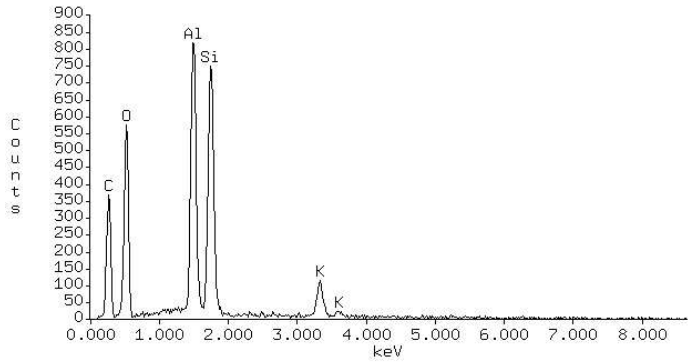


Figure F.12: EDS analysis - sample 6367

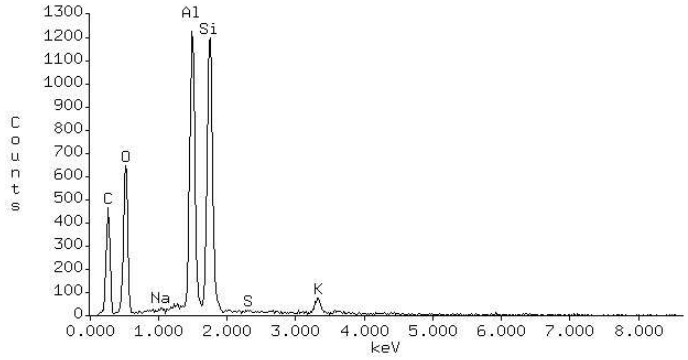


Figure F.13: EDS analysis, cross section in epoxy - sample 6353 overall

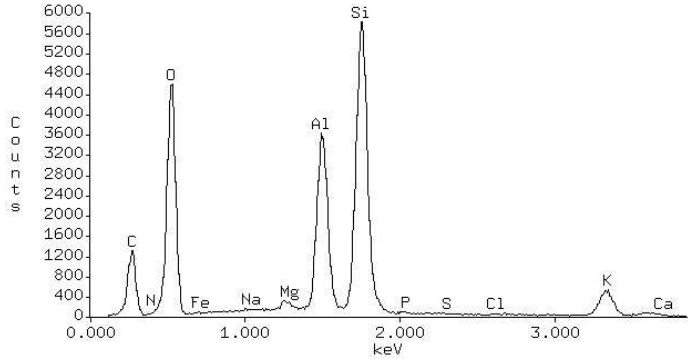


Figure F.14: EDS analysis, cross section in epoxy - sample 6353 - spot 1

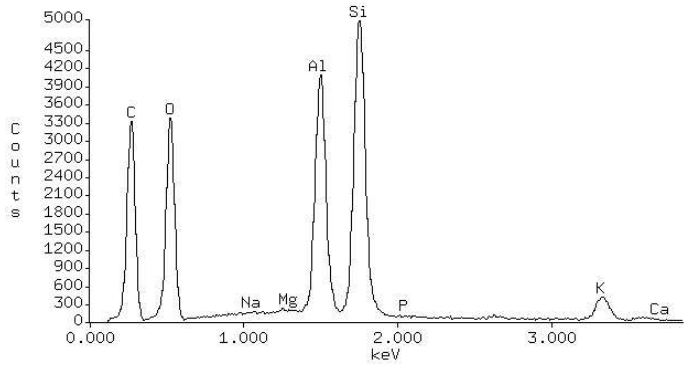


Figure F.15: EDS analysis, cross section in epoxy - sample 6353 - spot 2

	Test – 04.04.2005	Test - 13.04.2005	Test - 13.04.2005	Test - 18.04.2005	Test - 19.04.2005	Test - 19.04.2005	Test - 19.04.2005	Test - 19.04.2005
	bigger holder	bigger holder	bigger holder	bigger holder	bigger holder	bigger holder	bigger holder	bigger holder
	KCl + kaolin – 850oC	only kaolin - 800oC	only kaolin - 850oC	KCl + kaolin	KCl + kaolin	KCl + kaolin	KCl + kaolin	KCl + kaolin
	complete			10 min. - 850oC	20 min. - 850oC	10 min. - 800oC	20 min. - 800oC	full time - 800oC
NUMBER	6353	6355	6356	6357	6358	6359	6360	6361
BEFORE:	BEFORE:	BEFORE:	BEFORE:	BEFORE:	BEFORE:	BEFORE:	BEFORE:	BEFORE:
[mg]	[mg]	[mg]	[mg]	[mg]	[mg]	[mg]	[mg]	[mg]
TOTAL	5076.5	5073.9	5073.4	5073.3	5072.2	5071.6	5071	5070.5
U:	2762.3	2762.1	2761.9	2762.1	2761.8	2761.7	2761.5	2761.1
L:	2314.2			2310.8	2310.7	2310.1	2309.7	2308.8
L + KCl:							2400.7	
U + kaolin	2874.6	2858.8	2866.6	2870.6				
KCl:	91.2			93.7	90.6	91.2	91	90.5
kaolin:	112.3	96.7	104.7	108.4	98.1	99.1	101.8	101.1
KCl + kaolin:				202.1	188.7	190.3	192.8	191.6
TOTAL	5280	5170.4	5178.1	5275.5	5261.2	5262.2	5263.7	5262.2
AFTER:	AFTER:	AFTER:	AFTER:	AFTER:	AFTER:	AFTER:	AFTER:	AFTER:
TOTAL:	5181.5	5159.5	5165.7	5251.8	5227	5243.1	5234.8	5165.4
U + kaolin:	2865.9	2847.6	2853.9	2860	2852.1	2849.9	2852.3	2854.9
L:	2315.1			2391.8	2375	2393.3	2382.3	2310.4
L:KCL containing part								
U:kaolin containing part								

Table F.1: Experiments overview, the big sample holder

	Test - 26.04.2005	Test - 26.04.2005	Test - 26.04.2005	Test - 26.04.2005	Test - 26.04.2005	Test -
	smaller holder	smaller holder	smaller holder	smaller holder	smaller holder	smaller holder
	KCl - kaolin	KCl - kaolin	KCl - kaolin	KCl - kaolin	KCl - kaolin	KCl - kaolin
	10min. - 850oC	20min. - 850oC	10min. - 800oC	20min. - 800oC	complete - 850oC	complete - 800oC
NUMBER	6363	6364	6365	6366	6367	
BEFORE:	BEFORE:	BEFORE:	BEFORE:	BEFORE:	BEFORE:	BEFORE:
	[mg]	[mg]	[mg]	[mg]	[mg]	[mg]
TOTAL	5599.7	5599.6	5602	5598.2	5597.6	
U:	2762	2762.1	2761.7	2761.4	2761.3	
L:	2837.6	2837.8	2840.5	2837	2836.6	
L + KCl:						
U + kaolin	2858.8					
KCl:	65.8	64.7	64.6	67	61.5	
kaolin:	103.1	106.3	100.3	103.6	103.5	
KCl + kaolin:	168.9	171	164.9	170.6	165	
TOTAL	5768.8	5770.2	5766.8	5768.4	5762.7	
AFTER:	AFTER:	AFTER:	AFTER:	AFTER:	AFTER:	AFTER:
TOTAL:	5759.6	5749.1	5750.7	5749.5	5693.7	
U + kaolin:	2857.4	2856.4	2900.2	2853	2855.7	
L:	2902.2	2892.3	2850.7	2996.2	2837.9	
L:KCL containing part						
U:kaolin containing part						

Table F.2: Experiments overview, the small sample holder

Summary

Alkali metals in combustion of biomass with coal

Growing demand for energy in the world, depletion of fossil fuels and green house effect require from us to utilize alternative, renewable sources of power. Biomass gained in the last few years more and more attention especially in Europe. Many research programs focused on the various forms of thermal biomass utilization have been launched and successfully accomplished expanding our knowledge and contributing to the, so called, sustainable development. Utilization of straw, biomass present in Europe in large although spread quantities, is an interesting option among others for small decentralized CHP plants. On the other side, straw thermal utilization can cause serious problems resulting in power plant shut downs. The chemical composition of straw, especially high volatile alkali metals content in combination with other elements like chlorine causes corrosion and deposits formation problems, moreover, in combination with silica and calcium slagging and fouling problems.

The main goal of this thesis is to investigate the mechanisms responsible for alkali metals release and sequestering during combustion of straw and the influence of co-combustion of straw with coal. The knowledge regarding these mechanisms is necessary to operate biomass fired power plants in a safe, efficient and profitable way. The research has been done by means of experiments and system modeling. The tests have been done using pilot scale CFB combustor and bench scale heated grid reactor together with the fundamental studies over KCl-kaolin interactions in TG reactor.

After a general introduction in **Chapter 1**, description of the alkali metals behavior under combustion conditions combined with the extensive literature overview and discussion over the present state of the art is given in **Chapter 2**. Chapter 2 specifies the research goals for this thesis. Moreover, the possible alkali getters are discussed focusing on kaolin clays as the most promising ones.

In **Chapter 3** the experimental work using pilot scale CFB combustor is presented. For the tests various samples of straw and coal were used. The gaseous

alkali metals compounds were measured using the modern, on-line ELIF laser technique. This chapter presents data of unique scientific value because of the CFB reactor used and the selected fuels. Moreover, the observed substantial decrease in the gaseous alkali metals concentration during the co-combustion of straw with coal provided basis for further modeling work presented in the following chapter.

In **Chapter 4** the modeling work using chemical equilibrium modeling package is shown that was performed in order to simulate the system. The assumptions and restrictions to the model are pointed out. The chapter presents interesting data validating the experimental finding presented in the previous chapter. The co-combustion with coal has a strong effect on alkali sequestering and formation of relatively safe alkali-alumina-silicates thus this is positive for power plant operators. Moreover, the modeling work gives more insight into the complex system with multiple important compounds. In order to further investigate the alkali capturing phenomena by natural clays present in coal the fundamental studies were performed and presented in the following chapter.

In **Chapter 5** fundamental investigation of KCl and kaolin interactions is presented. This chapter reveals couple of interesting mechanisms including the influence of water on the system. Water in the system increased the sorbing capacity of kaolin. Moreover, it is presented that mechanism of absorption is the diffusion controlled and the presence of water speeds up the whole process.

Finally in **Chapter 6**, the thesis is concluded by a summary of the obtained results and original contributions, moreover recommendations for future research work are pointed out.

Michal Glazer

Samenvatting

Alkali metalen in verbranding van biomassa met steenkool

De groeiende vraag naar energie in de wereld, de uitputting van fossiele brandstoffen en het broeikas effect vragen ons om alternatieve, hernieuwbare bronnen voor elektriciteitsopwekking. Biomassa heeft in de afgelopen jaren meer en meer de aandacht getrokken, vooral in Europa. Veel onderzoeksprogrammas gericht op de verschillende vormen van thermische biomassa conversie zijn gelanceerd en met success afgerond, waardoor de kennis op dit gebied is vermeerderd en is bijgedragen aan de zogenaamde duurzame ontwikkeling. Het gebruik van stro, een agrarisch biomassa residu dat in Europa in grote hoeveelheden beschikbaar is, maar wel met een grote regionale spreiding, is een interessante optie samen met andere voor kleinschalige, decentrale gecombineerde warmte- en krachtcentrales. Aan de andere kant kan de thermische utilisatie van stro ernstige operationele problemen veroorzaken, resulterend in een gedwongen stop van de bedrijfsvoering van een centrale. De chemische samenstelling van stro, vooral het gehalte aan hoog-vluchtige alkalimetalen in combinatie met andere elementen zoals Chloor, veroorzaakt corrosie- en depositieproblemen. Erger nog, in combinatie met Silica en Calcium kunnen verslakkings- en vervuilingsproblemen ontstaan.

Het hoofddoel van dit proefschrift is het onderzoek naar mechanismen die verantwoordelijk zijn voor het vrijkomen van de alkalimetalen alsmede hun binding tijdens verbranding van stro en de invloed van het meestoken van stro samen met kolen. Kennis van deze mechanismen is nodig om biomassa gestookte elektriciteitscentrales op een veilige, efficinte en economisch voordelige manier te bedrijven. Het onderzoek is uitgevoerd middels experimenteren en systeemmodellering. Testen zijn uitgevoerd, gebruikmakend van een pilotschaal CFB verbrandingsopstelling en een labschaal heated grid reactor, tesamen met een fundamentele studie naar KCl-kaoliniet interactie in een TG reactor.

Na een algemene inleiding in **Hoofdstuk 1**, wordt een beschrijving van het gedrag van de alkalimetalen onder verbrandingscondities, gecombineerd met

een uitgebreide literatuurstudie en discussie omtrent de huidige stand van de techniek gegeven in **Hoofdstuk 2**. Hoofdstuk 2 specificeert de onderzoeksdoelen voor dit proefschrift. Bovendien worden de mogelijke alkalibinders besproken, waarin de nadruk wordt gelegd op kaoliniet kleimaterialen als de meest veelbelovende.

In **Hoofdstuk 3** wordt het experimentele werk rondom de pilotschaal CFB verbrandingsopstelling gepresenteerd. Voor de proeven werden verschillende soorten stro en kolen gebruikt. De gasvormige alkalimetaalverbindingen werden gemeten door middel van moderne, on-line ELIF lasertechniek. Dit hoofdstuk presenteert gegevens van een unieke technisch-wetenschappelijke waarde vanwege de toegepaste CFB opstelling en de geselecteerde brandstoffen. Bovendien vormt de waargenomen substantile afname van de gasvormige alkalimetaal concentratie tijdens co-verbranding van stro en kolen de basis voor verder modelleerwerk, dat wordt gepresenteerd in het volgende hoofdstuk.

In **Hoofdstuk 4** wordt het modelleerwerk gepresenteerd, waarbij gebruik wordt gemaakt van chemische evenwichtsmodellering om het systeem te simuleren. De aannames en beperkingen van het model worden hier uitgewerkt. Het hoofdstuk toont interessante gegevens, waarbij experimentele waarnemingen beschreven in het vorige hoofdstuk gevalideerd worden. Het meeverbranden van kolen met stro heeft een sterk effect op de alkalibinding en de vorming van relatief onschuldige alkalialuminosilicaten, hetgeen dus positief is voor het op die manier bedrijven van centrales. Bovendien geeft het modelleerwerk meer inzicht in het complexe systeem van meerdere belangrijke anorganische verbindingen. Om het fenomeen van alkalimetaalbinding door natuurlijke kleimaterialen in kolen verder te bestuderen, zijn er fundamentele studies uitgevoerd, welke worden gepresenteerd in het volgende hoofdstuk..

In **Hoofdstuk 5** wordt het fundamentele onderzoek naar KCl en kaoliniet interacties gepresenteerd. Dit hoofdstuk onthult een aantal interessante mechanismen waarbij de invloed van water op het systeem een rol speelt. Water in het system doet het absorptievermogen van kaoliniet toenemen. Bovendien wordt aangetoond dat het absorptiemechanisme wordt gelimiteerd door diffusie en de aanwezigheid van water versnelt het hele proces.

Tenslotte wordt het proefschrift in **Hoofdstuk 6** afgerond met het geven van een samenvatting van de verkregen resultaten en originele bijdragen. Bovendien worden aanbevelingen voor toekomstig verder onderzoekswerk aangegeven.

Michal Glazer

Selected Publications

Glazer, M.P., Khan, N.A., Schürmann, H., Monkhouse P., de Jong, W., Spliethoff, H. Alkali Metals in Circulating Fluidized Bed Measurements and Chemical Equilibrium Analysis. Energy&Fuels, vol. 19, 2005

Glazer, M.P., Schürmann, H., Monkhouse P., de Jong, W., Spliethoff, H. Co-combustion of coal with high alkali straw. measuring of gaseous alkali metals and sulfur emissions monitoring. International Conference on Circulating Fluidized Beds CFBC8 2005, Hangzhou, China

Wiebren de Jong, Michal Glazer, Marcin Siedlecki, Ömer Ünal, Hartmut Spliethoff High temperature gas filtration results obtained for fluidized bed gasification and combustion Biomass 2004, Rome, Italy

Glazer, M.P., Schürmann, H., Monkhouse P., de Jong, W., Spliethoff, H. Measurements of Flue Gas Alkali Concentrations in Circulating Fluidized Bed Combustion of High Alkali Biofuels Science in Thermal and Chemical Biomass Conversion STCBC Conference 2004, Victoria, Vancouver Island, Canada

Glazer, M.P., Spliethoff H., Chen G. Structural changes during rapid devolatilization of high alkali bio-fuels. Preliminary study for CFB combustion experiments. Clean Air 2003, Lisbon, Portugal

Glazer, M.P., Spliethoff H High Alkali Biofuels Combustion in CFBC systems state of the art and discussion Waste 2003, Sheffield, UK

Curriculum Vitae

Date and place of birth:	07 Jully 1977, Poznań, Poland
Master of Science:	Heating and Airconditioning Systems, Heat and Fluid Flow Laboratory, Poznań University of Technology, Poland (1996 – 2001)
Doctorate:	Alkali metals in combustion of biomass with coal, Section Energy Technology, Delft University of Technology, The Netherlands (2001 – 2005)
Marie Curie Fellow:	Marie Curie Training Site, Åbo Akademi Finland (March 2005 – July 2005)

Acknowledgments

This is the place for me to acknowledge many people who contributed to this thesis. Without them it wouldn't be written.

It is a great pleasure for me to express my sincere gratitude to Prof. Hartmut Spliethoff and dr. Wiebren de Jong who supervised this work. Wiebren I wish to express to you my sincere appreciation for the high quality of scientific discussions, the attention, the care and importance you gave to this work.

I would like to thank to Prof. Mikko Hupa for hosting me in his group for 4 month during Marie-Curie fellowship at Åbo Akademi, Finland. It was really great time of the highest scientific value and I really appreciated the engagement of the people there and the atmosphere in the group. Special thanks to Patrik Yrjas my direct supervisor. Special thanks as well to Peter Backman for his great help with the experiments, our discussions I enjoyed a lot and keeping my car in his garden for a week when I was in China.

I would like to thank to my former students: Marcin Siedlecki and Nafees Khan for their contribution to this thesis. Marcin, many thanks for your great help, hard working together to make "ciapuza" running, our scientific and non-scientific discussions and last but not least, friendship. Many thanks to the ET technical stuff.

This work could not have been completed in such a peaceful way without encouragements of my dear Beata and many friends whom I came to know. The greatest thanks to my Polish mates from Delft and surroundings: Michal and Ewelina, to Grzes, Zbyszek and Aneta, Wojtek and Ania, Radek and Agnieszka, Krzysztof, Anrzej and Ela, Adrian and Elwira. Many special thanks to Gianluca for the friendship and great time we had together during these years. Moreover great thanks to my old Polish mates Andrzej Tabaka and Andrzej Wandtke for the time we spend together being abroad.

Finally, I would like to dedicate this thesis to my parents and Beata, whose love is more than I can describe.

23rd January 2007, Delft

"By the grace of God, I am what I am...."
(1Cor 15:10)

Memo

.....